HITACHI

GE Hitachi Nuclear Energy

James Robinson
NPP Project Manager

3901 Castle Hayne Road, M/C A60
Wilmington, NC 28401
USA

T 910-819-6215
NE22472@ge.com

GEOE-ARC-2015-0022

Response required: Yes ☐ No ☒
Response required date: N/A

October 29, 2015

Procurement Services Division
U.S. Department of Energy
Idaho Operations Office
1955 Fremont Avenue
Idaho, Falls, ID 83415

Subject: DE-NE0000613, Final Scientific/Technical Report: Next-Generation Electromagnetic Pump Analysis Tools

Please find enclosed the "Final Scientific/Technical Report" deliverable titled: Next-Generation Electromagnetic Pump Analysis Tools (DOEGEHA00613).

As a team, we reviewed the content requirements for the Final Technical Report and looked at our two deliverable comprehensive final technical reports. We realized that the reports had the content, but it was not provided in a sequence easy 'checkoff' format. To make it easier for you to verify that GEH's two Final Technical Reports have the information required, we created a stand-alone Appendix in each report titled "Federal Reporting Checklist (FAR) Checklist." This Appendix follows exactly the sequence of the seven areas of information and provides the specific information identified. This is not new information but is pulled from both reports.

For the "FINAL TECHNICAL REPORT: NEXT-GENERATION ELECTROMAGNETIC PUMP ANALYSIS TOOLS," this information resides in Appendix B.

Both Appendices have the SAME content and were generated to 'tear' away from the report as a quick summary/reference/guide to our very thorough (long), final technical reports, as well as the project itself.

To better support your review and address the request in your October 1, 2015 email, this cover letter provides a guide to where these original proposal objectives can be found within the two final technical reports:

GE Hitachi Nuclear Energy (GEH):

GE Hitachi **GE Hitachi Nuclear Energy**

1 - Create database of EM pump design, development operation, and post operation experiences.

- Final Technical Report: Next-Generation Electromagnetic Pump Analysis Tools, Section 2.0
- Final Technical Report: Electromagnetic Pump Insulation Materials Development and Testing, Section 2.0

2 - Identify advanced materials for winding electrical insulation of pump coil.

- Final Technical Report: Electromagnetic Pump Insulation Materials Development and Testing, Section 3.0

3 - Identify replacement materials and design for previously used materials/design.

- Final Technical Report: Electromagnetic Pump Insulation Materials Development and Testing, Section 3.0

4 - Evaluate alternative materials through thermal, electrical, and mechanical testing to qualify longevity of insulation performance.

- Final Technical Report: Electromagnetic Pump Insulation Materials Development and Testing, Section 3.0

5 - Modernize GEH's legacy EM pump analysis tools and performance models.

- Final Technical Report: Next-Generation Electromagnetic Pump Analysis Tools, Sections 3.0 and 4.0
- Final Technical Report: Electromagnetic Pump Insulation Materials Development and Testing, Section 4.0

6 - Develop and demonstrate next generation EM pump analysis tools to further understand magnetic field and flux profiles.

- Final Technical Report: Next-Generation Electromagnetic Pump Analysis Tools, Section 5.0

Argonne National Laboratory (ANL):

7 - Perform testing of high temperature electromagnetic pump coils.

- Final Technical Report: Electromagnetic Pump Insulation Materials Development and Testing, Section 6.0

8 - Conduct alternative insulation material development and evaluation.

- Final Technical Report: Electromagnetic Pump Insulation Materials Development and Testing, Section 6.0

9 - Provide analysis and modeling needed to support efforts to upgrade the MATRIX code for modeling electromagnetic pump performance.

- Final Technical Report: Next-Generation Electromagnetic Pump Analysis Tools, Section 4.0
- Final Technical Report: Electromagnetic Pump Insulation Materials Development and Testing, Section 4.0

10 - Develop and calibrate multi-stress test facilities.

- Final Technical Report: Electromagnetic Pump Insulation Materials Development and Testing, Section 6.0

11 - Perform testing and validation of composite insulation developed.

- Final Technical Report: Electromagnetic Pump Insulation Materials Development and Testing, Section 6.0

12 - Identify the best insulation system for long-term reliability and safety.

- Final Technical Report: Electromagnetic Pump Insulation Materials Development and Testing, Section 6.0

If you have questions or concerns, I can be reached at 910-819-6215 or NE22472@ge.com.

Sincerely yours,

James Robinson

James Robinson
NPP Project Manager

Attachments: (1) DOEGEHA00613.pdf

cc: Willettia D. Amos (DOE) David Craig Welling (DOE) Eric Loewen

FINAL TECHNICAL REPORT: Next-Generation Electromagnetic Pump Analysis Tools (PLM DOC-0005-2188) - REPORT# DOEGEHA00613

Federal Grant Identification Number: DE-NE0000613

Project Title: Qualification of EM Pumps: Next Generation Electromagnetic Pump: Analysis Tools and Insulation Materials Development

Principal Investigator: Eric P. Loewen, Ph.D.
Chief Consulting Engineer, Advanced Plants
T 910-819-5190 F 910-363-5190
Email: eric.loewen@ge.com

Submitter: James Robinson
Project Manager
T 910-819-6215 F 910- 342-6215
Email: ne22472@ge.com

Date Submitted: 10/26/2015
DUNS Number: 800334570
Recipient Organization: GE-Hitachi Nuclear Energy Americas LLC
3901 Castle Hayne Road
Wilmington, NC 28401
Other Team Members: Argonne National Laboratory
9700 South Cass Avenue
Argonne, IL 60439

Project Start Date: 08/05/2013 **Project End Date:** 11/03/2015

10/29/2015

James Robinson Date

This page intentionally left blank

==

DOE Disclaimer

This report was prepared as an account of work sponsored by an agency of the United States Government. Neither the United States government nor any agency thereof, nor any of their employees, makes a warranty, express or implied, or assumes any legal liability or responsibility for the accuracy completeness, or usefulness of any information, apparatus, product, or process disclosed, or represents that its use would not infringe privately owned rights. Reference herein to any specific commercial product, process, or service by trade name, trademark, manufacturer, or otherwise does not necessarily constitute or imply its endorsement, recommendation, or favoring by the United States Government or any agency thereof. The views and opinions of authors expressed herein do not necessarily state or reflect those of the United States Government or any agency thereof.

DOE Acknowledgments

This material is based upon work supported by the Department of Energy under Award Number DE-NE0000613. This document is the result of the technical contributions from many individuals and organizations in addition to the authors of this document.

==

This page intentionally left blank

TABLE OF CONTENTS

LIST OF FIGURES

LIST OF TABLES

This page intentionally left blank

1.0 PROJECT OVERVIEW

In 2013, the Department of Energy (DOE) announced a $3.5 million investment opportunity for the further improvement of Advanced Nuclear Power Reactors to expand clean energy leadership and to empower a low-carbon economy[1]. For the past two years, GE Hitachi Nuclear Energy Americas LLC (GEH) with GE Global Research Center (GRC) teamed with Argonne National Laboratory (ANL) to perform Research and Development (R&D) for the next-generation analysis tools and insulation materials for Electromagnetic (EM) Pumps. These tools and insulation materials are necessary for the development and qualification of EM Pumps used in advanced liquid-metal reactor (ALMR) designs.

Figure 1-1 provides an overview of this project scope and deliverables. GEH led the research efforts to ensure the relevant pockets of individual expertise within industry and one of the DOE laboratories were incorporated into industry products for the benefits of the U.S.

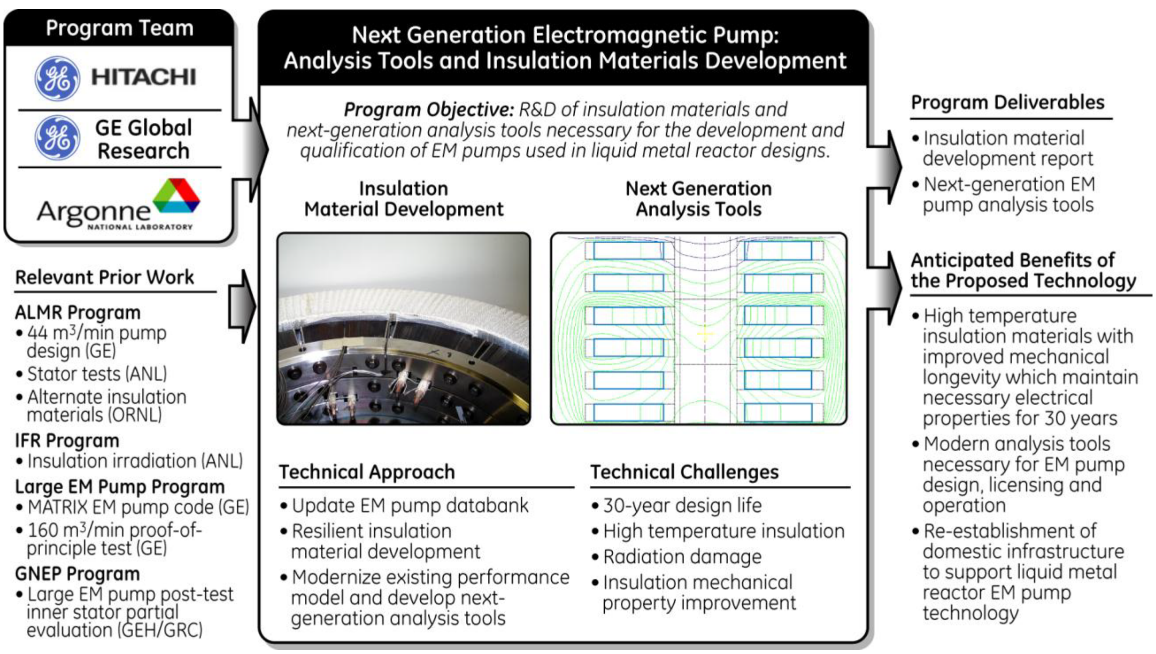

Figure 1-1: Overall EM Pump Project Overview

[1] U.S. Department of Energy, "Advanced Reactor Technologies", (2014) URL: http://www.energy.gov/ne/nuclear-reactor-technologies/advanced-reactor-technologies

In GEH's 2009 *Technology Development Roadmap: Facilities for Closing the Fuel Cycle* (#DE-FC01-07NE24504), the self-cooled EM Pump is defined as a "critical technology element" for the development of the Power Reactor Innovative Small Module (PRISM). This project advanced the roadmap to develop and qualify the EM Pump. The applicability of this R&D project towards commercialization is summarized in Figure 1-2.

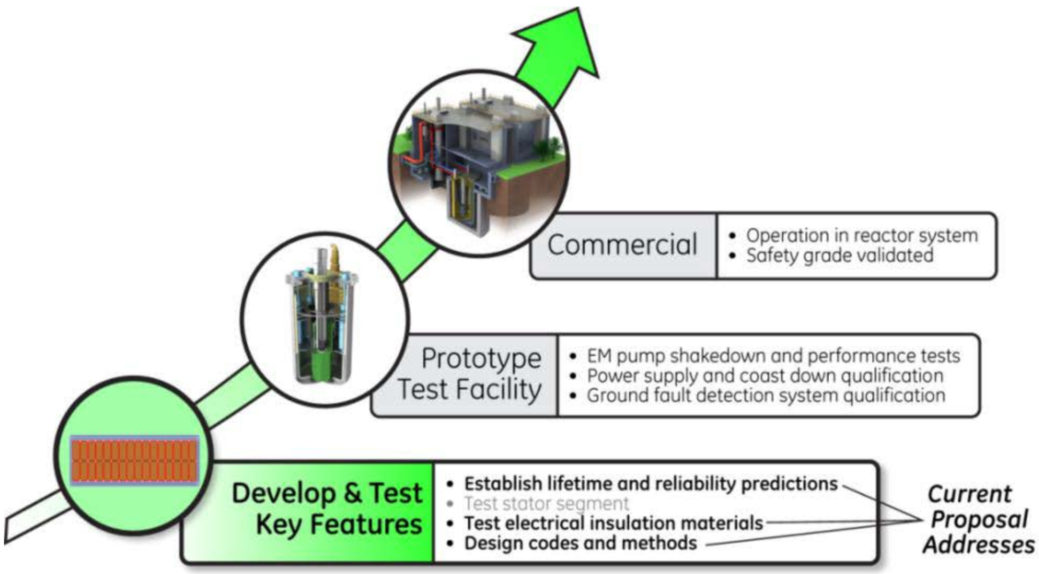

Figure 1-2: Technical Roadmap for the Self-Cooled EM Pump Deployment

1.1 Specific Objectives and Goals

There were five identified tasks submitted in the original proposal:

1. Update a searchable databank of EM Pump design, development, operating and post-operation experiences for assistance in further development.
2. Identify advanced materials for winding insulation of the pump coil, so that a new resilient engineered insulation system can be defined for future EM Pump construction.
3. Modernize legacy performance models used in the design of the 160 m³/min EM Pump, the largest ever built, [and] to capture previous EM Pump knowledge and modeling among early career engineers.
4. Develop and demonstrate next-generation EM Pump analysis tools to further understanding of magnetic field and flux profiles as they relate to thermal cycling and pumping efficacy of molten metal.

5. Provide an opportunity for U.S. industry to participate in collaborative research to facilitate greater engagement between the industry and national laboratories.

In support of this R&D project, each organization brought the following strengths in completing the project:

General Electric (GEH and GRC): GE Hitachi Nuclear Energy Americas LLC (GEH) brings over 50 years of commercial nuclear technology experience and has been a leader on sodium-cooled power reactor systems since 1946. GE amassed a significant amount of information and developed an extensive expertise in fast reactor design, including large-scale EM Pumps, available in GEH record repositories. GEH, as the steward of the PRISM technology, knows the challenges of deploying large EM Pump technology on a commercial scale.

GE's Global Research Center (GRC) dielectrics team is a 17-member team that blends many scientific and engineering disciplines: chemists, ceramists, material scientists, and physicists, as well as electrical, mechanical, and chemical engineers. All team members work in conjunction to understand the fundamental mechanisms of aging and failure of electrical insulation and dielectrics for the various products and new designs created by GE, as well as for fundamental government research. GRC personnel and analytical tools provided the necessary technical resources for material identification and next-generation analysis model development to seek a modern alternative insulation material that exceeds the properties of the insulation from previous EM Pumps.

Argonne National Laboratory (ANL):

ANL prepared and tested the precursor stators that served as prototypes for previous EM Pumps from the 1980s through the 1990s during DOE's ALMR Program. As a result, ANL has intimate knowledge of EM Pump coil and insulation system design.

ANL has performed radiation and thermal testing on binder materials and has an understanding how they may affect the physical properties of new EM Pump insulation materials over the 30-year life expectancy requirements. ANL has a vast array of laboratory testing capabilities, and heating systems and furnaces that were readily available to support testing. A multi-stress test apparatus was designed by the team and fabricated/assembled at ANL for testing insulation materials and system replacement candidates.

The project roles of each organization are provided in Figure 1-3.

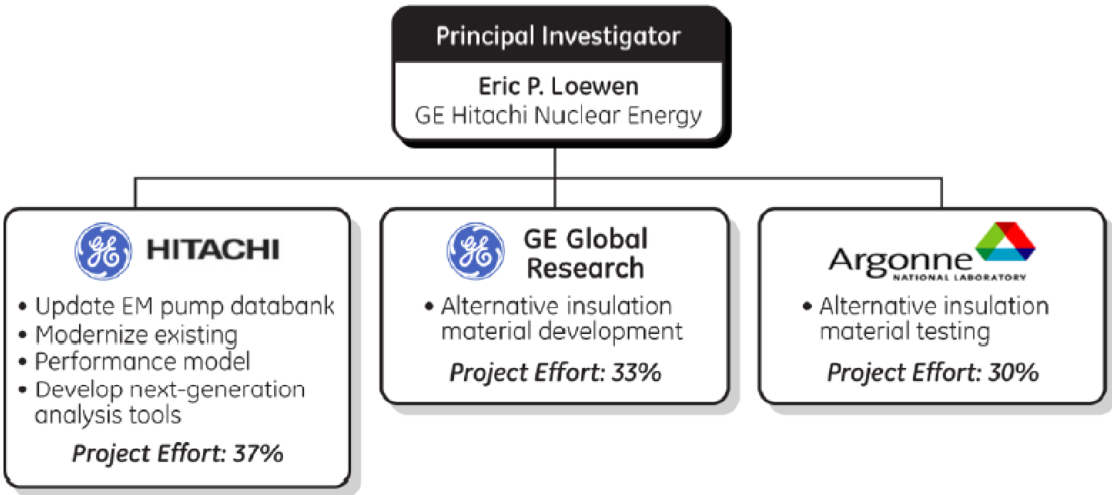

Figure 1-3: Roles of Each Organization

The key personnel from each organization are listed in Table 1-1.

Table 1-1: Key Personnel

Affiliation	Key Contriubtor	Technical Background	Project Role
GEH	Eric Loewen, Ph.D.	Nuclear Engineer	Principal Investigator
GEH	Ana Da Silva	Electrical Engineer	Individual Contributor
GEH	Pradip Saha, Ph.D.	Mechanical Engineer/Thermal Hydraulics	Individual Contributor
GEH	Seth Strege	Electrical Engineer	Individual Contributor
GRC	John Krahn, Ph.D.	Materials Scientist	GRC Leader
GRC	Manoj Shah, Ph.D.	Electrical Engineer	Individual Contributor
ANL	Claude Reed, Ph.D.	Mechanical and Electromagentic Scientist	ANL Leader
ANL	Ken Natesan, Ph.D.	Materials Scientist	Individual Contributor
ANL	Yoici Momozaki, Ph.D.	Nuclear and Electromagentic Scientist	Individual Contributor

Over the course of the past two years, the project schedule generally followed the original Gant Chart submitted in the proposal (Figure 1-4). Figure 1-4 provides a list of tasks and sequences to aid in the understanding of this project, dividing the responsibilities between the three organizations for each subtask as shown.

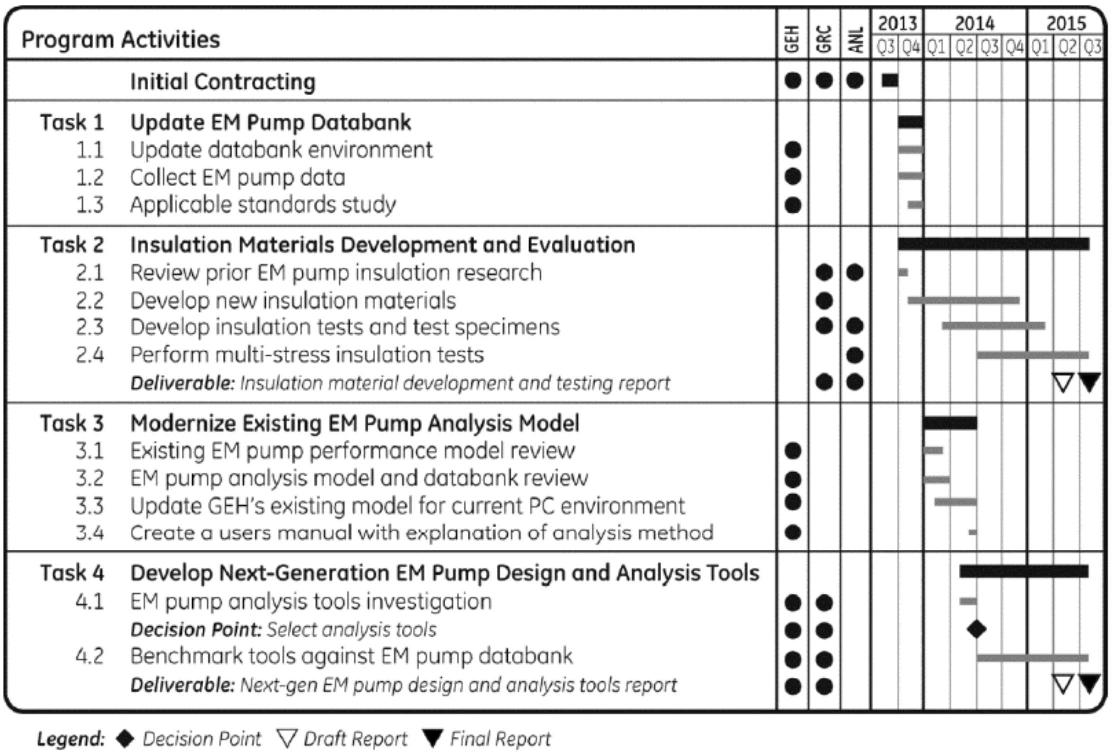

Figure 1-4: Project Task Sequence and Timeline

To support the technical objectives of the projects, the individual organizations established internal goals to aid in project tracking:

GEH & GRC Responsibilities:

1. Create a databank of EM Pump design, development, operation and post operation experiences.
2. Identify advanced materials for winding electrical insulation of pump coil.
3. Identify replacement materials and designs for previously used materials/design.
4. Evaluate alternative materials through thermal, electrical, and mechanical testing to qualify longevity of insulation performance.
5. Modernize GEH's legacy EM Pump analysis tools and performance models.
6. Develop and demonstrate next generation EM Pump analysis tools to further understand magnetic field and flux profiles.

Argonne National Laboratory (ANL) Responsibilities:

1. Perform testing of high temperature electromagnetic pump coils.
2. Conduct alternative insulation material development and evaluation.
3. Provide analysis and modeling needed to support efforts to upgrade the MATRIX code for modeling electromagnetic pump performance.
4. Develop and calibrate multi-stress test facilities.
5. Perform testing and validation of prototype, composite insulation systems.
6. Identify the best insulation system for long-term reliability and safety.

Throughout this project, quarterly progress reports were submitted to DOE.

During the advanced insulation-related efforts, the team evaluated the effectiveness of electrical insulation materials to effectively provide high temperature isolation within a self-cooled, submerged EM Pump. This task leveraged structure-property relationships of a previously operated EM Pump insulation system to improve insulation materials.

Another thrust of this research effort was to provide early career engineers opportunities to work with highly experienced engineers on theory of annular linear induction pumps (ALIPs) to modernize the GEH legacy EM Pump performance models, and leverage experience while building U.S. experience for the future.

The next-generation ALIP design and analysis tools were developed. Fluid dynamic and thermal aspects were added to the analysis tool.

These two project objectives were accomplished through an engagement between industry GE (GEH and GRC) and the DOE laboratories (ANL).

This report, Technical Report: Next-Generation Electromagnetic Pump Analysis Tools (PLM DOC-0005-2188), as previously shown in Figure 1-1, is one of the final two deliverables. To close the project, two separate reports titled: 1) Technical Report: Insulation Materials Development and Testing (PLM DOC-0005-2465) and 2) Technical Report: Next-Generation Electromagnetic Pump Analysis Tools (PLM DOC-0005-2188) are being submitted. The latter is the subject of this document.

1.2 Project Background

EM Pumps are a key component used in the operation of liquid-metal cooled nuclear reactors, such as PRISM, a small, modular, sodium-cooled reactor designed by GEH.

EM Pumps have been used since the beginning of nuclear reactor technology. Beginning with conceptual validation by GE in 1947, through initial deployment in the nuclear-powered USS Seawolf submarine, EM Pump technology has grown with nuclear reactors, as shown in Figure 1-5. As Sodium-cooled Fast Reactor (SFR) technology has changed (inset within Figure 1-5), EM Pump technology has evolved to support size and flow requirements as reactor designs improved.

The current PRISM reactor design uses six EM Pumps, four primary pumps, and two Intermediate Heat Transport System (IHTS) loop pumps. The primary EM Pumps are submerged in the primary sodium and are used to provide the sodium circulation through the reactor core. These pumps are made to interface with the reactor internals through two manifold assemblies, which collect the high-pressure sodium at the pump discharge and distribute it through pipes to the core inlet plenum. The IHTS EM Pumps, located in each cold leg of the loop with a capacity of 160 m^3/min, are intended to circulate the intermediate sodium through the tube-side of the intermediate heat exchanger (IHX) and the shell-side of the steam generator (Triplett, *et al.*, 2012).

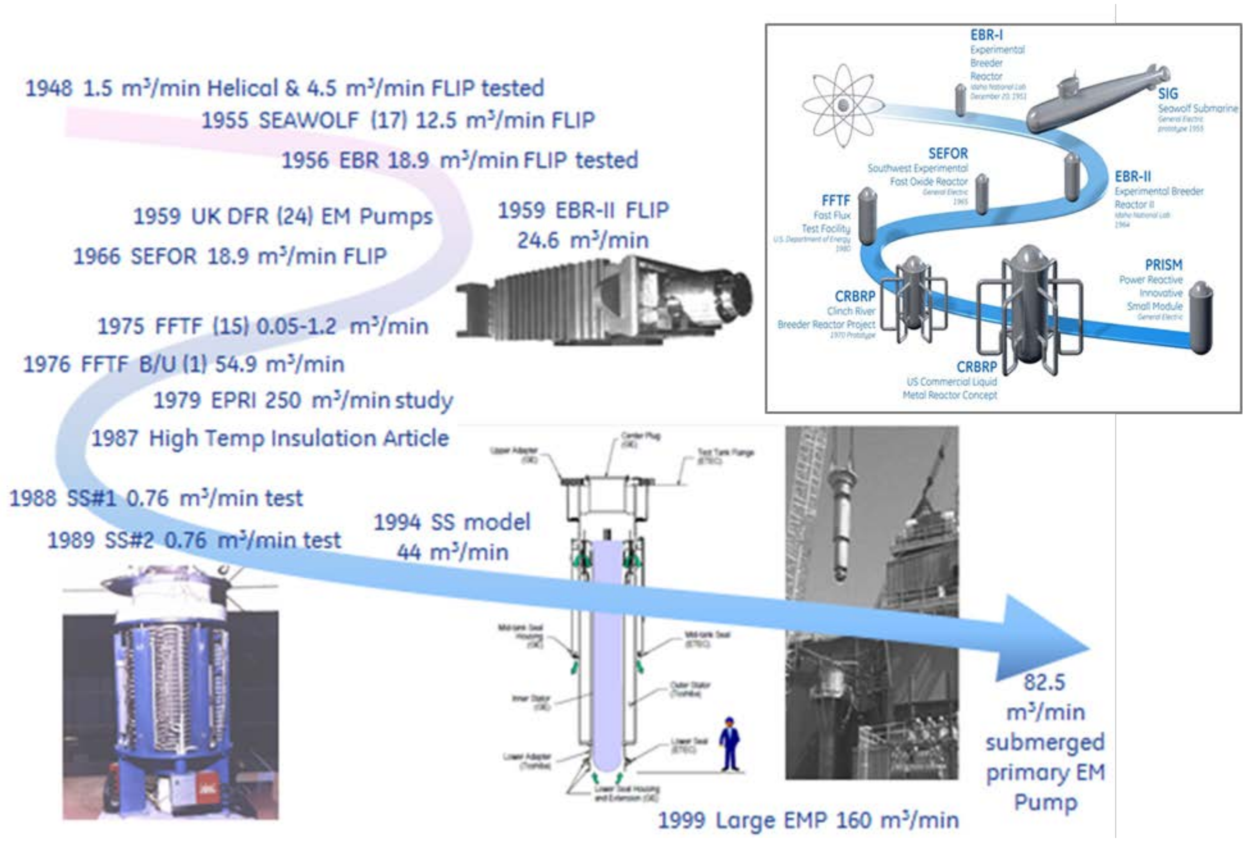

Figure 1-5: Fast Reactor and EM Pump Technology Evolution

As nuclear technology improves safety and reliability, the benefits of EM Pumps align well with these requirements. EM Pumps have no moving parts and eliminate the need for a mechanical pump shaft seal through the primary boundary, allowing the reactor vessel to be hermetically sealed. Self-cooled EM Pumps allow for full submersion in the pumping fluid, thus no rotating mechanical seals are needed. The benefits of EM Pumps have been well documented elsewhere (Fanning, *et al.*, 2003; Ota, 2004; Kane, 1964; Davis, 1970; Cook, 2007).

Early generation EM Pumps were mechanically air or water cooled and electrical insulation requirements did not require stringent, thermal criteria. The next generation EM Pumps is self-cooled. Compared to mechanically cooled pumps, however, self-cooling places harsher thermal requirements on the electrical insulation system. In the PRISM design, the primary EM Pumps are designed to be submerged within a pool of molten sodium that acts as the heat sink for the EM Pump. The demands of the internal electrical insulation system are unusual, involving temperatures far exceeding those that exist in conventional pumps and even above the conditions in so-called "harsh environments" such as down-hole, geothermal applications. The thermo-electrical properties of the insulation need to ensure safety over the life of the equipment.

In 1985 insulation evaluations were initiated in coordination with ANL to develop practical, high temperature, electrical insulation suitable for self-cooled EM Pumps operating at very high temperatures (Jaross, 1985). That research produced reduced-scale (so-called "pan-cake") coils, insulating them with mica mat. In subsequent testing (1988), the binder "Secon-5" became the binder of choice. The coil arrangement and insulation materials from these R&D efforts were subsequently tested in the large EM Pump program.

From the early 1990's through the early 2000's a large EM Pump program was funded by the Japan Atomic Power Company (JAPC) as a part of an overall program to further the research on advanced, liquid-metal cooled, reactor designs such as PRISM. This program was carried out by a series of partners including JAPC, GE, Toshiba Corporation (Toshiba), Kawaski Heavy Industries, and the Boeing Company. During the program, a full size 160 m^3/min (42,000 gpm) annular linear induction pump was designed, fabricated, and in 2000-2001, tested. This pump is approximately the size of one of the IHTS EM Pumps intended to be used by PRISM. Toshiba and GE shared the design and fabrication responsibilities, as well as the testing specifications, for the pump. GE used the MATRIX code (Elliot, 1975) as an EM Pump modeling and design tool.

The purpose of that test program was to demonstrate proof-of-principle for a large, self-cooled, annular linear induction sodium pump intended for use in liquid-sodium-cooled nuclear fast reactors. The pump windings employed a high temperature insulation system capable of 540°C continuous operation, using a proprietary binder. The pump operated over 106 days with 335°C molten sodium. Analytical models predicted that the copper conductors operated at 420-450°C within the EM Pump.

Long after operational testing, the pump was dismantled and the insulation system was evaluated by GRC. The 2009 analysis identified several weaknesses of the insulation system. First, the mechanical integrity was of concern due to thermal-induced embrittlement of the binder and glass support system used in the ground wall insulation. Second, the binder, being a natural product, was inconsistent in quality. Third, being hand-applied, this approach introduced manufacturing variability. Fourth, the binder was no longer commercially available. Finally, as documented in this report, dimensional analysis identified that there was some settling of the primary ground wall insulation. That settling could lead to loose coils in the slot over the 30-year design life.

Computer modelling coincided with EM Pump development, with the original version of MATRIX developed in 1975 by the Jet Propulsion Lab (Elliott, 1975). MATRIX was subsequently transferred from mainframe to PC platforms with new language compilers.

The MATRIX analysis code is a tool used to analyze the overall electric, magnetic, and fluid performance of EM Pumps. The code uses the well-established "MATRIX method" for the analysis of linear induction machines (Elliott, 1975; Kliman, *et al*., 1974). MATRIX can analyze both single- and double-sided linear induction motors, and both flat and annular linear induction liquid-metal pumps and generators. MATRIX incorporates features which allow a finite-length stator to be modeled on a slot-by-slot basis, with magnetic end effects explicitly considered. The code is based on a narrow gap, magnetic circuit approximation with correction factors for the various fringing fluxes, stator ends, and conductor skin effects. Given the frequencies and conductor diameter involved in the EM Pump, the skin effects are zero.

The MATRIX code was later modified in 1990 to be used for GE specific EM Pump applications. This update included calculations for the primary impedance and flux density of both single and double stator annular EM Pumps. It also included the addition of modeling with multiple circuits per phase and detailed tooth geometry. The original (1975) and 1990 versions of the MATRIX code were run on UNIVAC 1108 computers (or similar) that required computing times of about $(M/50)^{2.7}$ minutes, where M is the number of slots. A slot is comprised of one coil and all of the back iron associated with that coil. The inner and outer stator slots are lined up axially along the pump. The long slot computing times were one of the initial drawbacks of the earlier codes.

GE further updated MATRIX in 1999 during the JAPC EM Pump project, to run on the PC. This conversion involved the creation of a batch file method of running the MATRIX calculations. In this method, input files along with the MATRIX FORTRAN source code were compiled into an executable file that was re-compiled every time the case inputs were changed.

Throughout the development of the large EM Pump program, MATRIX and EAGLE (Toshiba's version of MATRIX) were used to analyze initial pump sizing and various operating conditions. After the construction of the pump, a series of operational tests were conducted at the Boeing Santa Susanna Test Facility (also known as the Energy Technology and

Engineering Center, or ETEC). Towards the end of the large EM Pump program, it was observed that the MATRIX code produced pressure rise and efficiency results that needed to be degraded by 30% in order to match the measured pump values. Based on those observations, a 0.7 multiplier was used on the MATRIX results.

The MATRIX outputs from the individual data runs at different frequencies, and currents can be combined for improved evaluation and assessment of EM Pump performance. The following 3-dimensional plots of slip, frequency and power (active, reactive and apparent) or slip, frequency and efficiency, are provided in Figure 1-6 through Figure 1-9 (Fanning, 2009).

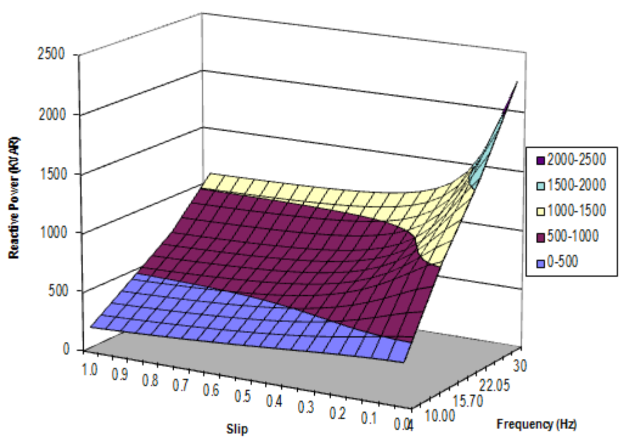

Figure 1-6: Reactive (Imaginary) Power

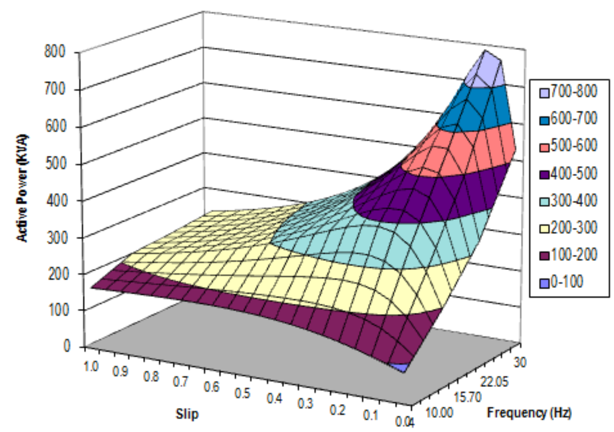

Figure 1-7: Active (Real) Power

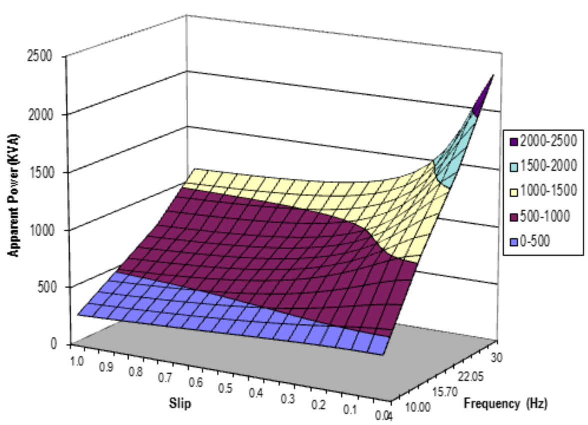

Figure 1-8: Apparent Power

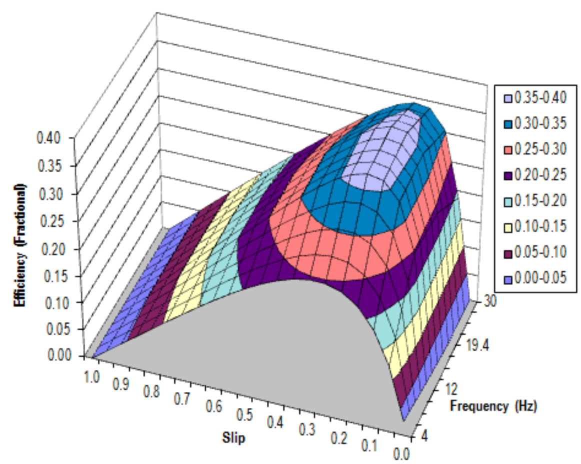

Figure 1-9: Pump Efficiency

These 3-dimetional graphs can provide additional evaluation tools when comparing different EM Pump designs.

To address the concerns of program execution time and the 0.7 multiplier, and provide the next generation of EM Pump modelling tools, this improvement effort was executed as a sub-task of the larger project effort. The primary objective of this sub-task is to develop and demonstrate next-generation EM Pump analysis tools for further understanding of magnetic field and flux profiles as they relate to thermal cycling and pumping efficacy of molten metal.

To progress along the technology development roadmap, the DOE 2013 investment opportunity has allowed GEH, teaming with ANL and GRC, to conduct R&D. This R&D on the next-generation analysis tools and insulation materials for EM Pumps is necessary for the development and qualification of EM Pumps used in future, advanced, liquid-metal reactor designs. As a part of this grant, the MATRIX analysis code was modernized, improved, and tested in order to enhance its overall design analysis capabilities.

1.3 Final Project Task Reports

Sections 1.1 and 1.2 provide the broad historical review of EM Pump development.

The Final Technical Report: Insulation Materials Development and Testing (PLM DOC-0005-2465) performed as part of this project is not the subject of this report. That report (PLM DOC-0005-2465) summarizes the information gathered from the analysis of the 160 m^3/min EM Pump insulation that was tested in 2000-2002 and additional evaluations of new resilient engineered insulation system evaluated and tested at both GRC and ANL under the present DOE R&D project.

The rest of this report provides details of MATRIX development under this project. This report, titled "Technical Report: Next-Generation Electromagnetic Pump Analysis Tools (PLM DOC-0005-2188), summarizes the efforts made to modernize the legacy performance models used in previous EM Pump designs and the improvements made to the analysis tools.

This report provides information on Tasks 1, 3, and 4 of the entire project.

1.4 Project Objectives

The research for Task 4 builds upon Task 1: Update EM Pump Databank and Task 3: Modernize the Existing EM Pump Analysis Model, which are summarized within this report. Where research for Task 2: Insulation Materials Development and Evaluation identified parameters applicable to the analysis model with Task 4, the analysis code was updated, and analyses were made for additional materials.

The important design variables for the manufacture and operation of an EM Pump that the model improvement can evaluate are provided in Table 1-2.

Table 1-2: Important EM Pump Design Variables

Space constraints (diameter, length, etc.)
Voltage capability of insulation system
Maximum flux density through iron
Flow rate and outlet pressure
Efficiency
Manufacturability

The development of the next-generation EM Pump analysis tools during this two-year program provides information in three broad areas:

- Status of analysis model development
- Improvements made to older simulations
- Comparison to experimental data

This page intentionally left blank

2.0 Update EM Pump Databank

The initial creation of the EM Pump databank was completed within the first two quarters of the project. The databank structure was designed, and consists of, topical areas for ease of use. These topical areas are: reference material, analysis tools, design and drawings, fabrication, disassembly, insulation materials, and photos. To further increase the navigability of the databank, searchable cover sheets were appended to each legacy document in order to enable key word search, as well as providing a short abstract to define the subject matter of the document, as shown in Figure 2-1. To have all the legacy documents converted by optical character recognition (OCR) to a verified searchable document was beyond the scope of the proposal resources.

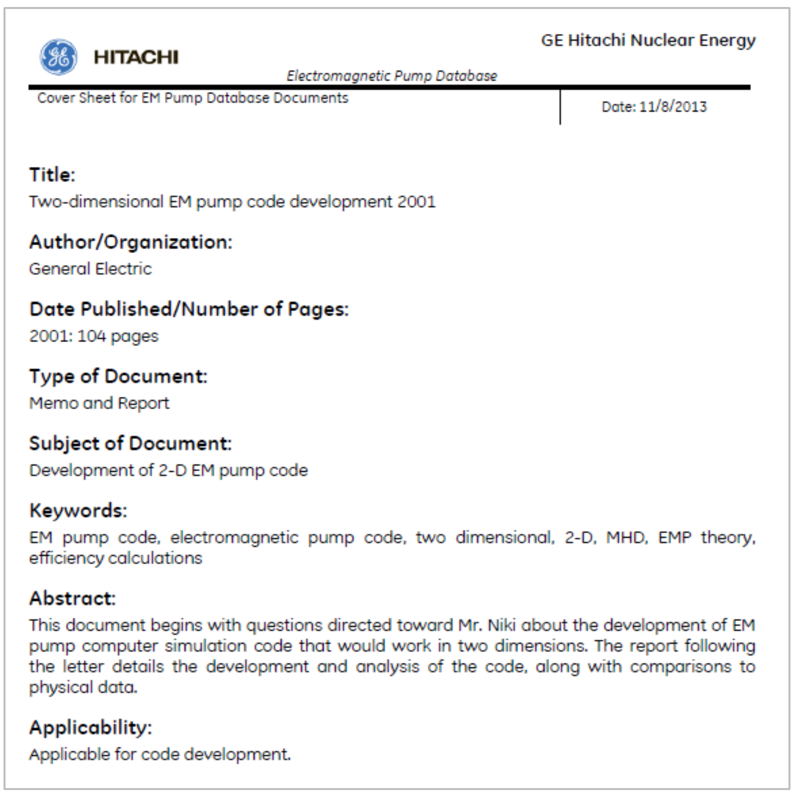
HITACHI

GE Hitachi Nuclear Energy

Electromagnetic Pump Database

Cover Sheet for EM Pump Database Documents

Date: 11/8/2013

Title:
Two-dimensional EM pump code development 2001

Author/Organization:
General Electric

Date Published/Number of Pages:
2001: 104 pages

Type of Document:
Memo and Report

Subject of Document:
Development of 2-D EM pump code

Keywords:
EM pump code, electromagnetic pump code, two dimensional, 2-D, MHD, EMP theory, efficiency calculations

Abstract:
This document begins with questions directed toward Mr. Niki about the development of EM pump computer simulation code that would work in two dimensions. The report following the letter details the development and analysis of the code, along with comparisons to physical data.

Applicability:
Applicable for code development.

Figure 2-1: Example Searchable Cover Sheet

A directory was placed within the databank that lists every scanned document, the number of pages of each document, and its location within the databank in order to enable specific document searches and quick identification of the desired materials. The current contents of the databank are included in this report as Appendix A. Figure 2-2 provides a pictorial representation of the databank architecture.

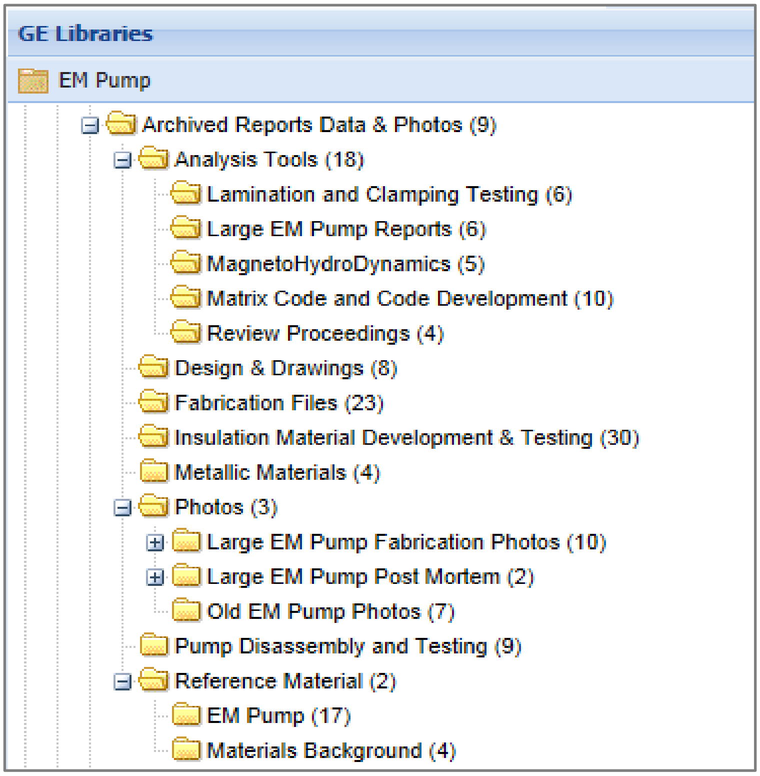

Figure 2-2: EM Pump Databank Structure

The GEH team went through the legacy files and determined which ones were needed for success of this project. Then, ANL team leader, Dr. Reed, visited GEH, Wilmington, NC, and completed an independent physical review of GEH files on EM Pumps in Q4 2013. After this independent review, the development started using the forms in Figure 2-1 and archiving into the structure identified in Figure 2-2. The initial legacy EM Pump databank contained a total of 165 documents numbering 25,234 pages with 2.6 GB worth of data. Several of these documents are compilations of legacy documents, which were combined for ease of topical understanding, as well as ease of identifying important topical areas.

Over the course of the project, new documents were added to the EM Pump databank collection, which has grown to 3.4 GB worth of data and were distributed in the file structure as shown in Figure 2-3. As new documents become available, they will be added to the EM Pump databank, and it will be kept up to date as the team works to commercialize EM Pumps for metal-cooled reactors.

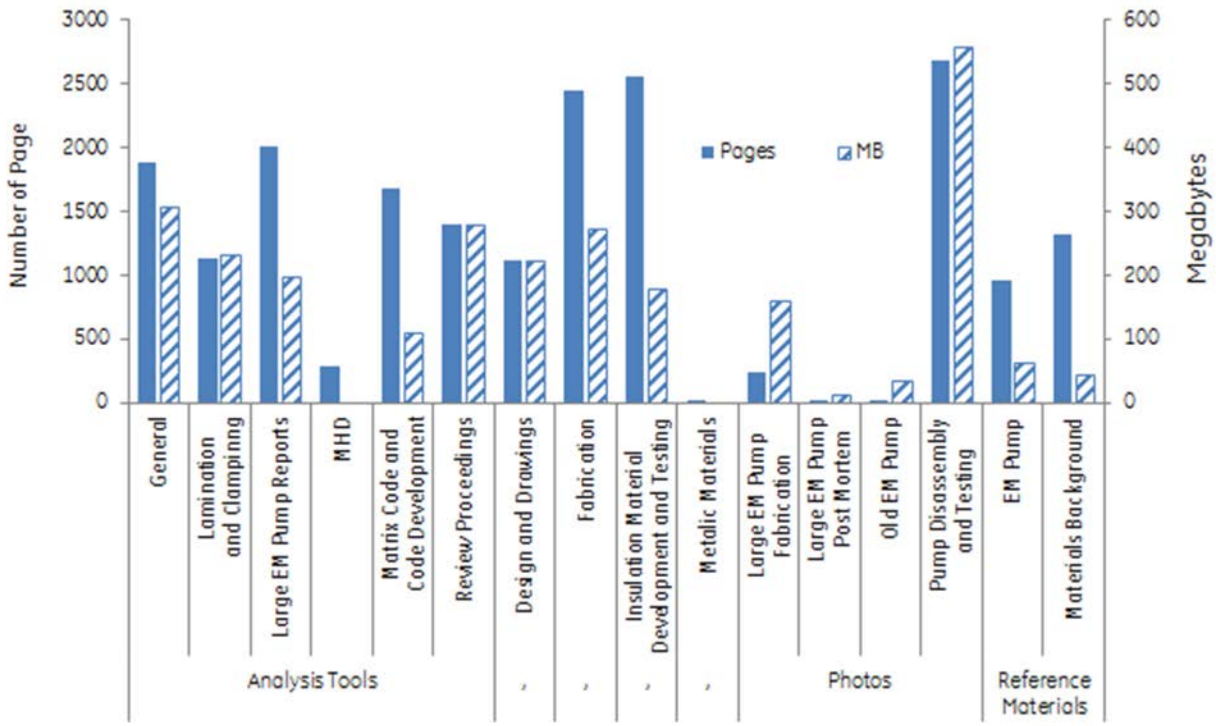

Figure 2-3: EM Pump File Size and Number

2.1 EM Pump Analysis Model Databank

The legacy MATRIX software was extracted and the major subroutines were identified. Investigation of the full capabilities of MATRIX occurred from thorough review of the analysis model databank.

In the large EM Pump project, three main analysis tools were used: MATRIX, GE2D, and AGENA. MATRIX was the pump performance code, GE2D was the magnetic analysis code, and AGENA was a general purpose, advanced network analysis tool used for the thermal analysis of EM Pumps. It was planned that the main portions of these three codes would be combined into a comprehensive, modern EM Pump analysis tool. Further investigation identified the GE2D magnetic analysis was already incorporated into MATRIX code in the EM Pump Magnetohydrodynamics (MHD) Stability Update 1997, leaving only the thermal analysis to be developed and implemented in the improved MATRIX code, discussed in Section 5.0, Develop the Next Generation EM Pump Analysis Tools.

2.2 EM Pump Insulation Databank

A review of the prior EM Pump post-mortem analysis and electrical testing was performed. The results of this effort were used to guide the team in selecting candidate insulation materials for initial screening. The initial screening results were used in discussions with the current day mica tape suppliers to identify existing candidate fiber-backed mica tape systems for subsequent insulation tests. Custom-built insulation tapes could also be pursued using the initial screening criteria. A history of Argonne National Labs (ANL) and GEH insulation development under PRISM was collected, described and discussed. The parts of the databank that best served the insulation work in this project were: lamination and clamping, design and drawings, insulation material development and testing, pump disassembly and testing, and materials background per Figure 2-3.

2.3 Analysis and Performance Models Electronic Databank Usage

The EM Pump analysis model and the EM Pump performance model databanks were updated and utilized to support developments for both the Next-Generation EM Pump Design and Analysis Tools and Insulation Materials Development and Testing.

As the AGENA code was evaluated, additional thermal analysis references were added to the databank as support documentation to the MATRIX code. The updated code and a new MATRIX user manual (PLM DOC-0003-7657) were also added to the databank. The Industry Codes and Standards are identified in the EM Pump Modifications for 3 Pump Operation (PLM DOC-0004-7828).

This new MATRIX user's manual will allow the continued use of the code for further EM Pump design work in the future. Recorded results of thermal analyses of the large EM Pump design performed in the past were used as reference during the development of the thermal analysis model implemented in MATRIX.

3.0 Modernize Legacy EM Pump Analysis Code MATRIX

The 1999 version of the MATRIX Code was updated during the 2014-2015 project, which collectively is referred to as the 2015 MATRIX code. The 1999 MATRIX code was run on a computer platform that was no longer supported. Modernization was needed to ensure continued commercial use in the future.

In the modernization efforts, the MATRIX code was restructured into the GE Data Transfer Array (DTA) format, which is based on common data memory blocks. This vastly improved the data transfer and running efficiency of the code without using a fixed-sized data structure. The new code structure eased the maintenance and the ability for future modification of MATRIX. Validation of the MATRIX code version upgrade is described in Section 3.2.

The improvements made to the code during this upgrade, including the code to adjust the number of meshes per slot pitch and a description of the post-processing tool capabilities, are described in Section 3.3.

3.1 MATRIX CODE BACKGROUND

The MATRIX analysis code is a tool used to analyze the overall electrical, magnetic, and fluid performance of EM Pumps. The code uses the well-established "MATRIX method" (Elliott, 1975; Kliman, *et al*., 1974). The original 1975 objective of the MATRIX method was analysis of liquid-metal MHD generators with end-effect compensation windings, insulating vanes to reduce the effective conductivity of the fluid at the ends, and variation of fluid velocity along the channel. The advantages of the MATRIX method are 1) more accurate modeling of the magnetic field, accounting for finite iron length, slot effects, air-path fields, and gap variation; and 2) the ability to handle arbitrary winding distributions, conducting walls, and variations of secondary velocity, thickness, and conductivity. The MATRIX method also permits determination of the primary-current distribution for maximum efficiency. Other analysis methods have shorter computing times than the MATRIX method but can be expected to be less accurate due to their simpler model of the finite-length iron; but none of the other methods have all of the capabilities of the MATRIX method (Elliott, 1975).

In general, the MATRIX method provides more accurate results than other methods for machines with unusual windings; unbalanced excitation; velocity, conductivity or gap variations; short length; few slots; wide slots; or large gaps (Elliott, 1975).

MATRIX Analysis Method performs the basic linear induction machine analysis to find the secondary currents given the primary currents:

1. MATRIX calculates the field and flux coefficients (B1, B2, Φ1, Φ2).
2. The field and flux coefficients are combined to form the influence coefficient matrices (Z1 and Z2).
3. The mesh resistances (R2) from the secondary dimensions, with skin-effect correction, are determined.
4. The influence coefficients and resistances are combined to form the left-side coefficient MATRIX.
5. The primary currents are multiplied by Z1 to obtain the right-side voltage vector (V1).
6. The secondary current equation is solved using Gaussian elimination to find the secondary currents (I2).

The MATRIX Code went through several updates since the 1975 creation. During the large EM Pump test program, a 160 m3/min (42,000 gpm) at 0.25 MPa (37psig) linear induction pump was designed, built, and tested as part of a major program to develop an advanced sodium-cooled nuclear reactor. The pump is essentially a large linear induction motor with a liquid secondary. It was designed to operate immersed in liquid sodium and cooled by it, hence winding temperatures exceeding 450° C were expected. The pump was built and tested under prototypic pressure, flow, and temperature conditions with outstanding success. It was observed however, during the testing that the MATRIX code used to predict pressure rise and efficiency results needed to be degraded by 30% in order to match the measured pump values.

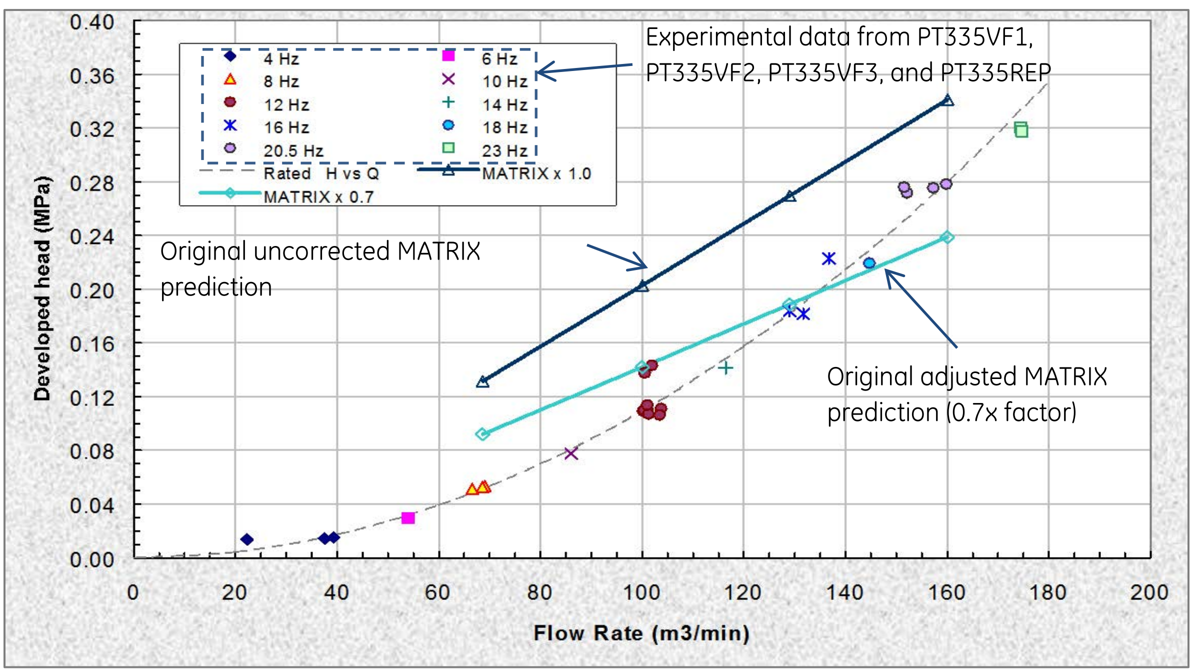

Figure 3-1: Head versus Flow Rate (Experimental Data versus 1999 MATRIX Code)

The experimental EM Pump data from 2001 testing, the 1999 MATRIX code results, and the 0.7 adjusted MATRIX results are shown in Figure 3-1, extracted directly from the reference material (Fanning, *et al.*, 2003) annotated with updated labels added for clarity. The 0.7 multiplier provided a better fit than the uncorrected MATRIX results, but it does not provide a perfect fit to the experimental data, and the 0.7 multiplier is not a fully accurate predictor.

3.2 MATRIX PROGRAM CODE UPDATE

3.2.1 EM Pump Induction Theory Used in MATRIX

The MATRIX analysis code solves Maxwell's equations in a series of mesh calculations using the "MATRIX method" for the analysis of linear induction machines (Elliott, 1975; Kliman, 1974). Linear induction machines utilize the rotating magnetic fields created by the AC current passing through their stator coils to generate a force or torque. In an induction motor, this force turns a rotor, and in the case of a pump this force pushes a conductive fluid. In an EM Pump, the rotating magnetic field of the stator induces a current in the fluid, and the resultant axial force on the fluid induces a directional flow. The main objective of the linear induction machine analysis is, given the primary currents, to find the secondary currents within the system. After MATRIX solves for these currents, the performance of the machine can be found using basic electromagnetic principles. A basic depiction of how an annular linear induction pump (ALIP) operates is shown in Figure 3-2. The inner and outer stator coils (1) are first energized with a power supply to create a circulating current within the pump. The coils are energized using three-phase alternating current (AC) ranging from 600 to 1,000A at a voltage ranging from 500 to 1,700 V (line-to-line). This circulating AC current induces a magnetic field, ranging from 0.5 T to 0.65 T, within the inner and outer stator iron cores (2). The changing magnetic field, with a magnitude of around 0.1 T, inside the flow annulus (3) further induces a current in the pump fluid. The resultant axial force on the fluid induces a directional flow.

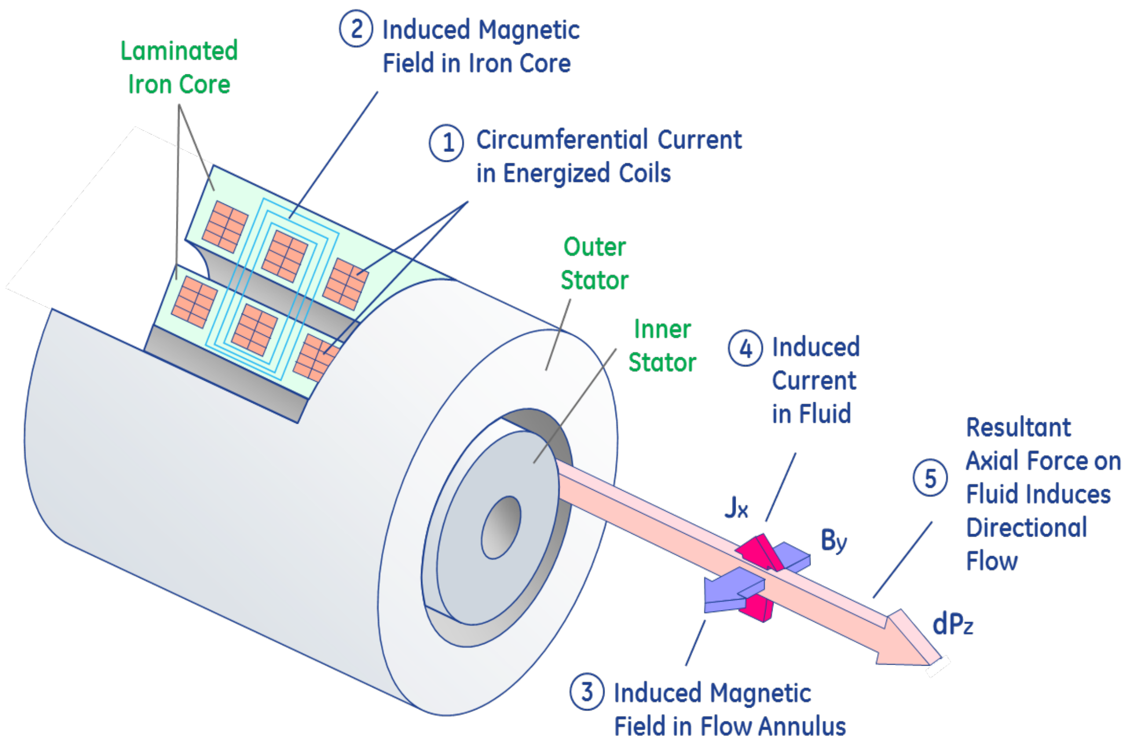

Figure 3-2: Double Stator Annular Linear Induction Pump (ALIP) Operation

This axial force is derived from a phenomenon known as the Lorentz force, which is defined as:

$$dP_z = J_x \times B_y \qquad (3.1)$$

where Jx is the current density in the sodium, By is the magnetic field in the pump flow annulus, and dPz is the incremental pressure rise in the axial direction of the pump (Sadiku, 2009). During the modernization of MATRIX, the main electromagnetic MATRIX computing structure was not altered; however, several functional structures were combined to help the code run more efficiently. Three main FORTRAN input files were combined into one simplified, main routine, and the code was restructured into the GE Data Transfer Array (DTA) format. Additional pre- and post-processing tools were added to improve processing and data evaluation.

For the 1999 code, the input files, along with the MATRIX FORTRAN source code, were compiled into an executable file that was re-compiled every time the case inputs were changed. Figure 3-3 shows the process flow for running one input case through MATRIX using this batch file method.

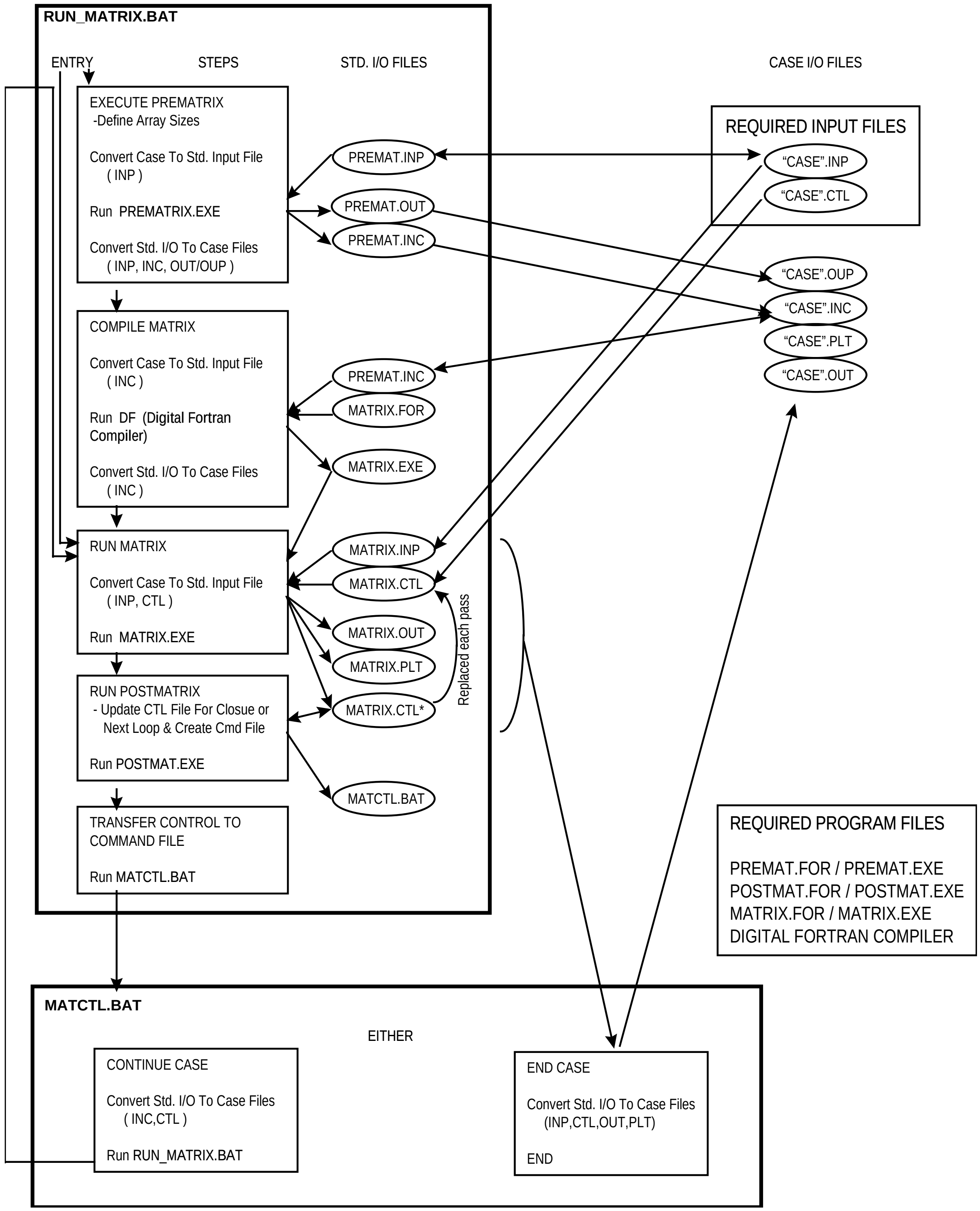

Figure 3-3: Batch File Process Flow for MATRIX (circa 1999)

The process flow for the 1999 batch file mode running of MATRIX had a series of steps: 1) Execute PREMATRIX.EXE with input files, 2) Compile MATRIX.FOR into MATRIX.EXE, 3) Run MATRIX.EXE, 4) Run POSTMAT.EXE, 5) Transfer command to MATCTRL.BAT (which will either loop back to Step 3 or end the case and create the final output files), and finally 6) Use manual post-processing to create data plots.

3.2.2 2015 MATRIX Code Modernization

To streamline the batch running process from the 1999 MATRIX code, the 2015 MATRIX code was restructured into the GE Data Transfer Array (DTA) format. The DTA structure, which is based on common data memory blocks, vastly improved the data transfer and running efficiency of the code, without using a fixed sized data structure. In addition, the reorganization eases the maintenance and the ability for future modification of MATRIX. The original code, which was split into three main FORTRAN files, PREMAT.FOR, MATRIX.FOR, and POSTMAT.FOR, was consolidated into one, main routine controlled by MAIN.FOR. The modernized MATRIX block flow is illustrated in Figure 3-4.

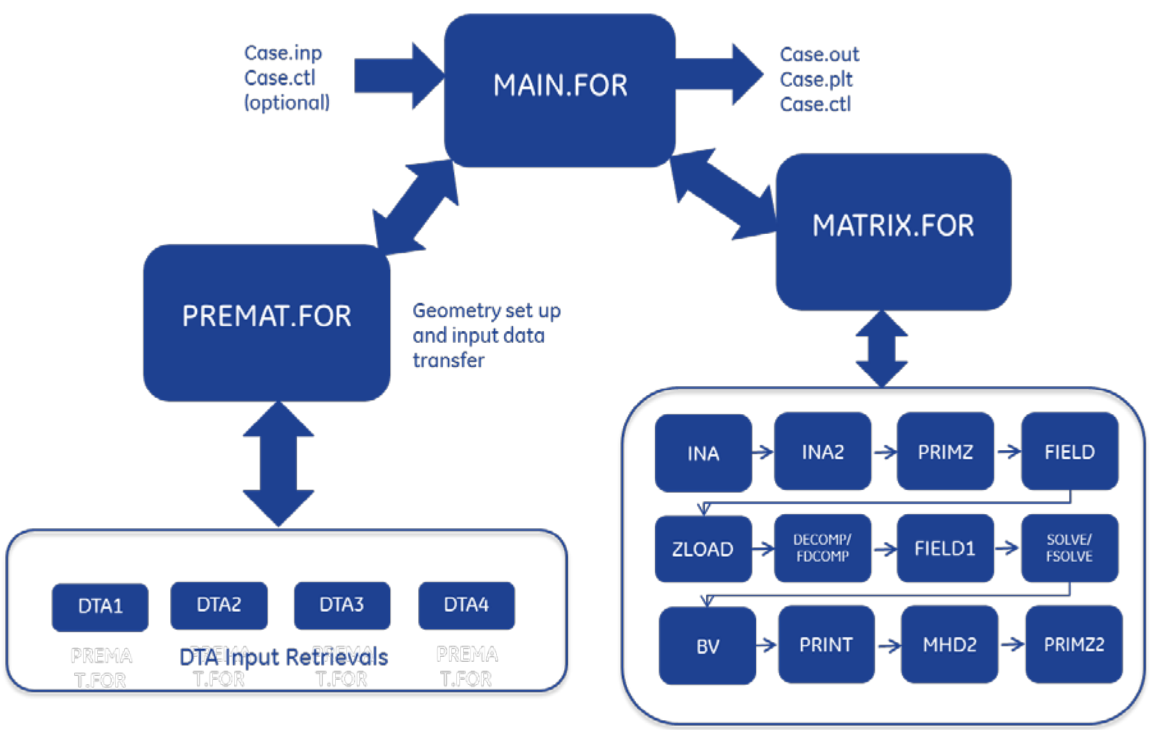

Figure 3-4: 2015 MATRIX Code Computation and Data Flow (circa 2015)

The elimination of the three, separate FORTRAN source files which had to be compiled separately for each file and each MATRIX run streamlined code performance. Figure 3-5 illustrates the modernized process flow for running a single test case through MATRIX. The process now only uses one, generic compiled FORTRAN file.

A pre-preprocessing executable was created to work in conjunction with a multiple case post-processing tool, which takes output text files from multiple MATRIX test cases and automatically creates output and plot files corresponding to the data.

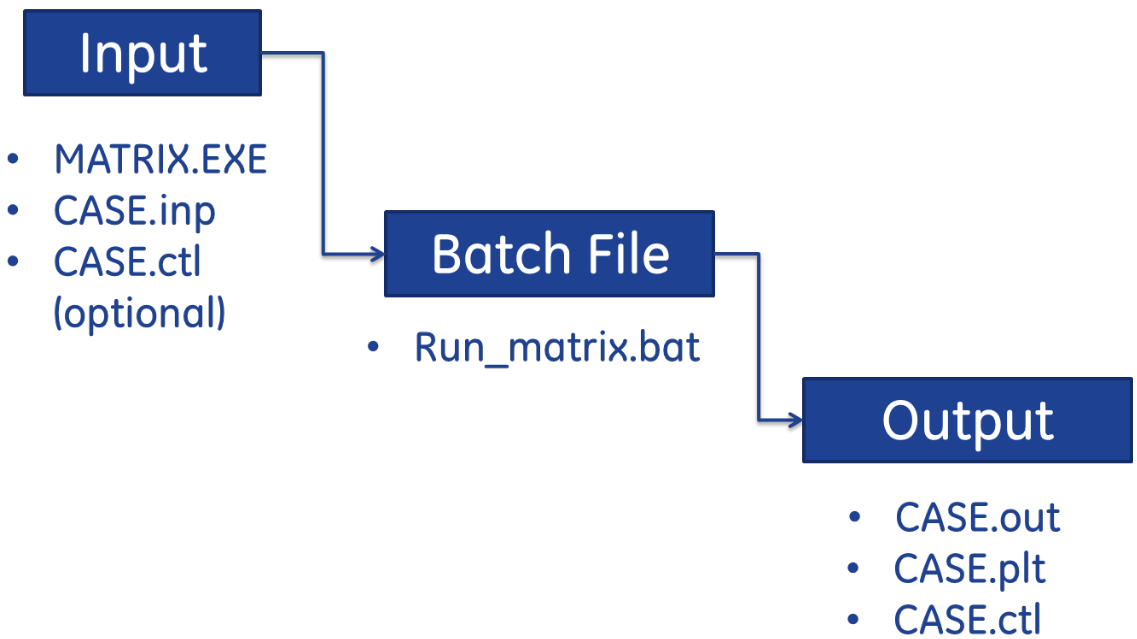

Figure 3-5: Modernized DTA MATRIX Basic Process Flow

3.2.3 2015 MATRIX Code Validation

Legacy test conditions provided eight test cases to validate the code upgrade and compare the 2015 MATRIX code and the 1999 MATRIX code results. The current and frequencies used for these test cases are shown in Table 3-1.

Table 3-1 Test Cases Used for MATRIX Upgrade Comparisons

Amps	Frequency (Hz)			
	4	12	19	30
884	X	X	X	X
1,060	X	X	X	X

For each test case, the operating slip condition was varied, since altering the slip effectively changes the fluid flow being used for the code input. Slip is defined in Equation 3.2.

$$Slip = \frac{Synchronous\ Speed - Fluid\ Speed}{Synchronous\ Speed} \quad (3.2)$$

In Equation 3.2, the synchronous speed is the speed of the magnetic field (or current frequency) and the fluid speed is the average speed of the sodium moving through the pump. When the pump is energized from a stopped condition and the fluid is not in yet in motion (fluid speed is zero), there is maximum slip between the field and fluid and a maximum induced current into the fluid. This induced current causes the fluid to speed up, to some maximum point. If the fluid speed reaches the field or synchronous speed, the fluid will be moving as fast as the field, and slip would be zero. However, since there is no relative motion between the fluid and the field, there would be no current generated in the field and the fluid would slow down. As the fluid slows down and the slip increases from zero, the current in the fluid increases, which then increases the driving force in the fluid up to some maximum. If the fluid is slowed by external forces (shutting a valve in the system), the field moves faster than the fluid, and the induced voltages in the fluid cannot keep up with the field.

Figure 3-6 through Figure 3-8 shows various characteristic plots versus slip for one test case (19 Hz and 884 amps). The other test cases have similar plots. Fluid motion is stopped at slip values of one on the right side of the plots and fluid motion is synchronous to the field at slip values of zero on the left side of the plots.

Figure 3-6 depicts the power factor and the net efficiency of the pump versus slip for one of the test cases (19 Hz and 884 amps). The net efficiency is at a maximum at 0.2 slip and is above 35% with slip values between 0.1 and 0.3.

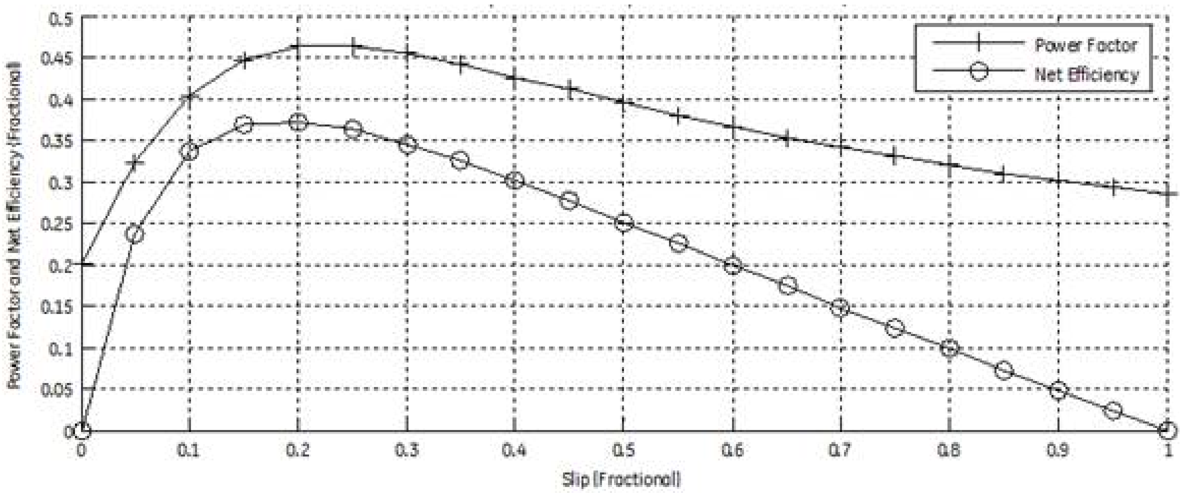

Figure 3-6: Power Factor and Net Efficiency at 884 Amps at 19 Hz

Figure 3-7 depicts the active (real), reactive (imaginary), and apparent (real and imaginary) powers versus slip. The line voltage is what is provided to the pump coils. The reactive and apparent powers within the pump are calculated by MATRIX. The active power is above 500 line volts when slip values are between 0.1 and 0.2.

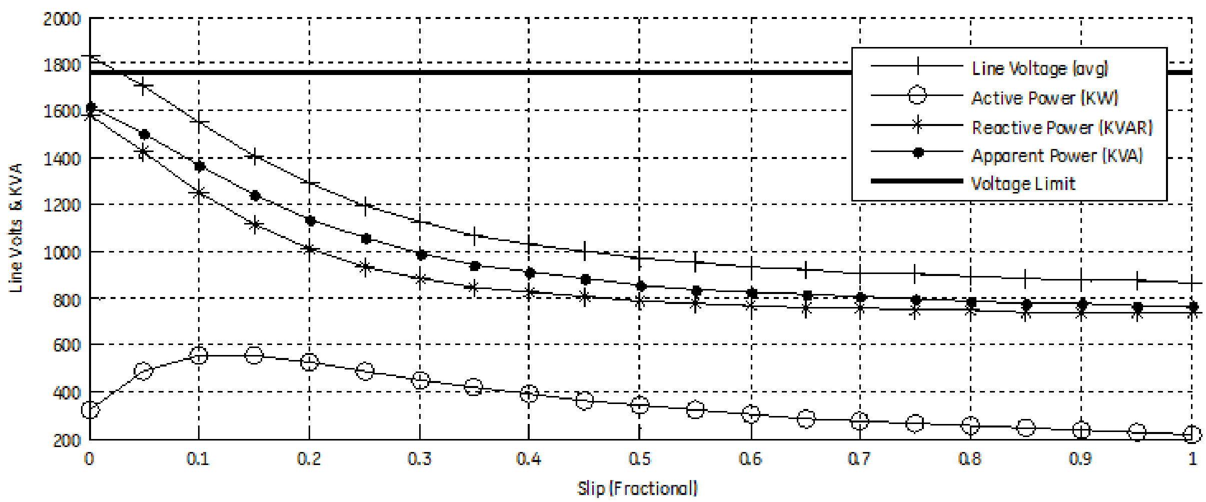

Figure 3-7: Line Volts and KVA at 884 Amps at 19 Hz

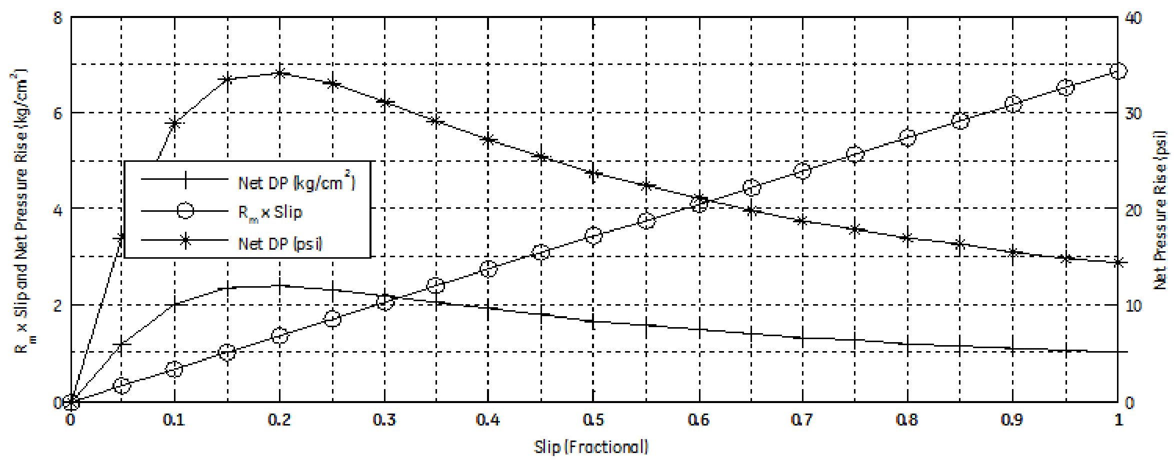

Figure 3-8: Net Pressure Rise at 884 Amps at 19 Hz

Figure 3-8 depicts the MATRIX-developed head (multiplied by 0.7 in psi and kg/cm2) as well as the Rm x Slip curve. The net differential pressure is provided in a doubly Y plot in two different units. This shows a maximum pressure rise of about 34 psi at a slip of 0.2. The R_m x Slip increases from 0 to 7 as slip increases from 0 to 1. The product of the magnetic Reynolds number (R_m) and the slip provide regions of potential stability limitations for the pump. Areas where the R_m x Slip is less than 1 the pump will operate without stability issues; areas where the R_m x Slip is between 1 and 2 have potential for operating without stability issues; areas where the R_m x Slip is between 2 and 3 may have some instabilities; and areas where the R_m x Slip is greater than 3 will have even more instabilities.

For this test case (884 amps at 19 Hz):

- When the slip is less than 0.15, the pump operation is stable.
- When the slip is between 0.15 and 0.3, the pump has the potential for operating without stability issues.
- When the slip is between 0.3 and 0.45, the pump may have some flow instabilities.
- When the slip is greater than 0.45, the pump operation is unstable.

The other seven test cases generated plots similar to Figure 3-6, Figure 3-7, and Figure 3-8 from the updated MATRIX code. The outputs from the 2015 MATRIX code test cases were plotted and visually compared to the 1999 MATRIX code outputs. The results from these test cases were combined into a pressure map. The results for eight test cases from the 1999 MATRIX large EM Pump testing with the 0.7 multiplier applied is shown in Figure 3-9 (Fanning, et al., 2003), and the pressure map developed from updated 2015 MATRIX code with the 0.7 multiplier applied is shown in Figure 3-10.

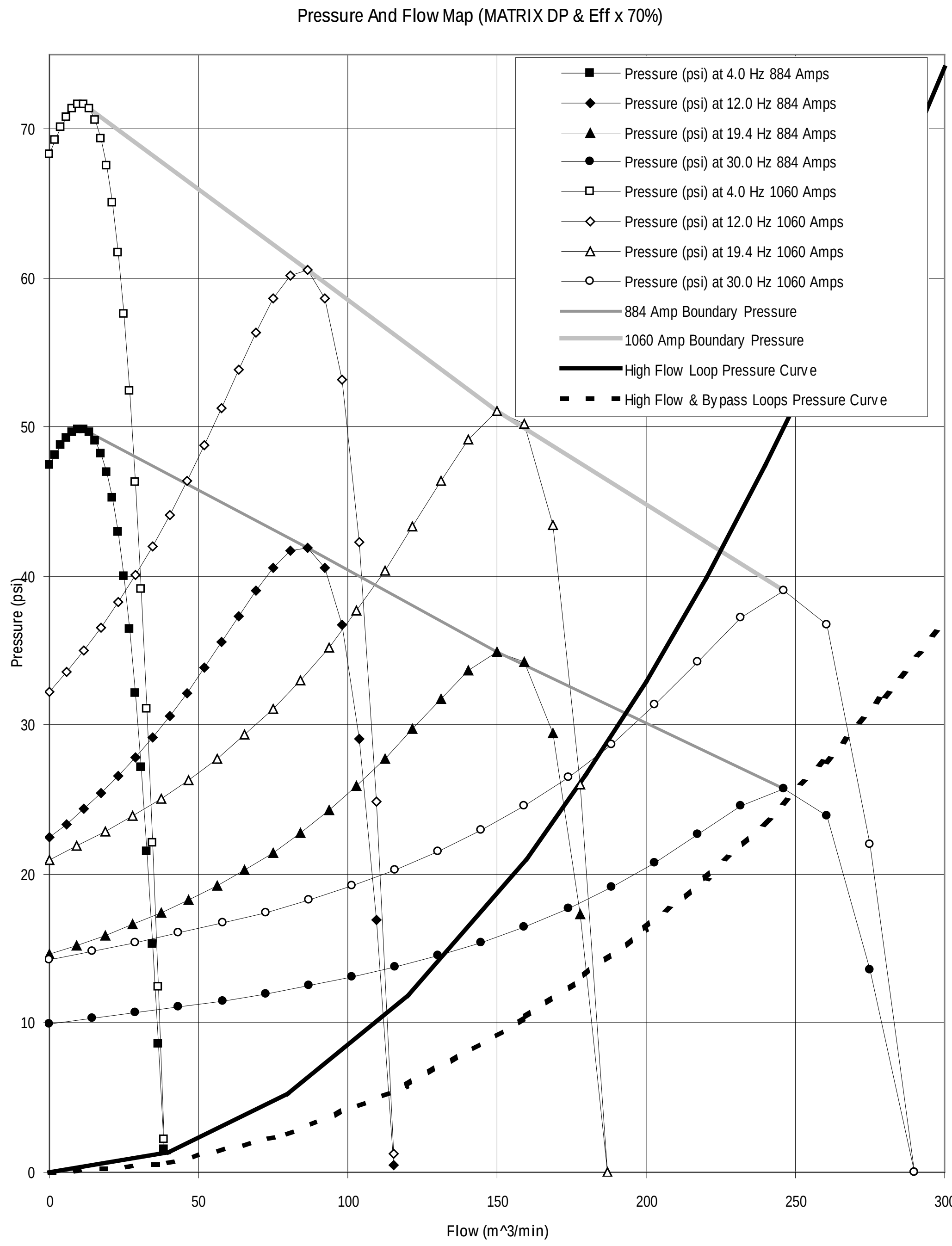

Figure 3-9: 1999 MATRIX Pressure Map (with 0.7 Multiplier)

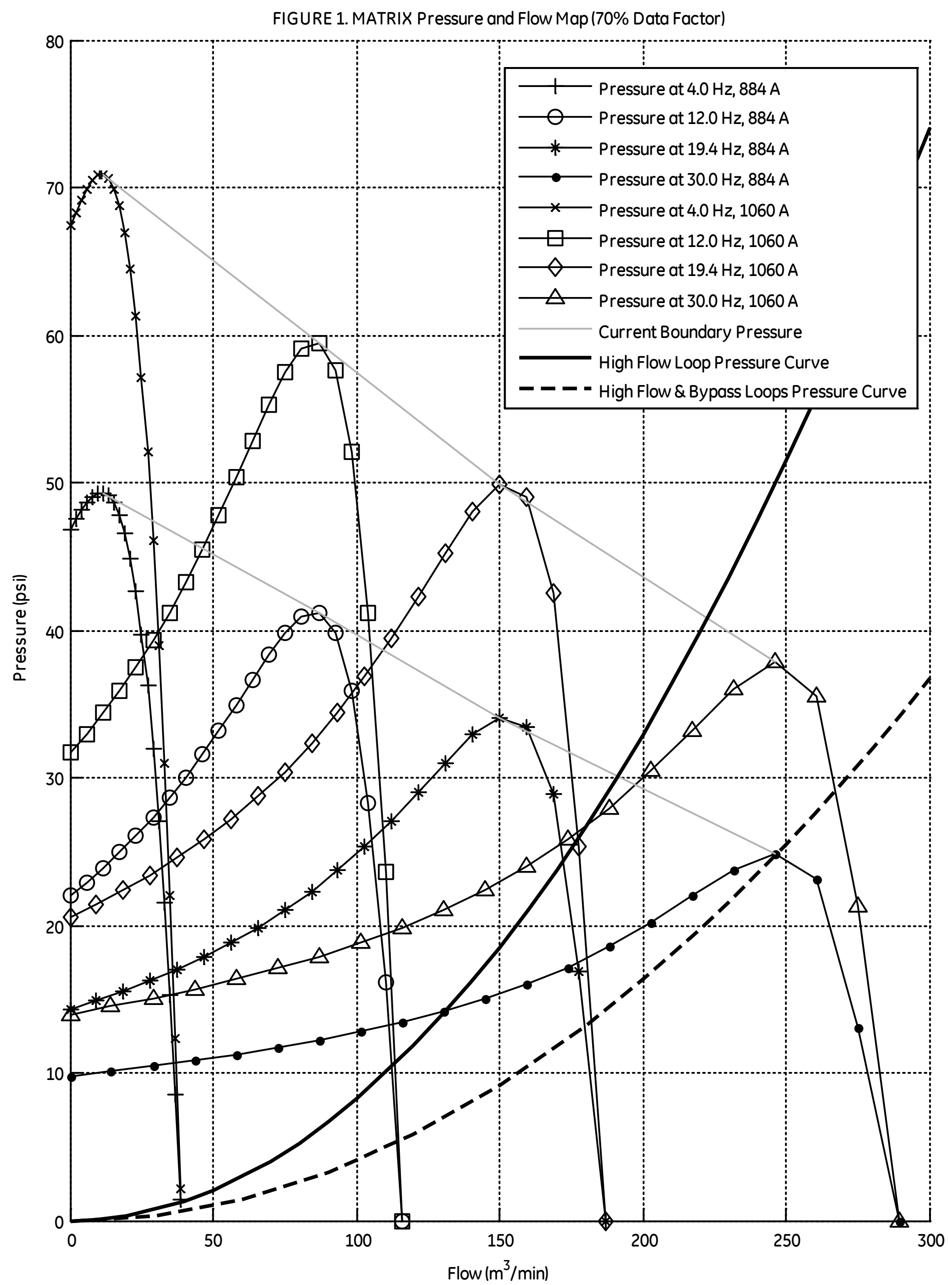

Figure 3-10: 2015 MATRIX Pressure Map (with 0.7 Multiplier)

Figure 3-9 and Figure 3-10 show the pressure developed (with the 0.7 multiplier for comparison purposes) versus the pump flow results from the 1999 and 2015 MATRIX codes, respectively. In general, the developed pressures from the modernized code were 0-0.007 MPa less than those from the legacy code.

The individual output values from the 1999 and 2015 MATRIX codes were compared, with the ratio or normalized 2015 / 1999 MATRIX data plotted for all flow rates, (Figure 3-11).

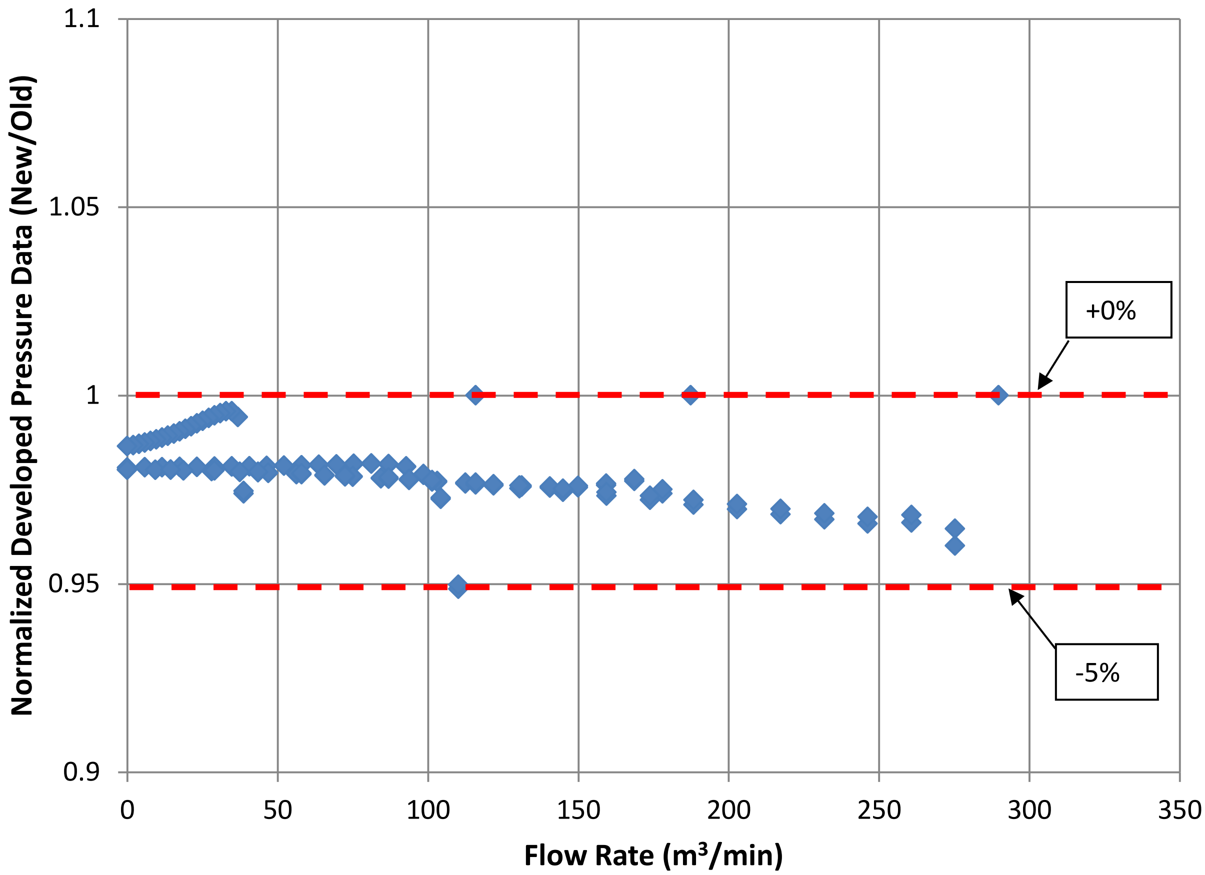

Figure 3-11: Normalized 2015 / 1999 MATRIX Data

All of the normalized data fell within the 0 to -5% (shown as dashed lines) confirming constant results after the code modernization. A majority of the normalized data is centered on 0.97. This trend supports the visual differences that were seen between Figure 3-9 and Figure 3-10 and also indicates that the update to MATRIX slightly reduced the discrepancy between the simulated and measured pump data. Additional output plots from both the 1999 and 2015 code were compared. For example, the power factor, net efficiency, line volts, KVA, and net pressure versus slip plots between the two versions of the code, depicted in Figure 3-6 through Figure 3-8 showed similar effects. This supports that the modernized MATRIX code is operating as expected.

The small discrepancies between 1999 and 2015 MATRIX results, with no normalized values equal to one, are due to using different compilation software with different mathematical operations. The modernized code utilized an Intel compiler instead of a Digital FORTRAN compiler. The relevant Visual Studio Compiler Settings that were used during the modernization of the MATRIX can be seen in Table 3-2.

Differences in the varying slips that were used to create Figure 3-9 and Figure 3-10 also have an impact on the results. The legacy results used varying slips of 0.00021, 0.050021, 0.10021, etc., and the new results used varying slips of 0, 0.05, 0.1, etc. The legacy slip values where calculated using an unknown pre-processing algorithm. These differences show that the flow rates are slightly different when running the new MATRIX code.

Table 3-2: MATRIX Code Compiler Options and Settings

Compiler Menu	Compiler Option	Compiler Setting
Diagnostics	Generate Interface Blocking	Yes (/gen-interfaces)
Diagnostics	Check Routine Interfaces	Yes(/warn;interfaces)
Data	Local Variable Storage	All Variables SAVE (/QSAVE)
Data	Initialize Local Saved Scalars to Zero	Yes (/QZero)
Libraries	Runtime Library	Debug Multithreaded (libs;static/threads/dbglibs)

3.2.4 Modernization and Verification Summary

The 2015 MATRIX code was verified using a series of input-output tests to ensure that the legacy MATRIX results and the new MATRIX results matched. A pressure and flow map for the prototypic 160 m^3/min EM Pump was developed using the updated MATRIX code. This was compared to the 1999 MATRIX performance mapping curves. The pressure and flow map (Figure 3-10) and the individual test case performance plots

(Figure 3-6, Figure 3-7, and Figure 3-8) showed equivalent comparison results.

The updated code showed a slight improvement in predicting EM Pump performance, but the 0.7 multiplier was still needed to match actual measured data. Eliminating the 0.7 multiplier became the goal to improve the code.

3.3 MATRIX Improvements Made During the Code Upgrade

During the modernization from 1999 MATRIX Code to the 2015 MATRIX Code, several improvements were added to improve the flexibility of the code and improve the processing of the MATRIX data beyond improving the inputs and modernizing the code to run on a supported platform.

These improvements include an expanded range of the code variable for the number of meshes per slot pitch and adding a post processing tool to simplify data evaluation.

3.3.1 Number of Meshes per Slot Pitch Code Upgrade

The number of meshes per slot pitch (NMS) variable is an independent determination on how the overall MATRIX code simulation is modeled.

The NMS variable has been in the code since its origin in 1975; however, the computers from the past (including 1999 update) could not effectively use NMS values greater than 10 due to slow processor speeds. The modernization expanded this value to 35.

An analysis to evaluate the effect on the MATRIX calculation when adding more meshes has on the output and code runtime was performed. An increased number of meshes requires longer calculation times but achieves refined results. Nominal NMS values ranging from 1-35 were used to evaluate the convergence of the MATRIX developed pressure results. The upper NMS value of 35 represents the concentrated approach to output convergence.

Table 3-3 shows the various developed pressures when changing the NMS value, with the 1999 MATRIX code NMS value of 10, highlighted.

Table 3-3: Varying Developed Pressures from Different NMS Values

NMS Number	Electrical Developed Pressure (MPa)	Frictional Pressure Loss (MPa)	Total Developed Pressure (MPa)	% CHANGE
1	-	-	-	-
2	0.38	0.02	0.36	10.92%
3	0.37	0.02	0.35	7.33%
4	0.36	0.02	0.34	5.43%
5	0.36	0.02	0.34	4.25%
6	0.35	0.02	0.33	3.44%
7	0.35	0.02	0.33	2.86%
8	0.35	0.02	0.33	2.43%
9	0.35	0.02	0.33	2.08%
10	0.35	0.02	0.33	1.80%
11	0.35	0.02	0.33	1.58%
12	0.35	0.02	0.33	1.39%
13	0.35	0.02	0.33	1.23%
14	0.35	0.02	0.33	1.09%
15	0.35	0.02	0.33	0.97%
16	0.35	0.02	0.32	0.87%
17	0.35	0.02	0.32	0.77%
18	0.35	0.02	0.32	0.69%
19	0.35	0.02	0.32	0.61%
20	0.34	0.02	0.32	0.55%
25	0.34	0.02	0.32	0.29%
35	0.34	0.02	0.32	-

Figure 3-12 shows a visual representation of the results seen in Table 3-1, with the original NMS value highlighted by an "X". It was observed that this original NMS value produced a net developed pressure that was 1.8% off from the pressure developed using the maximum NMS value of 35. This slight difference shows that the number of meshes per slot used in the MATRIX calculation is important for accuracy.

If not enough meshes are utilized, the output values could be as much as 10.9% off (higher), which was the case when using an NMS value of only 2. An NMS value of 25 was chosen for both accuracy and time constraint purposes (about 20 minutes for one MATRIX run) when determining the flow correction values in Section 5.1.

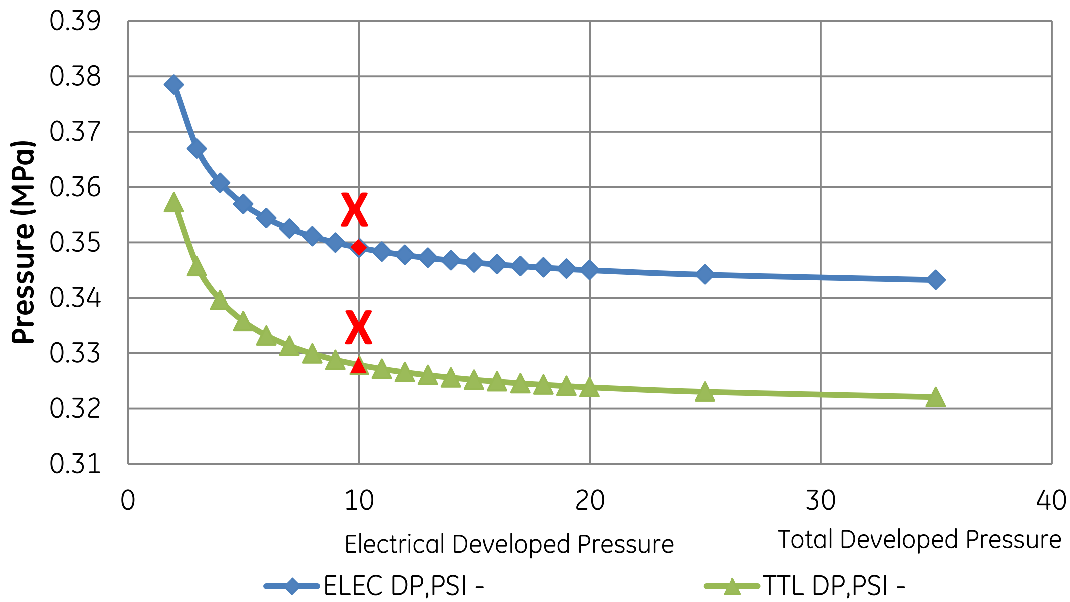

Figure 3-12: Pressure Developed Versus NMS Number

The NMS number used in original MATRIX code was 10 as highlighted in Table 3-3 and shown as an "X" in Figure 3-12. The effect of varying the NMS number on MATRIX thrust and attraction calculations are discussed in Section 4.1.

3.3.2 Post Processing Tools

In addition to streamlining the MATRIX batch file process, several post-processing tools were developed for improved analytical capabilities of the code. For the post-processing of the MATRIX output variables for an individual input case, an executable file takes output text files from MATRIX and automatically creates output plot files corresponding to the data.

The post processing tool is a MATLAB executable that takes the output text files (.out) and automatically creates output plot files. These output plot files are saved in a working directory in an MS WORD format. MS Excel Spreadsheet files can also be generated.

Table 3-4: Single Case MATRIX Run

Plots	Description
1	EM Pump Position vs. Mesh Number
2	EM Pump Slot Number vs. Mesh Number
3	Fluid Current and Phase Angle vs. Mesh Number
4	Annulus Magnetic Field vs. Mesh Number
5	Force vs. Mesh Number
6	Ohmic Power vs. Mesh Number
7	Slot Current and Phase Angle vs. Slot Number
8	Slot Voltage and Phase Angle vs. Slot Number
9	Wall Current and Phase Angle vs. Mesh Number
10	Pressure vs. Mesh Number
11	Tooth Root Magnetic Field vs. Slot Number
12	Stator Core-Iron Magnetic Field vs. Slot Number

Two examples of the post processing tool are plots 5 and 12. Plot 12 is discussed below with Figure 3-13. Example Plot 5 from the post-processing tool is discussed in Section 4.1.

The 2015 MATRIX post-processing tool can run multiple cases for comparison. The number of plots identified in Table 3-4 automatically adjusts in the post-processing software, with the multiple case plots labeled as identified in Table3-5.

Table 3-5 Multiple Case MATRIX Run Post-Processing Tool

Plots	Description
1	MATRIX EM Pump Performance Map Plots
2	EM Pump Performance Map for Case XX
XX+1	Rm x Slip Operating Ranges

These plots give the overall operating characteristics of a specified EM Pump design. Having them helps the designer see the exact operability of the pump under design.

3.3.3 MATRIX Post Processing Plot 12 Example

Figure 3-13 shows plot 12, the magnetic field versus slot number, from Table 3-4. The transient or end effects, seen at the beginning (slots 0-15) and end (slots 80-85) of the plot, illustrate the build-up and decay of fields and forces at the entrance and exit of the pump. The saw-tooth phenomenon results from the alternating slot current angles provided in the MATRIX simulation.

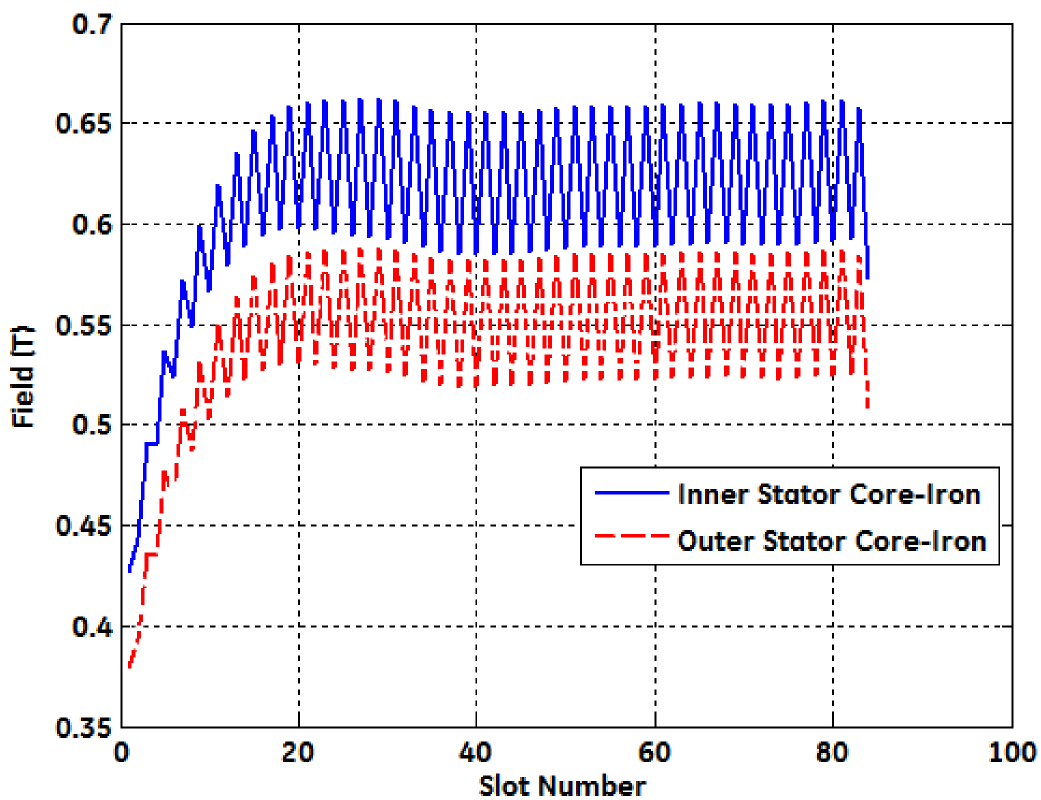

Figure 3-13: Example Field Plot Created by MATRIX Post-Processing Tools

The inner stator field average is higher than that of the outer stator field due to the increased area of the outer stator back iron. The magnetic flux density B is directly related to the magnetic flux per area, is defined in equation 3.3:

$$B = \frac{\Phi}{A} \quad (3.3)$$

3.3.4 NMS and Post Processing Tool Upgrade Summary

The NMS upgrade expanded the range of the number of meshes per slot variable that was limited to 10 in the 1999 Code due to processor speed to a maximum value of 35. The MATRIX output for developed pressures was analyzed when changing the NMS value. A reduction in variability of the predicted output from 1.80% to 0.29% was achieved when the NMS variable was changed from 10 to 25. The tradeoff between increasing the NMS number is between prediction accuracy and MATRIX model run time, with a value of 25 used for determining the flow correction values.

The post-processing tool works in conjunction with pre-preprocessing executable to improve the flexibility of the MATRIX Tool and the comparisons, which can be made of EM Pump independent and dependent variables. This post-processing tool reduces the external analysis of data from a MATRIX run and more effectively presents the pertinent data for evaluation.

This page intentionally left blank

4.0 Analysis and Modeling to Support Upgrades to the MATRIX Code for Modeling EM Pump Performance

The two electromagnetic forces on the EM Pump coils are the axial force and radial force used to model EM Pump performance and electromagnetic coil motion.

The axial force is along the axis of the EM Pump (typically upward) and the radial force is along the radius of the pump and is perpendicular to the axial force.

The MATRIX Model thrust and attraction calculations were compared to analysis done independently by GRC and ANL.

4.1 MATRIX Determinations

MATRIX does not use the terms axial and radial force but instead uses the terms Thrust and Normal Force. Normal Force may also be termed “Attraction”. Verifying the MATRIX terms equate to axial and radial forces is part of the validation process.

The MATRIX code modernization and update, performed as part of Tasks 3 and 4 of this project, calculated the thrust and attraction forces.

4.1.1 MATRIX Definitions

In the 1975 MATRIX documentation (Elliott), the axial force was called thrust and associated with mechanical power, and the radial force was called the Normal Force or Attraction.

There are no clear cut definitions within the early MATRIX documentation, but the definitions can be the drawn from text or tables in several different locations, summarized as follows:

- Thrust is the instantaneous force in the positive direction, and the overall thrust has an oscillating component. The instantaneous thrust, the total average thrust, and the frequency and magnitude of the oscillation was derived therein. The mechanical power is the product of thrust and velocity.
- Normal force is perpendicular to thrust, and the normal force is an attraction force between the iron blocks and a repulsion force between the secondary and the iron blocks. This is a net Y-directed force on each primary of a double-sided machine, or on the single primary of a single-sided machine (See Figure 4-1 for the Y-direction). The Y-direction is the radial direction for the EM Pump.

The MATRIX Groups 3 and 5 tables further define terms with a note that the Group 5 values [outputs] are the most accurate (Elliott, 1975), as follows:

- Thrust (N): The average over one cycle of the normal force <u>per mesh</u> on the secondary in the positive X-direction, in Newtons (Groups 3 and

5) (See Figure 4-1 for the X-direction); [The X-direction is the axial direction in the EM Pump.]

- Normal Force (N) average over one cycle of the normal force per mesh between the two primaries in a double-sided machine or between the primary and secondary-plus-iron in a single sided machine, in Newtons (Group 3)
- IRON ATTR (N) is the part of the normal forces (always positive) due to the field between the iron blocks, in Newtons (Group 5)
- CURR ATTR (N) is the part of the normal force (always negative due to the repulsion effects of the currents in the secondary and the walls, in Newtons (Group 5)
- ATTR (N): The average value over one cycle of the total normal force between the primaries of a double-sided machine or between the primary and secondary-plus-iron of a single sided machine, in Newtons (Group 5)
- Center of Attraction, is the X coordinate (meters) at which the normal force is centered (Group 5)

The 1975 MATRIX manual, the Thrust Force, and Mechanical Power equations are listed with 7 code terms, and the Normal Force equations are listed with 10 code terms, defined therein. The parenthetical statement, “Attraction is Positive”, is included in the header for this Normal Force (Elliott, 1975).

The attraction force on the primaries due to instantaneous field Bk(t) and the derivation of both components of the normal force is provided in that document (Elliott, 1975), supporting the information shown in Figure 4-1.

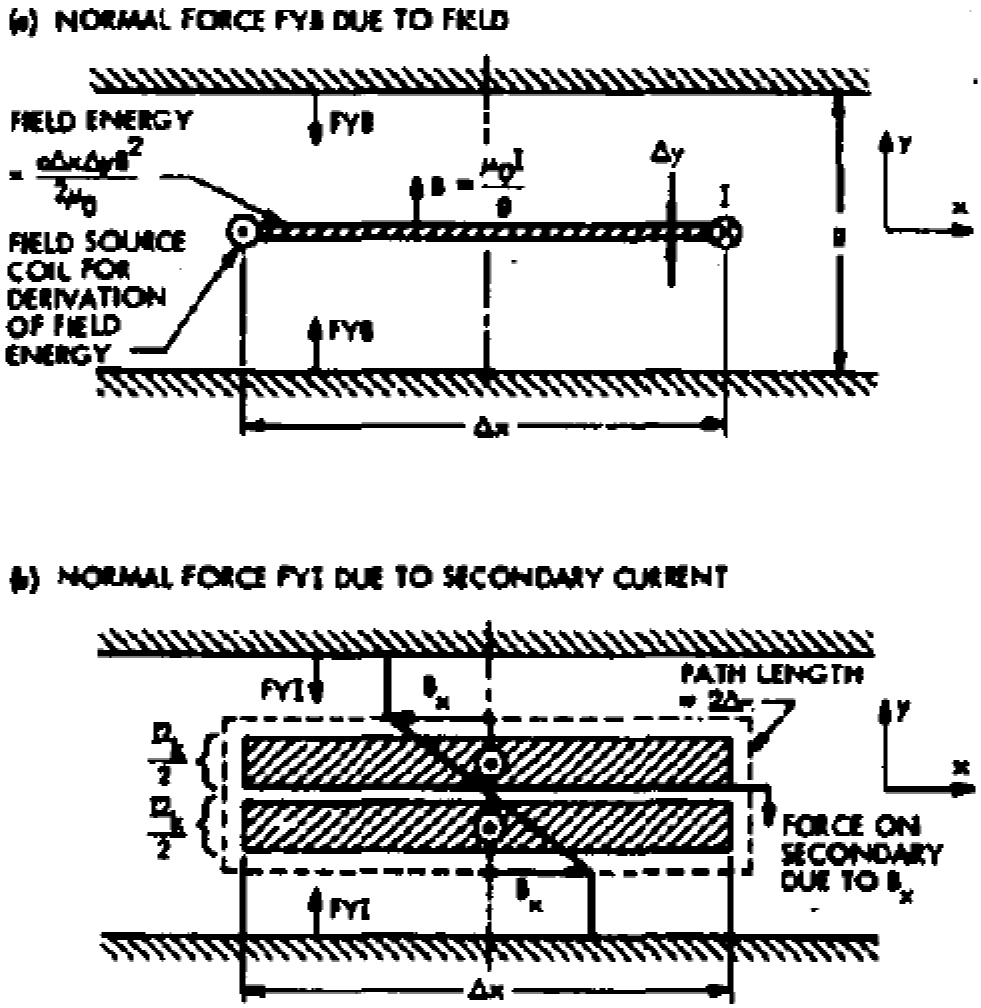

Figure 4-1: Source of Normal Force (Elliott, 1975)

The normal force is made up of two components: the first, the field force, labeled "Iron ATTR" in the code; and the second, the force from the secondary current, labeled "Curr ATTR" in the code (Elliott, 1975). The field force is always positive, the current force is always negative; and these two forces sum together to make a net "Attraction" force, labeled "ATTR" in the code, that "is positive."

It was concluded that attraction is the radial force.

4.1.2 Updated MATRIX Model Outputs

The post-processing tool, described in Section 3.3.2, provided output graphs for thrust and attraction for three MATRIX evaluation runs with NMS values of 2, 10 and 25, as shown in Figure 4-2, Figure 4-3, and Figure 4-4, respectively.

MATRIX calculates the Thrust (axial force) and Attraction or normal force per mesh number from which the forces can be calculated.

Figure 4-2 shows the force calculated with two meshes per slot (NMS=2) thus the force identified would be multiplied by two, so the resultant force per coil or slot calculated from MATRIX is approximately 1,250 N axially and 400-500 N radially.

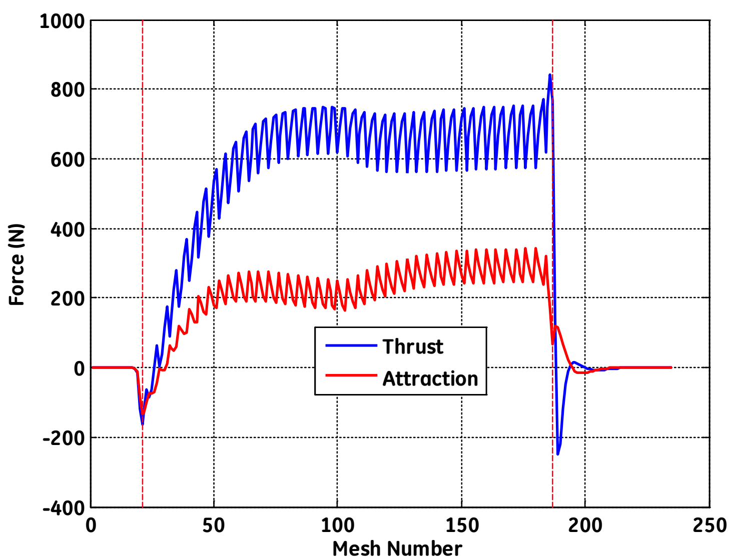

Figure 4-2: MATRIX Thrust and Attraction Plots for NMS = 2

Figure 4-3 shows the force calculated with NMS increased to ten meshes per slot (NMS=10). The force identified in Figure 4-3 would be multiplied by ten. The resultant force per coil calculated from MATRIX is approximately 1,250 N axially and 500 N radially.

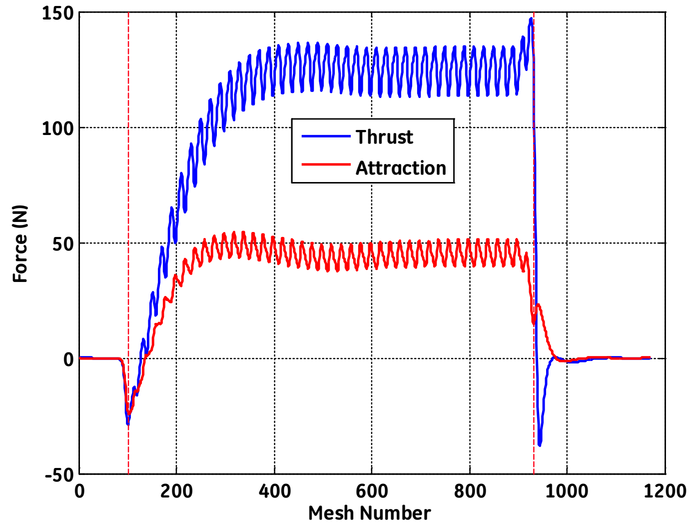

Figure 4-3: MATRIX Thrust and Attraction Plots for NMS = 10

Finally, Figure 4-4 shows the force calculated with twenty-five meshes per slot (NMS=25). The resultant force per coil or slot calculated from MATRIX is approximately 1,250 N axially and 500 N radially. So the forces per slot are about the same for NMS=10 and NMS=25.

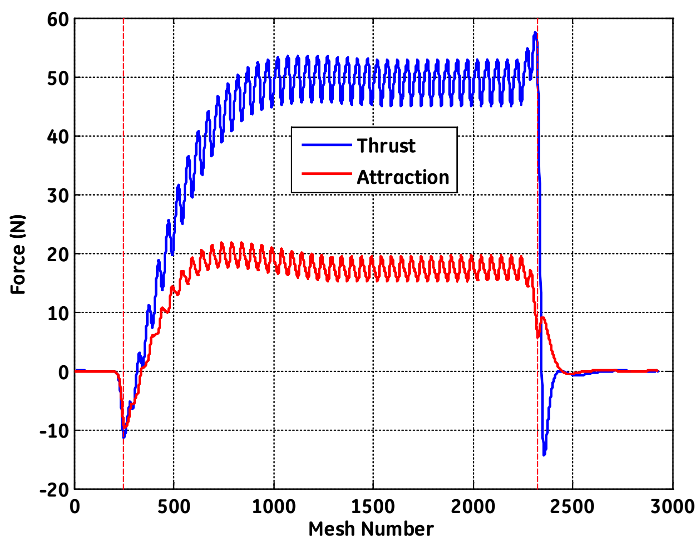

Figure 4-4: MATRIX Thrust and Attraction Plots for NMS = 25

4.1.3 MATRIX Thrust and Attraction Values

MATRIX shows a good correlation between NMS runs (as expected) with the thrust or axial force at 1,250 N and the attraction or radial force of about 500 N. Whether this attraction represents the radial force needs to be verified, and the distribution of the axial and attractive forces across the inner coil of an EM Pump also needs further investigation.

The MATRIX model contains some error in calculating the normal force. The 1975 MATRIX document states "Different average values should be used for calculating the normal force, but such averages have not been derived. Therefore, the same average currents and fields [are] used for calculating the normal force as for calculating thrust and power. The resulting error in the normal force is perhaps 20 percent for typical transportation motors." However, when compared to other predictive models at that time, the "thrusts agree within 2.0 to 2.5 percent with other analysis methods, and the normal forces agree within 10 percent in some cases but differ as much as a factor of three in others."

The GRC and ANL analyses were used to confirm the modernized MATRIX results.

4.2 GRC Finite Element Analysis (FEA)

GRC performed an FEA to evaluate the electromagnetic forces as part of the larger evaluation on EM Pump coil movement for insulation material evaluations. The electromagnetic forces that could be compared to MATRIX outputs are discussed herein.

4.2.1 Electromagnetically-Induced Motion of Coils via FEA

Prior to this DOE Advance Reactor project, the electromagnetic forces that exist on the coils during operation were never effectively documented. These electromagnetic forces act to move the coils and movement poses a risk to the electrical insulation mechanical integrity. New insulation materials and designs being evaluated require knowledge of these forces for designing the multi-stress testing equipment (see Technical Report: Insulation Materials Development and Testing (PLM DOC-0005-2465)).

4.2.2 FEA Parameters

MagNet[2] software used a 3D axisymmetric analysis to estimate the radial and axial forces on various components (Lipo, 1979).

The FEA analyzed a full pump section consisting of fourteen poles stacked on top of one another, where each of the coils forms a toroid, along with the stator pole sections, which also forms a toroid. The arrangement contains two stators, an inner as well as the outer stator, where the

[2] MagNet 2D/3D electromagnetic field simulation software, manufactured by Infolytica Corporation.

rotor is liquid sodium being pumped. An inner and an outer sleeve are also included, forming a separation between the stator components and the moving sodium. The 3D and 2D cross sections are shown in Figure 4-5.

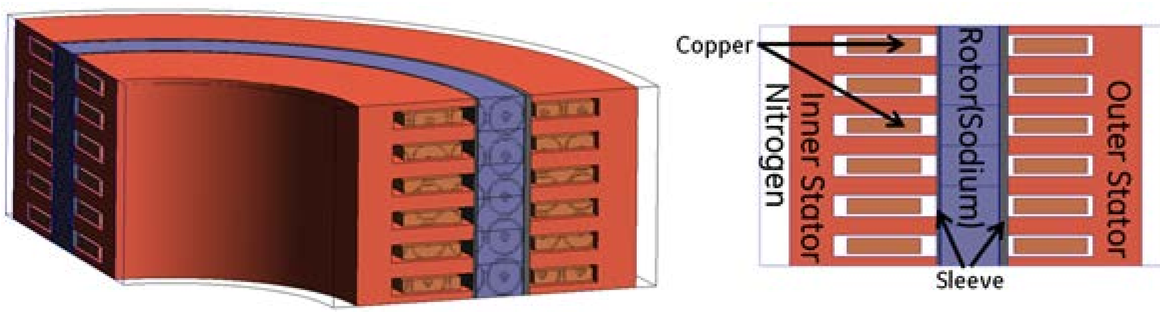

Figure 4-5: Axisymmetric 3D (one quarter section) and 2D Views of the Pump

A summary of the MagNet inputs are given in Table 4-1. The geometry is discussed in Section 4.2.3. The rotor is formed by the liquid sodium. A sodium temperature of 335°C moving at an average velocity of 10.4 m/s was used for this analysis. The resistivity of the sodium is considered at this hot temperature. On the other hand, the excitation frequency is 19.4 Hz in the coils, with each of the coils having a current of 884 Amps, which is equivalent to a stator current density of 2 Amps/mm^2. The sleeve material chosen was stainless steel, although the simulations also include results with an Inconel sleeve, at a temperature of 335°C.

Table 4-1: MagNet Inputs

Parameter	Value	Item	Value
Geometry	Given	Rotor	Sodium at 335°C
Slots/pole/phase	2	Sodium linear velocity	10.4 m/s
Excitation frequency	19.4 Hz	Travelling wave velocity	12.104 m/s
Resistivity of sodium	1.854E-7 Ω-m	Input current	884 Amps
Stator current density	2 Amps/mm2	304 Stainless Steel sleeve material	9.222E-007 Ω-m

4.2.3 EM Pump Dimensions used in the FEA

The EM Pump hot dimensions for each slot are shown in Figure 4-6. All of the dimensions are given at a temperature of 335°C, accounting for thermal growth of the components.

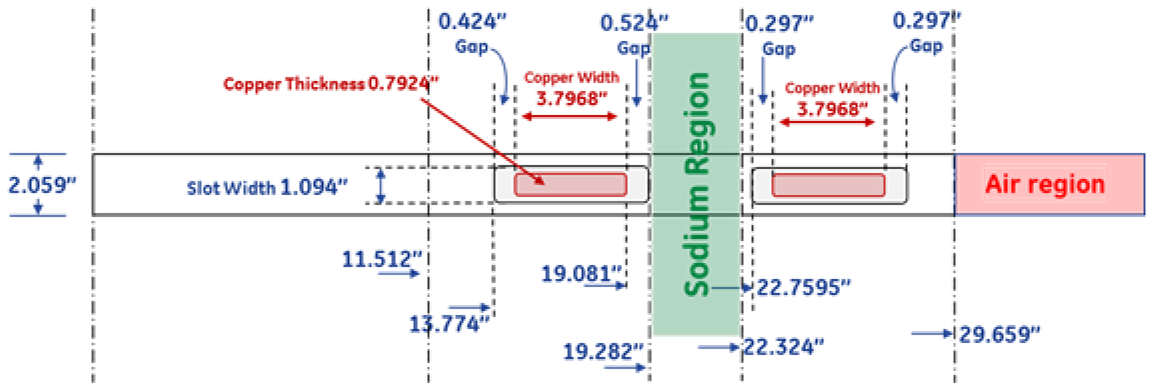

Figure 4-6: EM Pump "Hot" Dimensions. Centerline of Pump is to the Left.

The "Air region" identified on the right of Figure 4-6 is for a secondary EM Pump. This region for the primary EM Pump would be primary tank sodium at 335°C.

4.2.4 FEA Results

The forces on the sodium, as well as the axial and radial forces on the copper and the duct sleeve, are calculated. The summary of the results are provided in Table 4-2, comparing results for stainless steel versus Inconel sleeves. The variation of this material did not result in a statistically significant change of the forces on the sodium. The axial force on the sodium is estimated to be 1,315 N per slot, while the sum of the forces on the static components, namely the sleeve, slots and stator are equal and in the opposite direction. The force on the inner sleeve is about 695 N, while the outer sleeve force is 599 N.

Table 4-2: FEA Results

	1	2
Sleeve material	Steel	Inconel
Velocity [m/s]	10.4	10.4
RMS current	884	884
Force on sodium/slot	1315N	1365N
Force on inner sleeve/slot	695N	714N
Force on outer sleeve/slot	599N	631N
Radial force on inner slot	See Figure 4-7	
Radial force on outer slot		
Axial force on inner slot	Minimal	
Axial force on outer slot		
Sodium ohmic loss/slot	3217W	3298W
Outer sleeve loss/slot	3549W	3145W
Inner sleeve loss/slot	1778W	1574W
Line-line RMS voltage per pole	120V	122V
Power factor	0.388	0.385

An average of 8.5 N radial force is seen on each of the slots, added to which there is an AC component of 8.5 N occurring at twice the excitation frequency, *i.e.* 38.8 Hz is present. On the outer slots, the DC radial force is about 3.8 N along with an AC component of 3.8 N, also at twice the excitation frequency. While the direction of the radial forces on the inner slots is inward, the direction of the radial forces on the outer slots is outward.

Since the sodium is conductive, an average of 3.2 kW per slot of Ohmic losses is seen. These losses, combined with the outer and inner sleeve loss of 3.5 kW and 1.8 kW respectively, produce a heat influx into the sodium.

Based on the voltage waveform, the line RMS voltage per pole is estimated to be 120 V, which leads to a power factor of 0.388, based on the current of 884 Amps.

4.2.5 FEA Estimation of Radial and Axial Forces

The MagNet software does not output the radial forces, so the forces are estimated from the current density and the magnetic field. A multiplying factor of the volume is applied to get to the final forces per the equation 4.1:

$$Force = l\,(i \times B) = V\,(J \times B) \quad (4.1)$$

where V is the volume of the slot copper, J is the current density in the copper, and B is the net flux density in the copper.

The radial and axial forces are computed from the product of the current density and the field density, which is available as a post processed parameter in MagNet. The radial forces on the slots are shown in Figure 4-7.

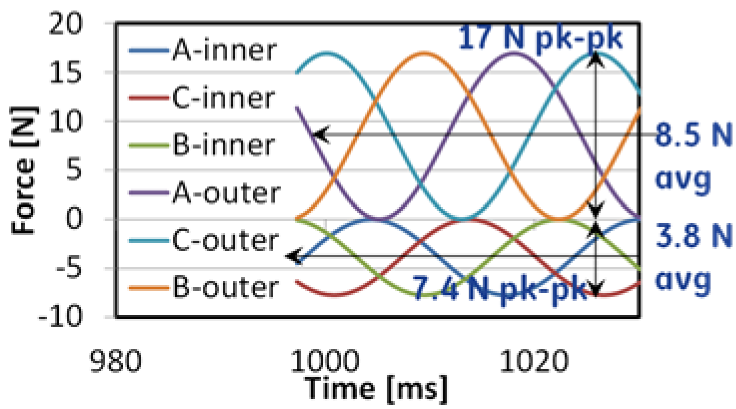

Figure 4-7: Slot Radial Forces

While the forces are in opposite directions on the inner and outer slots, what is also evident is that the forces are time-shifted between slots of the pump. In other words, the force on slot-A repeats in slot-B but at a different instant in time. The frequency of the forces is 38.8 Hz and is twice the excitation frequency delivered to the EM Pump from the power supply.

In contrast to the radial forces, the axial forces on the slots are negligible (Table 4-2). Most of the equal and opposite axial forces occur in the sleeves, which accounts for the reaction forces on the sleeves.

4.2.6 FEA Pressure Calculations

Based on the radial and axial forces, the pressure on the slots is estimated from the equations provided by MATRIX.

These pressure calculations in the fluid are as follows:

$$1315\ N\ \rightarrow 295.67\ lbf \tag{4.2}$$

$$Duct\ Area = \frac{(OS_{id}^2 - IS_{od}^2)\pi}{4} = \frac{(44.409^2 - 38.358^2)\pi}{4} = 393.2\ in^2 \tag{4.3}$$

$$DP = \frac{295.67\ lbf}{393.2\ in^2} = 0.752\ PSI\ (per\ slot - 2D\ zone) \tag{4.4}$$

The pump contact pressure calculations are as follows:

$$110460\ N\ \rightarrow 24{,}872\ lbf \tag{4.5}$$

$$Pump\ Area(IS) = \frac{(IS_{od}^2 - IS_{id}^2)\pi}{4} = \frac{(38.36^2 - 27.4^2)\pi}{4} = 565.94\ in^2 \tag{4.6}$$

$$Pump\ Area(OS) = \frac{(OS_{od}^2 - OS_{id}^2)\pi}{4} = \frac{(55.51^2 - 44.41^2)\pi}{4} = 871.25\ in^2 \tag{4.7}$$

$$Total\ Surface\ Area = 1437.19\ in^2\ (per\ mesh) \tag{4.8}$$

$$Total\ DP = \frac{24872\ lbf}{1437.19\ in^2} = 17.3\ PSI \tag{4.9a}$$

$$DP\ per\ slot = 17.3/84 = 0.2\ PSI \tag{4.9b}$$

where OS_{id} is the outer diameter of the sodium channel, IS_{od} is the inner diameter of the sodium channel, DP is the pressure of the sodium, IS_{od} is the outer diameter of the inner stator, IS_{id} is the inner diameter of the inner stator, OS_{od} is the outer diameter of the outer stator, and OS_{id} is the inner diameter of the outer stator. Note that the contact pressure or force between the ground insulation and copper coil is rather small and should not cause any appreciable axial movement of the insulation.

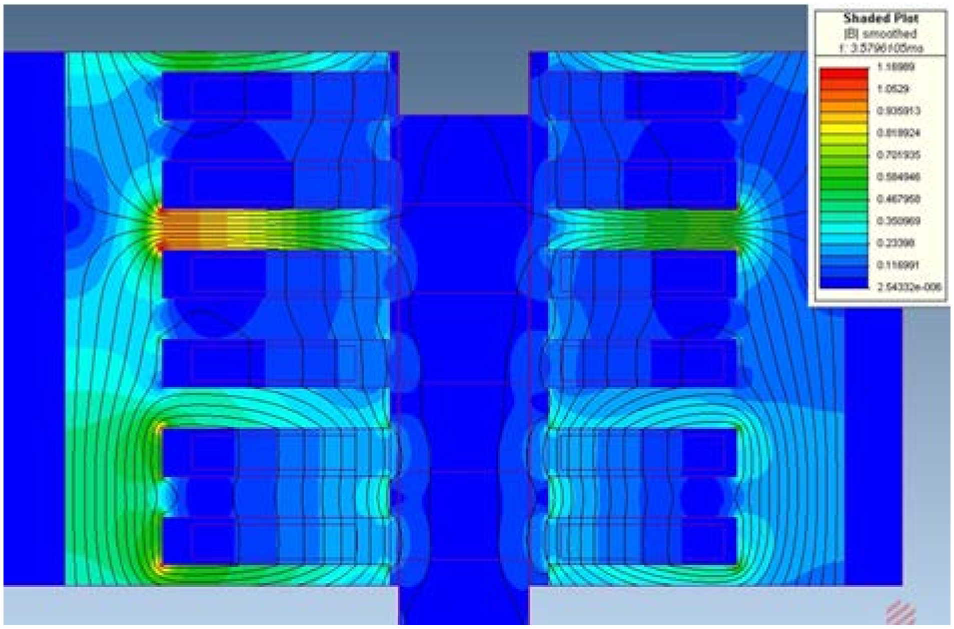

Figure 4-8: Flux Density Contours

4.2.7 FEA Flux Density Fields

Figure 4-8 shows the flux density contour along with the movement of the fluid between the two stators. The flux density in the machine is only 1.16 T, while the iron tolerates a maximum flux density of 2.0 T. The EM Pump design can be further optimized for performance, and insulation system performance reliability can be improved as well.

4.2.8 FEA Analysis Conclusions and Forecasts Regarding Coil Motion and Forces

The FEA of the EM Pump shows the radial and axial forces on the slots, sleeves, and sodium. The outer slots see a peak-to-peak outward radial force of 17 N, while the inner slots see a peak-to-peak inward radial force of 7.4 N. The axial force per slot as per the FEA calculation (1315N) is comparable to that of MATRIX (1250 N). No appreciable coil motion is expected because of these forces.

4.3 ANL Coil Force Calculations

ANL performed systematic, independent testing via the following analysis of the axial forces on the coils of the double stator pump (supporting ANL Objective 2-4) as an independent check.

4.3.1 Axial direction

As a counter action to the pump head, the coils in an ALIP receive thrust force. The summation of the all thrust forces acting on each coil is approximately equal to the force due to the pump head. For qualitative consideration, a simple picture of the electromagnetic interaction within the pump is shown in Figure 4-9.

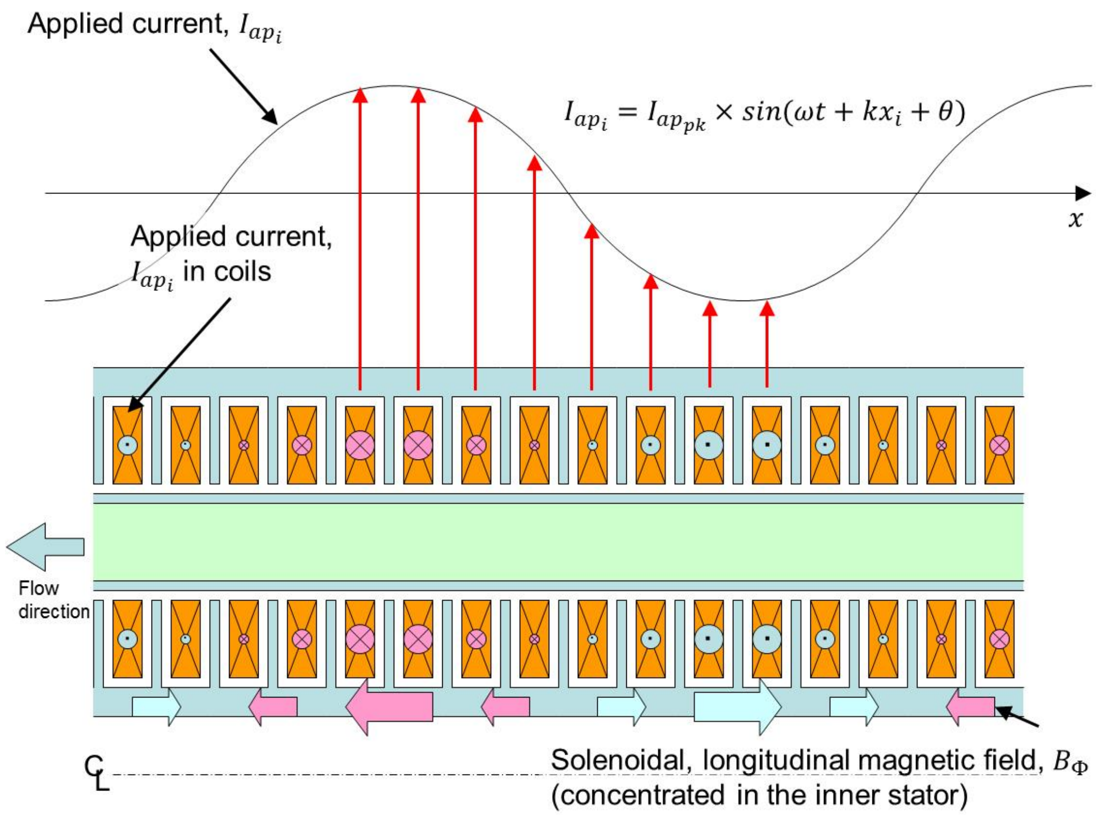

Figure 4-9: Applied Current and Induced Solenoidal Magnetic Flux in a Double Stator ALIP

To find the spatial and temporal distribution of the thrust, the applied current to a coil may be expressed as:

$$I_{ap_i} = I_{ap_{pk}} \times sin(\omega t + kx_i + \theta) \quad (4.10)$$

where $I_{ap_{pk}}$ is the peak applied current and ω is the angular velocity of the rotating magnetic field as a function of time, t.

Then, the produced solenoidal magnetic field in the center core or the flux in the perimeter of the stator along the axial direction of the pump is proportional to the applied current (thus in phase with it) given by

$$B_\Phi = B_{\Phi_{pk}} \times sin(\omega t + kx + \theta) \quad (4.11)$$

Where B_Φ is the longitudinal magnetic field.

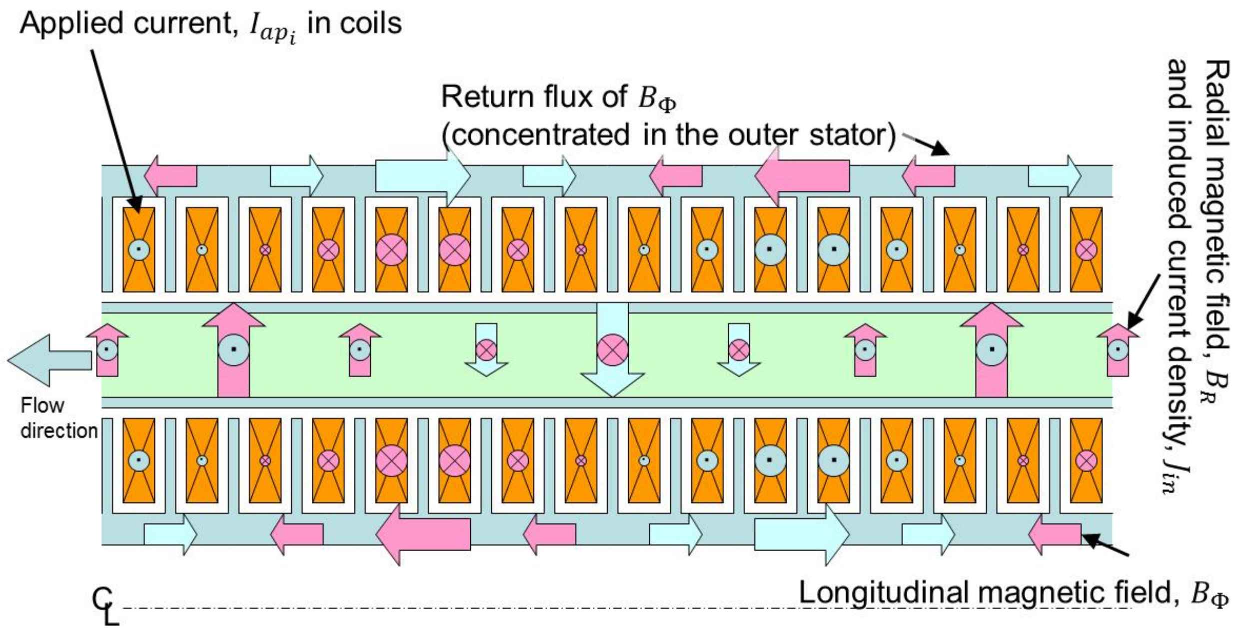

Figure 4-10: Longitudinal Magnetic Field, the Resultant Radial Magnetic Field and the Induced Current in the Sodium Fluid

The continuity of the magnetic flux and the radial magnetic field are shown in Figure 4-10, which is proportional to the spatial change of the axial magnetic flux given by:

$$B_R \propto -\frac{dB_\Phi}{dx} \tag{4.12}$$

and

$$B_R = -B_{R_{pk}} \times cos(\omega t + kx + \theta) \tag{4.13}$$

where B_R is the radial magnetic field and B_Φ is the longitudinal magnetic field.

The radial magnetic field is 90 degrees shifted to the phase of the current. The induced current J_{in} in the sodium is proportional to the temporal change of the radial magnetic field.

$$J_{in} \propto -\frac{dB_\Phi}{dt} \tag{4.14}$$

and thus

$$J_{in} = -J_{in_{pk}} \times cos(\omega t + kx + \theta) \tag{4.15}$$

The axial forces applied to the coils from the induced current density in the working fluid are shown in Figure 4-11.

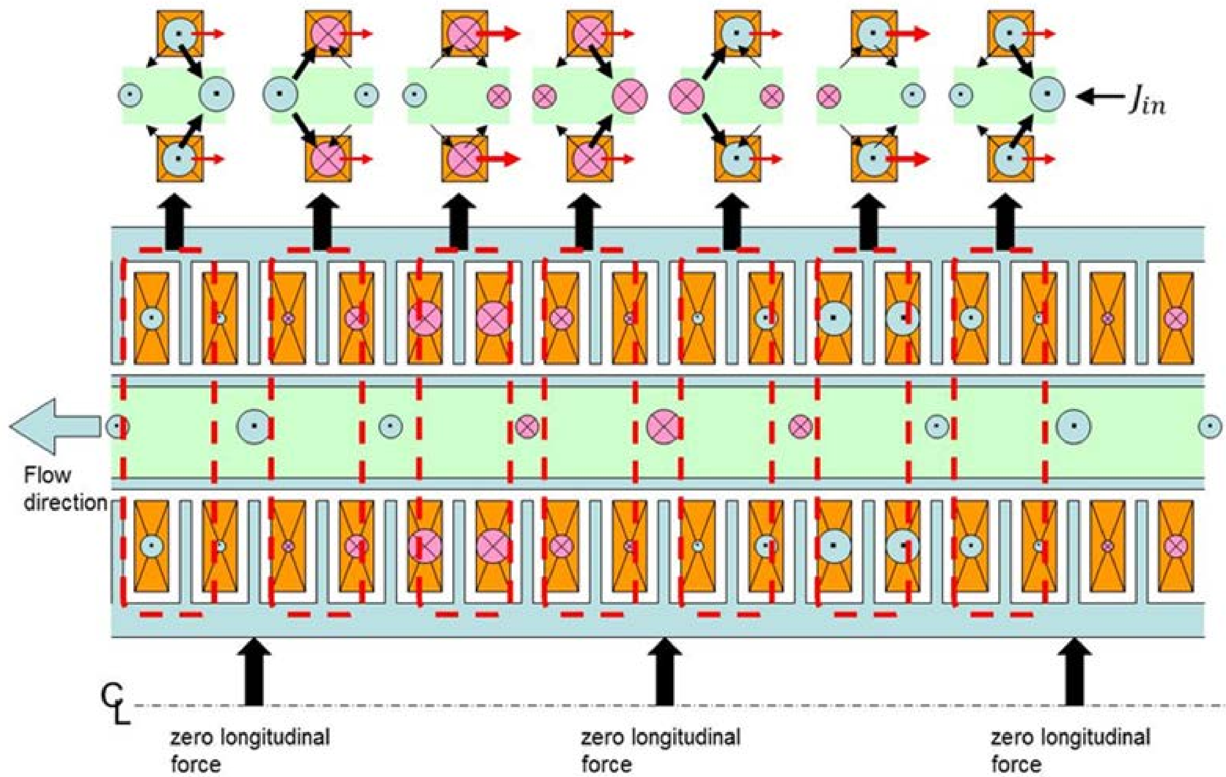

Figure 4-11: Resultant Longitudinal Force (red arrows) that Each Conductor Experiences Due to Ampere's Force Law

Force analysis only considers Ampere's Force Law, thus eliminating the need to obtain the magnetic field distribution. Only the forces due to the closest current carrying components are considered. In Figure 4-11, the forces between the conductors in the outer coils and those in the inner coils are assumed negligible when compared to those between the conductors in each coil and the adjacent current flowing working fluid. The longitudinal force (or thrust) on each coil, F_{Φ_i} is proportional to the product of the applied current, I_{ap_i} and the gradient of the induced current, $\left.\frac{dJ_{in}}{dx}\right|_{x=x_i}$

For quantitative consideration, ANL identified the total force that the pump produces to propel the working fluid, F_P is:

$$F_P \equiv S_d P \qquad (4.16)$$

where S_d is the cross section of the pump annulus and P is the pump head.

The sum of F_{Φ_i} is the counteracting force of F_P, so

$$F_P \equiv -\sum_i F_{\Phi_i} \qquad (4.17)$$

Also from the result of the qualitative analysis above,

$$F_P \equiv -\sum_i F_{\Phi_i} \propto I_{ap_i} \times \left.\frac{dJ_{in}}{dx}\right|_{x=x_i} = -I_{ap_{pk}} J_{in_{pk}} \sum_i sin^2(\omega t + kx_i + \theta) \qquad (4.18)$$

And

$$\lambda \equiv \frac{L_{pump}}{(N_{pole}/2)} \qquad (4.19)$$

where λ is the wavelength defined as $\equiv \frac{2\pi}{k}$ where K is the wave number and the wavelength is twice the pole lengths, and L_{pump} is the length of the ALIP, N_{pole} is the number of poles in the ALIP. N_{pppp} is the number of coils per pole per phase and is 2 for the case in Figure 4-12.

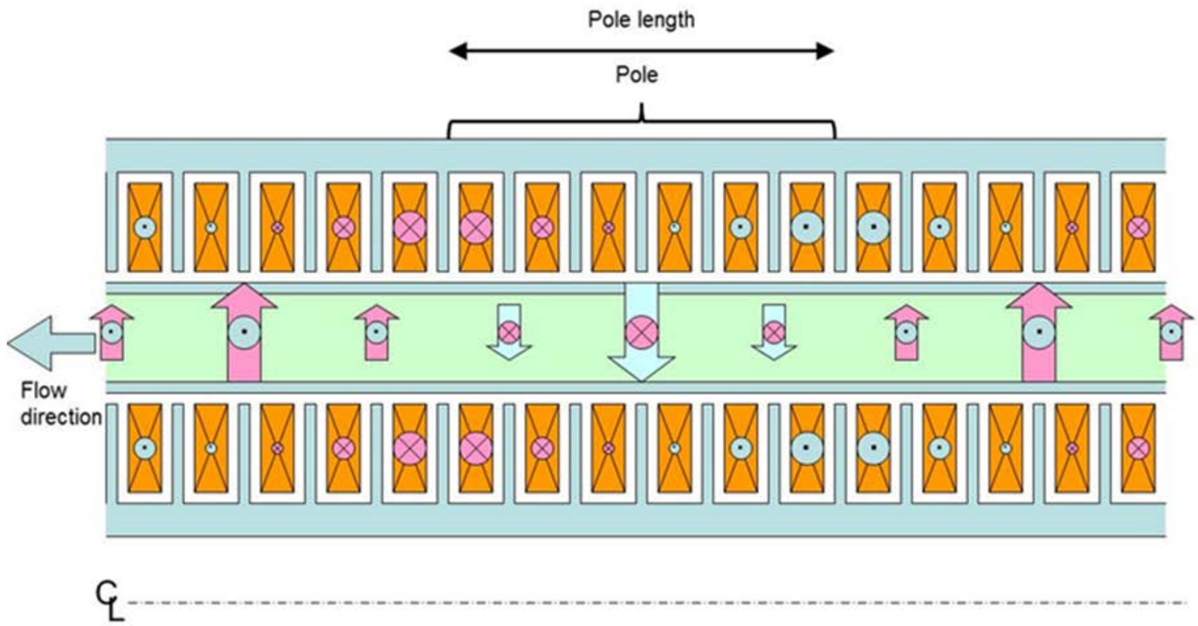

Figure 4-12: Pole and Wave Length of the Applied Field

For a 3 phase driven ALIP, each coil (or a group of coils in the same phase, where $N_{pppp} > 1$) in a pole is separated by $\frac{\pi}{3}$ or 60 electrical degree such that

$$x_{i+1} - x_i = \frac{\lambda}{6} \tag{4.20}$$

Also for $x_{i+1} - x_i = \frac{\lambda}{6}$

$$\sum_{i=0}^{5} \sin^2(\omega t + kx_i + \theta) = 3 \tag{4.21}$$

where $i = 0$ to 5 corresponds to one full cycle (2 pole length), see Figure 4-12. For $N_{pppp} > 1$, one full cycle corresponds to

.

$$N_{pppp} \times \sum_{i=0}^{5} sin^2(\omega t + kx_i + \theta) = 3N_{pppp} \tag{4.22}$$

Since there are $\frac{N_{pole}}{2}$ full cycles in the ALIP,

$$\sum_{i} sin^2(\omega t + kx_i + \theta) \ = 3N_{pppp} \times \frac{N_{pole}}{2} \tag{4.23}$$

And

$$F_P \propto -3N_{pppp}\frac{N_{pole}}{2}I_{ap_{pk}}J_{in_{pk}} \tag{4.24}$$

Or simplified to

$$I_{ap_{pk}}J_{in_{pk}} \propto -\frac{2F_P}{3N_{pppp}N_{pole}} \tag{4.25}$$

Finally, each coil experiences a time varying force that is equal to F_{Φ_i} that is acting along the axial direction where F_{Φ_i} is given as:

$$F_{\Phi_i} \approx \frac{2PS_d}{3N_{pppp}N_{pole}} sin^2\omega t \tag{4.26}$$

Noting that $3N_{pppp}N_{pole} = N_{coil}$ for a regular three-phase ALIP, the above expression can be further simplified as

$$F_{\Phi_i} \approx \frac{2PS_d}{N_{coil}} sin^2\omega t = \frac{PS_d}{N_{coil}}[1 - cos(2\omega t)] \tag{4.27}$$

As a note, it can easily be seen that since $sin^2\omega t$ changes from 0 to 1, the peak value of F_{Φ_i} is $\frac{2PS_d}{N_{coil}}$ and the thrust component does not become negative. Also from the $cos(2\omega t)$ term, the frequency of the longitudinal force is twice as high as the frequency of the applied current.

For the GE ALIP, P = ~0.3 MPa, $S_d = \frac{\pi}{4}\left({D_O}^2 - {D_I}^2\right)$ = 0.254 m^2, where D_O = 44.4 inch or 1.1 m, D_I = 38.4 inch or 1.0 m, N_{coil}= 84 and see Figure 4-13.

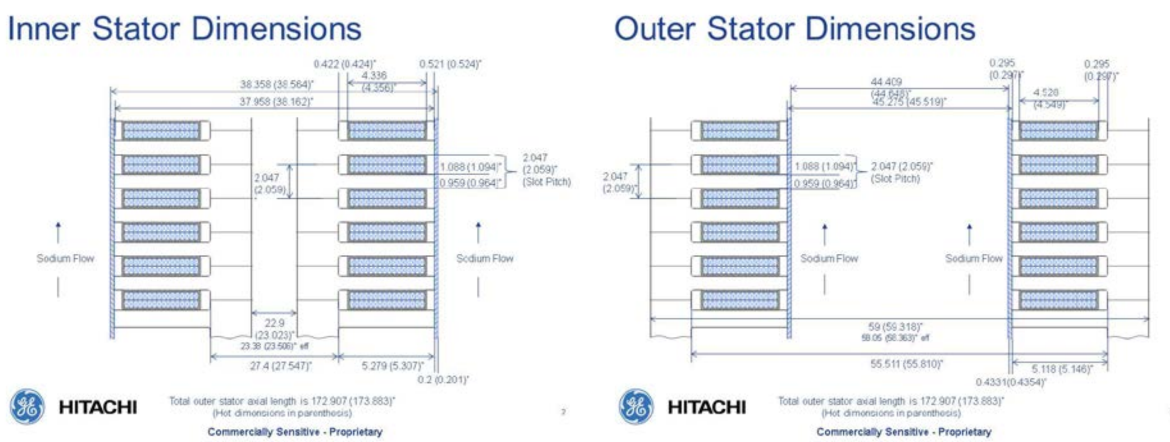

Figure 4-13: Inner and Outer Stator of the GEH ALIP

This gives $F_P = PS_d$ = 76,200 N and the peak of F_{Φ_i} = 1,814 N. Since this pump is a double stator coil configuration, and assuming the inner and the outer equally produce the thrust, each coil may be expected to experience 907 N in axial direction.

4.3.2 Radial Direction

For qualitative consideration, ANL assumed that the use of the concept of Ampere’s Force Law is also valid for the radial forces. There are radial components of forces acting on each conductor due to Ampere's Force Law, as indicated by the small red arrows in Figure 4-14.

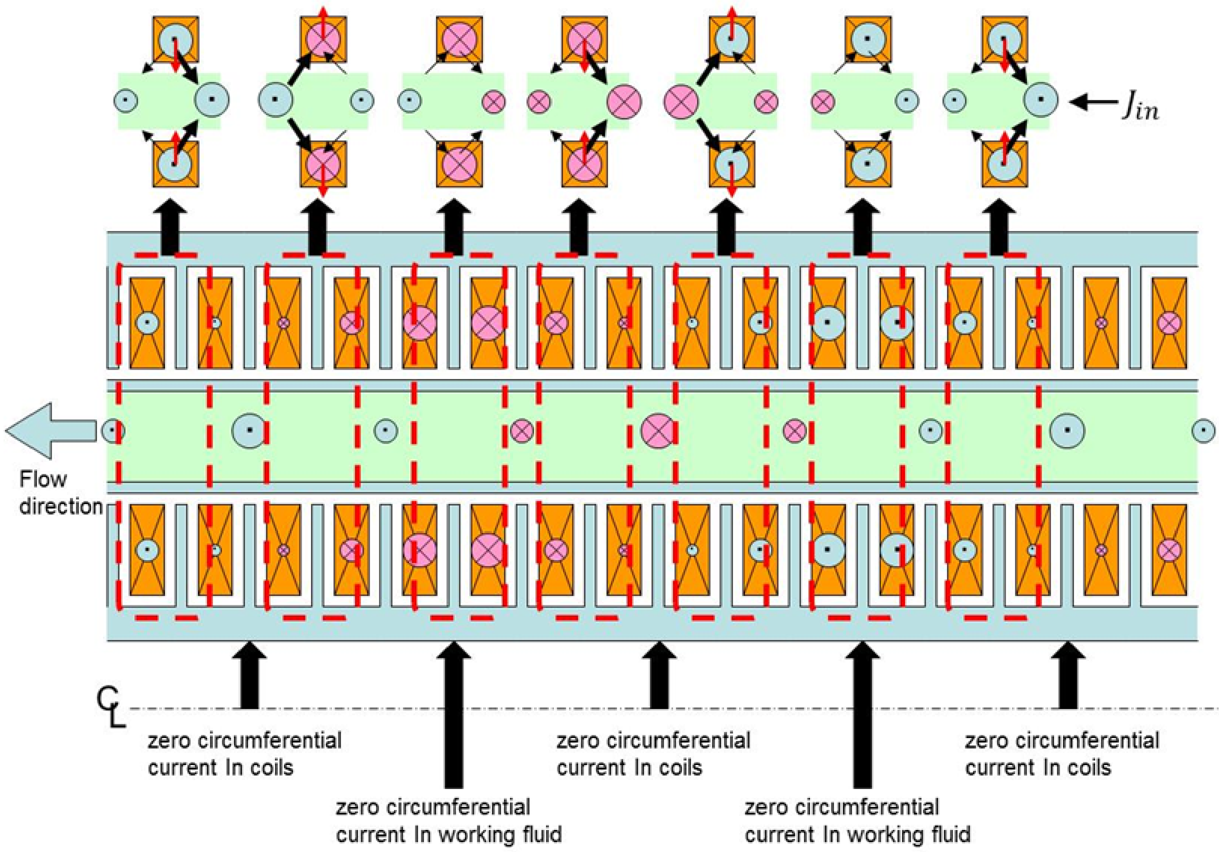

Figure 4-14: Forces to the Coils from the Induced Current Density in the Working Fluid

The net radial force is zero at locations where either conductor (coil or working fluid) carries zero circumferential current as shown in Figure 4-14. Also it changes the direction of the force at those locations (repulsive and attractive). This means that the radial force appears to have the same frequency as that of the longitudinal force (or thrust), but the phase is only 90 degrees.

The assumption that the forces between the conductors in the outer coils and those in the inner coils are assumed negligible when compared to those between each coil and the adjacent current flowing working fluid must be assessed. At locations where the circumferential current in the working fluid is zero, the conductors are assumed to have no radial force components; however, the applied current flowing in the outer coil and the inner coil at that location is at its peak and should produce some attraction between the coils. Figure 4-15 shows the phase and amplitude relationship between the longitudinal and radial forces and the applied current.

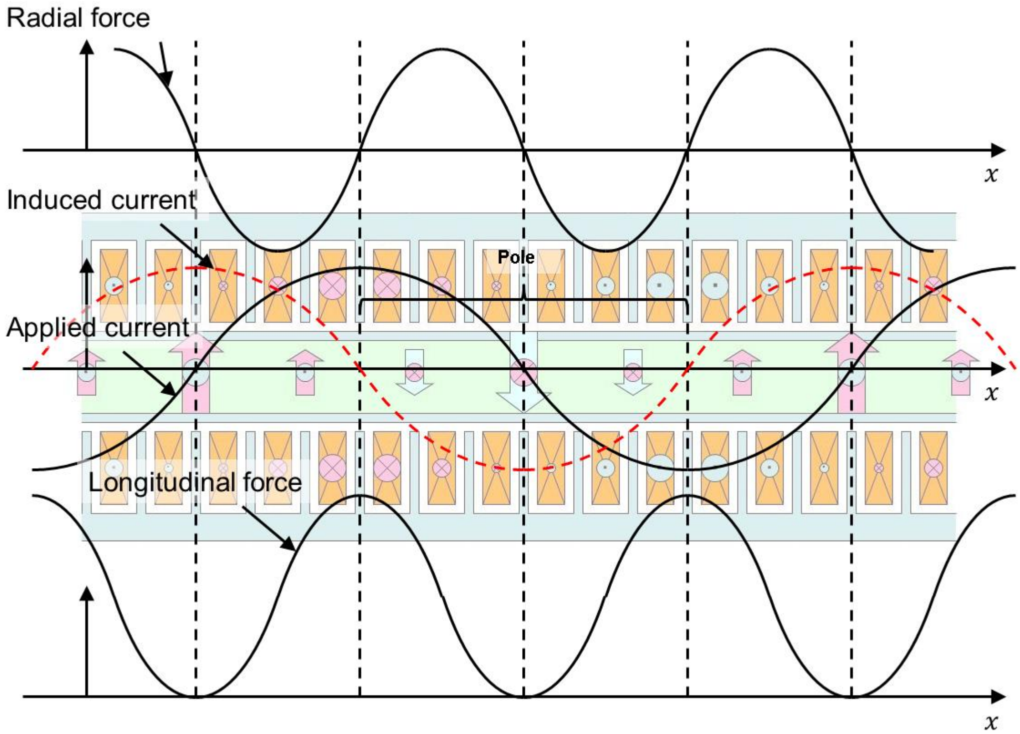

Figure 4-15: Phase and Amplitude Relationship between the Longitudinal, Radial Forces and the Applied Current

For quantitative consideration, ANL determined it was difficult to estimate the radial forces since the sum of the radial force components is zero. However, from the concept of Ampere's Force Law, the radial components may be estimated from the geometrical relationship between the pole length and the distance between the cross-sectional center of the coil to the sodium flow. Further work was needed in this regard.

4.3.3 ANL Coil Force Summary

ANL determined the axial force, or thrust, upon the each coil to be 907 N and was not able to quantify the radial force.

4.4 Coil Force Comparisons

The results of the three calculation methods, MATRIX, FEA and the ANL Force calculations for axial and radial forces upon the coils due to electromagnetic influences are summarized in the following subsections.

4.4.1 Thrust or Axial Force Comparisons

MATRIX calculated the thrust, or total axial force of 1,250 N per slot. MATRIX did not breakdown the forces to subcomponents in the EM Pump design to determine how much force is upon the sleeves compared to the coils.

The FEA estimated the axial force on the sodium is estimated to be 1,315 N per slot, while the sum of the forces on the static components, namely the sleeve, slots, and stator are equal and in the opposite direction. The force on the inner sleeve is about 695 N, while the outer sleeve force is 599 N, and per Table 4-2, the axial force on the coils is minimal.

ANL calculated the axial force 907 N per slot.

The FEA calculates thrust 5.2% higher than MATRIX, which is about twice the 2-2.5% agreement of other analysis methods in 1975. The ANL force calculates thrust 27% lower than MATRIX.

4.4.2 Attraction or Radial Force Comparisons

MATRIX calculated an attraction force of 500 N, which 1975 MATRIX documentation suggests is the sum of the radial force components. MATRIX did not breakdown the forces to subcomponents in the EM Pump design.

The FEA determined the outer slots see a peak-to-peak outward radial force of 17 N, while the inner slots see a peak-to-peak inward radial force of 7.4 N.

ANL did not quantify the radial force vector.

The FEA calculates the maximum radial force is only 3.4% of the MATRIX "Attraction" value. This is significantly outside the 10% agreement of other analysis methods in 1975 and even beyond the 2-3 times different of some 1975 comparisons. This difference from the GRC FEA caused some to question whether the MATRIX "Attraction" was indeed the radial force" because MATRIX is not clearly identified. Other reasons for this difference may include forces applied to the sleeve materials (See Table 4-2) and inaccurate code assumptions.

At twice the excitation frequency of 19.4 Hz, or 38.8 Hz described in Section 4.2.4, a coil would experience 1,224,000,000 cycles per year or 37,700,000,000 cycles in 30 years. However, at the small force with a maximum of 17 N identified by the FEA, little, if any, motion would be applied to the coils and the amplitude of this movement, if any, would be very small. The EM Pump lamination clamping pressures would easily overcome this force to prevent motion. In contrast to the FEA, the Attraction force identified by

MATRIX was 500 N. If the attraction force is the radial force, this force is more significant and may impart motion to the coils if the clamping force of the lamination is not sufficiently high. Such might help explain the early failures experienced in SS #1 tests described in Section 3.1 of the Technical Report: Insulation Materials Development and Testing (PLM DOC-0005-2465).

4.5 MATRIX Coil Force Recommendations

The axial or thrust calculations agree in relative magnitude between MATRIX and the FEA; however, the FEA distributes those forces to the EM Pump components, whereas MATRIX does not have such delineations.

The radial or attraction force results do not agree within previous model comparisons. Resolving these differences would help better understand the forces on, and motions of, the coils with minimal lamination clamping. The MATRIX code and the FEA code should be compared side by side to evaluate where the differences are. The MATRIX code should be improved, incorporating FEA elements distributing forces to other EM Pump components.

Improvements to the MATRIX code to identify the forces applied to the coil and the pump sleeve would aid EM Pump designers in developing insulation components and lamination yoke clamping parameters.

Elliot (1975) identified that extending the matrix method to provide a solution in the z direction would eliminate the problem with the transverse variations, but the computing time would be greatly increased. With computing times significantly reduced with faster processors, this improvement could be explored.

5.0 Develop the Next Generation EM Pump Analysis Tools

Significant changes were made to improve the accuracy of the MATRIX prediction through flow correction. These changes are described in Section 5.1.

Section 5.2 discusses how the Matrix code was updated for material properties including 1) the thermal expansion of duct and black iron materials, 2) the electrical resistivity of copper conductor materials, duct material, and sodium, and 3) the density and viscosity of sodium. Pre-processing material properties spreadsheets of the MATRIX were directly implemented in the improved code. Overall, these code improvements were verified by a side-by-side comparison with only slight difference of pressure head versus flow rate predictions caused by compiler difference.

The last section, Section 5.3, explains the thermal analysis implementation. A thermal analysis model for calculating the copper, lamination, and duct temperature profiles was incorporated into the MATRIX code. The main goal of developing a thermal analysis model was to obtain the maximum temperature in the copper block that the insulation material installed in the EM Pump must withstand. Such an analysis had never been implemented within the MATRIX code until this project. The program uses a thermal, network method consisting of nodes and connections patterned after the Advanced General Electric Network Analyzer (AGENA) program (Salamah, *et al., 1991*) used to analyze the 160 m^3/min EM Pump test. The MATRIX nodes have both heat capacitance and heat generation capabilities. The connectors transfer heat between the nodes by conduction.

5.1 Flow Correction Improvements

Eliminating the 0.7 multiplier and improving the MATRIX prediction by flow correction is described next.

5.1.1 Identifying the Discrepancies

The 1999 MATRIX code calculated pressure rise and efficiency results 30% greater than experimentally measured pump values. The code assumed a flat sodium velocity profile in the duct; however, a series of experiments conducted by Eckert *et al., 2002,* revealed that when sodium flows under a strong transverse magnetic field, an M-shaped velocity profile occurs within the flow duct. The application of an electromagnetic field causes a different flow structure phenomenon to occur within a duct than expected in non-conducting fluid. As the magnetic field is increased, the sodium velocity in the core of the flow is slowed while the velocities on the edges of the flow are enhanced. A relation to estimate the ratio between the velocity rises seen in the edges of the flow compared to the core of the flow δu and the mean velocity u is as follows (Eckert *et al., 2002*):

$$\frac{\delta u}{u} \approx 10 * \beta \frac{\mathrm{Ha}}{\mathrm{Re}} \tag{5.1}$$

where Re and the Ha variables are the Reynolds Number and the Hartmann number, respectively (Krasnov, *et al.; 2012;* DePuy, 2010). The aspect ratio of the flow duct β for the subject experiment was unity. The Hartmann number (Ha) is a non-dimensional ratio of the electromagnetic force to the viscous force as defined by:

$$Ha = B * a \sqrt{\frac{\sigma}{\rho * v}} \tag{5.2}$$

where $B, a, \rho, \sigma,$ and v are the magnetic flux density, half-width of the duct, fluid density, electrical conductivity, and kinematic viscosity, respectively. One half of the M-shaped velocity profile, from the center of the duct to the outer wall, is shown in Figure 5-1, as adapted from Eckert *et al.*, (2002.). Figure 5-1 shows the changing shape of the mean velocity profile for sodium flow at a Reynolds number of approximately 57,000 as the transverse magnetic field (which directly affects the Hartmann number, Ha) within the duct is changed.

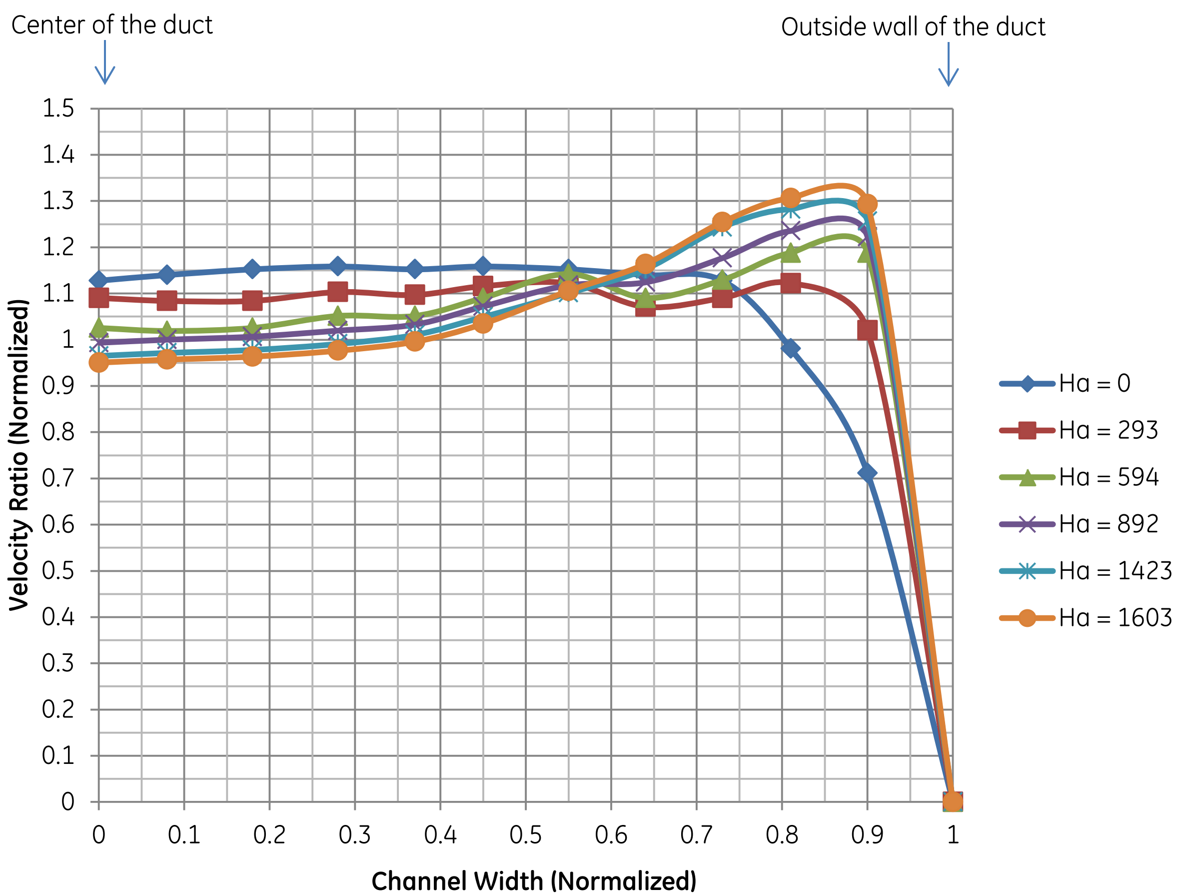

Figure 5-1: Transverse Magnetic Field Effects on the Mean Velocity Profile at a Reynolds Number of 57,000

The Hartmann number, Ha, is proportional to magnetic field B. For Ha = 0, no magnetic field is present and the velocity profile is similar to the standard shape of turbulent flow through a duct as shown in Figure 5-1. As the Hartmann number increases, corresponding to an increasing transverse magnetic field, the M-shape flow profile develops. For an EM Pump operating in the intermediate loop of the PRISM reactor system (sodium temperatures near 335°C), the Hartmann number is near 500, which results in a velocity profile somewhere between the Ha = 293 and Ha = 594 curves in Figure 5-1, if the operating Reynolds number is about 60,000. For a much higher Reynolds number, typical for EM Pump operation, but at a Hartmann number of about 500, the sodium velocity profile would most probably be like the "turbulent" flow seen somewhere between the Ha = 0 and Ha = 293 curves in Figure 5-1.

An alteration to the MATRIX input velocity is needed to adjust for the actual velocity profile ("turbulent" to "M" shaped shown in Figure 5-1). Since MATRIX is a 1-D code with a flat velocity profile, it is not possible to create the M-shaped velocity profile within the simulation.

5.1.2 Obtaining the Necessary Data

To validate the modernized MATRIX code, the input flow rate and current values from the experimental data was needed; however, no record of the experimental inputs was found in the EM Pump databank created in Task 1.

To create a comparison between the modernized MATRIX simulation and the experimental data, the input flow rate and current values needed to be found for frequencies of 4, 6, 8, 10, 12, 14, 16, 18, 20, and 23 Hz. These were the frequencies at which the large EM Pump (160 m^3/min design) was tested for obtaining operational data. The frequencies per experiments are identified in Table 5-1.

Table 5-1: Frequency Data Obtained from Experiments

Experiment	Frequency (Hz)									
	4	6	8	10	12	14	16	18	20	23
PT335VF1	X	-	X	-	X	-	X	-	X	-
PT335VF2	-	-	-	-	-	-	-	-	X	X
PT335VF3	-	X	-	X	-	X	-	X	-	-
PT335REP	X	-	X	-	X	-	-	-	-	-

Although the necessary input data was not directly available, the data could be back-calculated from the frequency versus flow rate and the frequency versus average phase current plots for the experimental data, which were available, as seen in Figure 5-2 and Figure 5-3. A second order polynomial best fit was found for each plot. The best fit lines provide equations for the flow rates and currents that were used as inputs into MATRIX for each of the test frequencies under consideration.

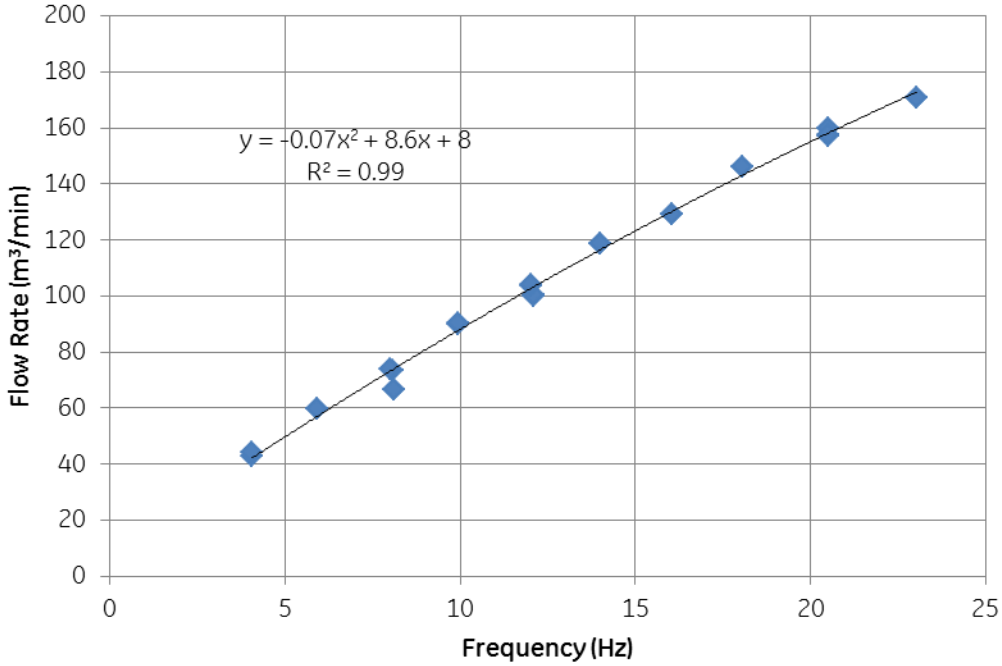

Figure 5-2: Frequency versus Flow Rate from Experimental Data

Figure 5-2 shows the frequency versus flow rate test data from the experiments listed in Figure 5-1. The non-linear nature of the data is due to the overall resistance within the pump, which changes as the voltage over frequency (V/f) control increases due to eddy currents and other current leakages.

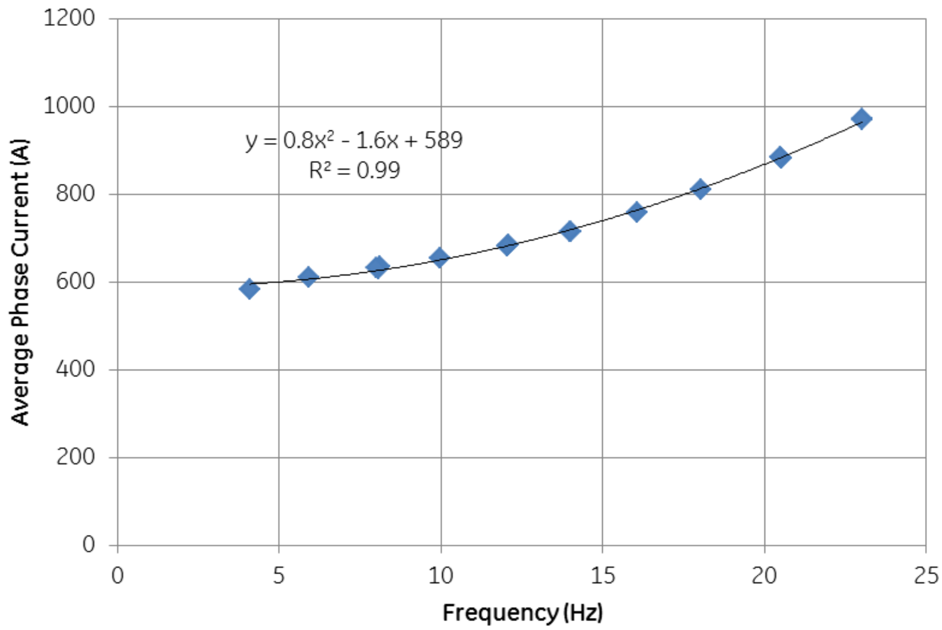

Figure 5-3: Frequency versus Phase Current from Experimental Data

Figure 5-3 shows the frequency versus phase current test data from the experiments listed in Figure 5-1. The non-linear nature of the data is due to the overall resistance within the pump, which changes as the voltage over frequency (V/f) control increases due to eddy currents and other current leakages.

5.1.3 Determining the Flow Error

With the needed input data from the best fit lines from Figure 5-2 and Figure 5-3, the calculated input flow rates versus developed head was plotted for the modernized MATRIX code in Figure 5-4 along with the experimental test data for comparison.

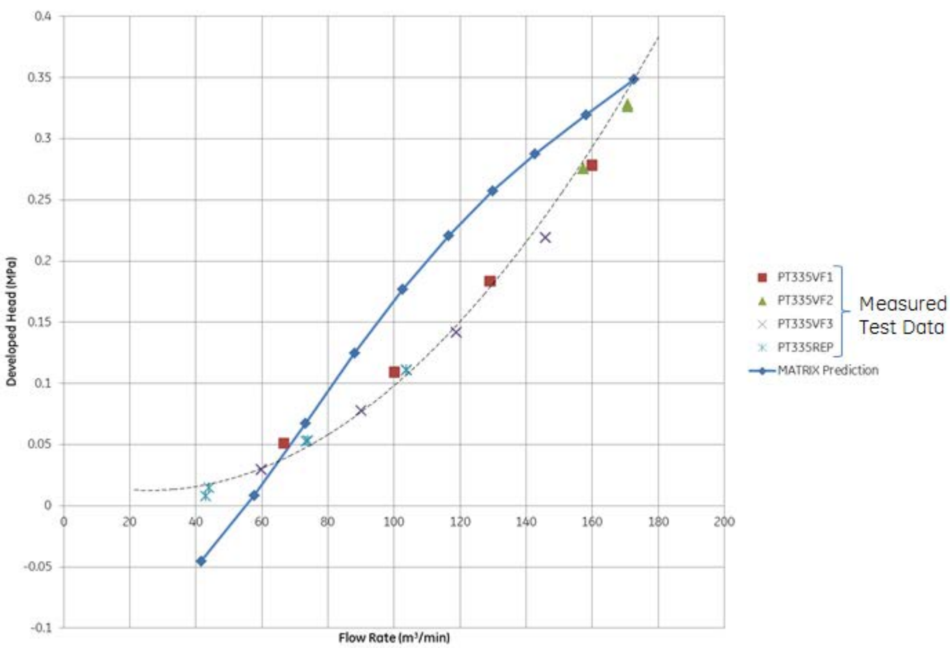

Figure 5-4: Developed Head versus Flow Rate (without flow correction)

As was the case shown in Figure 3-1, there is an inconsistency between the simulated and experimental data. As no changes were made to the input flow data to account for the velocity profile, this difference is to be expected; however, this time the simulation can be fitted with a polynomial curve instead of being completely linear. The simulated and experimental curves cross at a flow rate of 70m^3/min and again near 170 m^3/min.

A normalized curve (MATRIX/Experimental) of the developed head shows most of the data fell outside of the ± 5% lines, shown as dashed lines depicted in Figure 5-5. The data points near 170 m^3/min were close to the ± 5% zone, which confirms the observations seen during the large EM Pump testing, depicted in Figure 3-1.

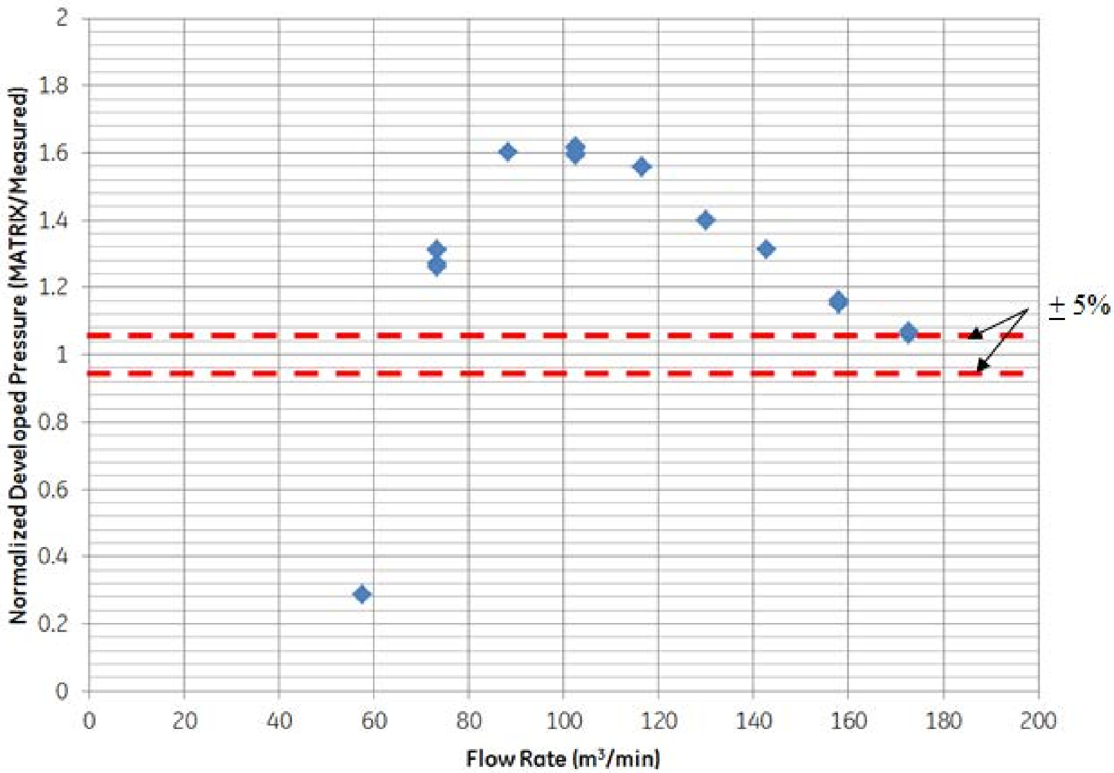

Figure 5-5: Normalized MATRIX/Experimental Data

This discrepancy between the simulated and measured data was analyzed further in order to improve the overall predictability of the MATRIX code.

5.1.4 MATRIX Prediction Improvement by Flow Rate Correction

Section 5.1.1 identified a difference between the MATRIX "flat" velocity profile and the Eckert experimental "turbulent" to "M-shaped" velocity profile. To adjust for the difference, new values for the sodium input or effective flow rates were needed to match the experimental data.

Throughout the process of determining effective flow rates, it was observed that MATRIX was extremely sensitive to any perturbations (negative or positive) of the input flow rate. This is because of the steep slopes of the EM Pump characteristic curves at the main pump operating points (Figure 3-10). Changing the input flow rate by a small amount changes the calculated, developed pressure, depending on where that flow rate is located on the characteristic curve.

The optimal corrected flow rate, which matched the developed pressure for each original flow rate during the trial and error analysis, was obtained. The original (input) flow rate versus the corrected (input) flow rate needed to produce the improved predictions is shown in Figure 5-6. The 2nd, 3rd, and 4th polynomial best fit lines were applied to best predict the corrected flow rates.

It is observed that the corrected flow rate fit lines cross the original flow rate line at about 70 m^3/min, about the cross-over point in Figure 5-4 and for original flow rates larger than 70 m^3/min, the corrected flow rate is greater than the original flow rate. This is consistent with the "turbulent" like velocity profile for higher Reynolds numbers discussed in Section 5.1.1.

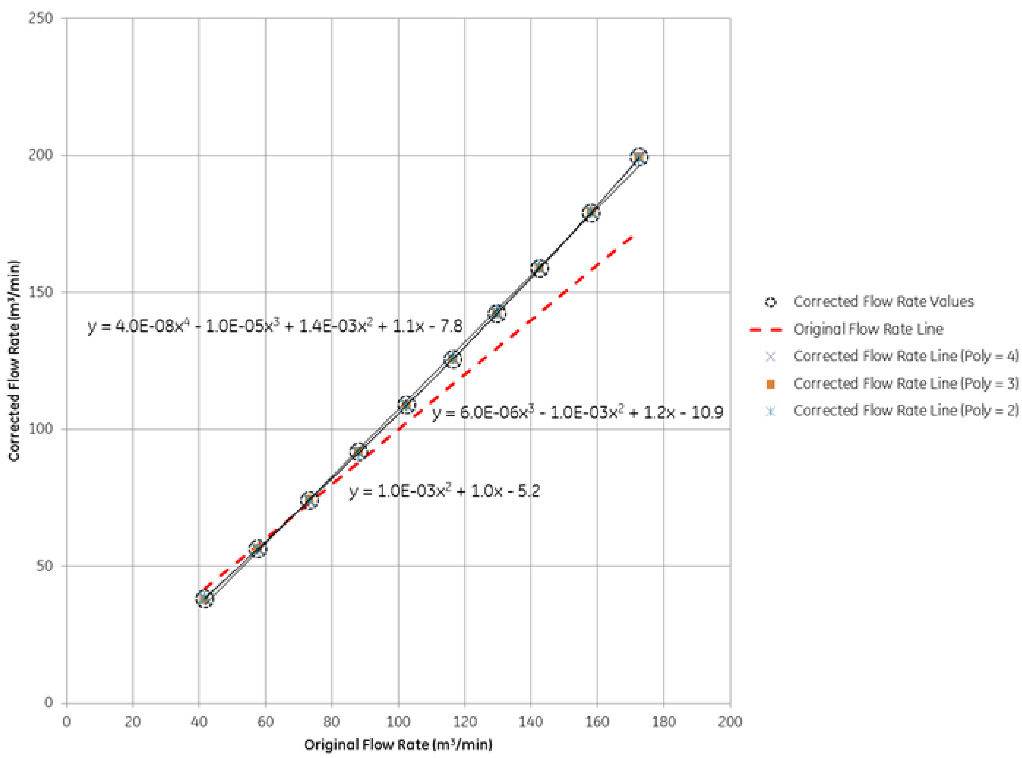

Figure 5-6: MATRIX Flow Rate Correction Equations

The normalized (corrected/original) flow rate curves corresponding to the best fit lines are seen in Figure 5-7, and the corrected flow rates needed in each of the cases do not vary more than ± 15% from the original flow rates.

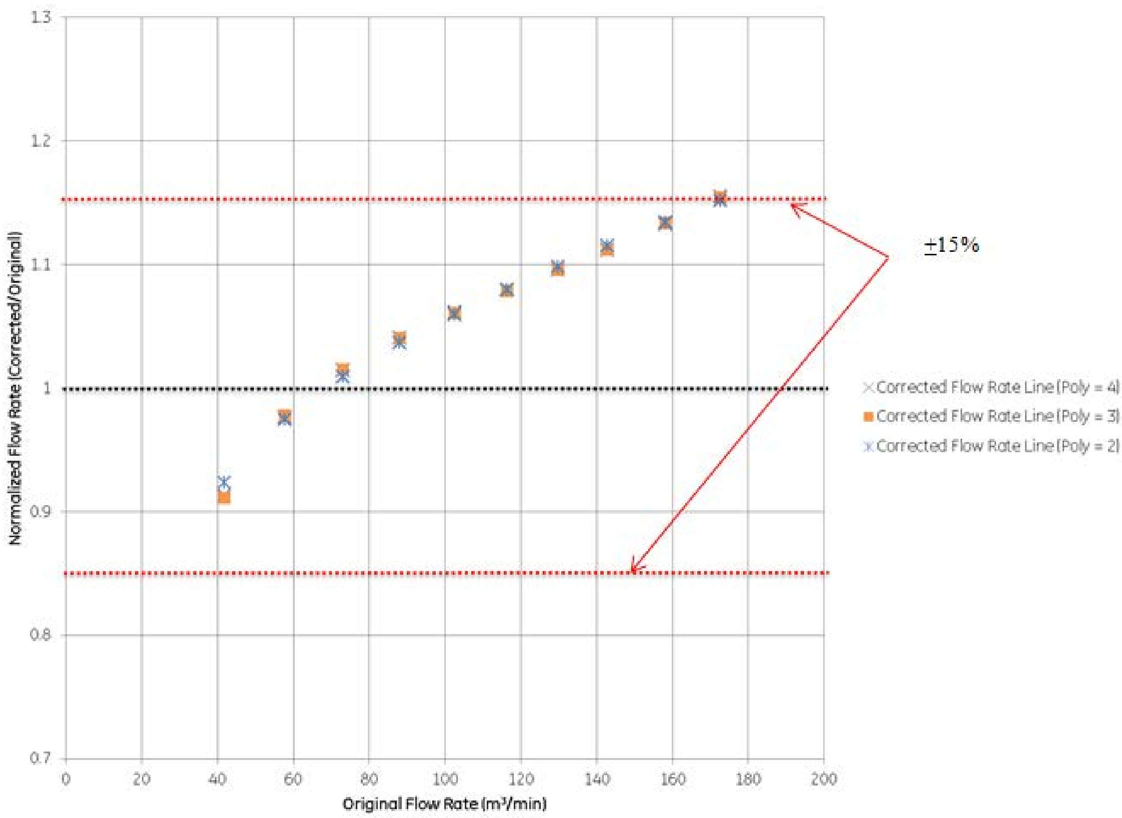

Figure 5-7: MATRIX Correction/Original Flow Rate Normalization

The 2^{nd}, 3^{rd}, and 4^{th} order flow rate correction equations shown in Figure 5-6 were used in the MATRIX Code. These corrections significantly improved the MATRIX developed head prediction, as shown in Figure 5-8.

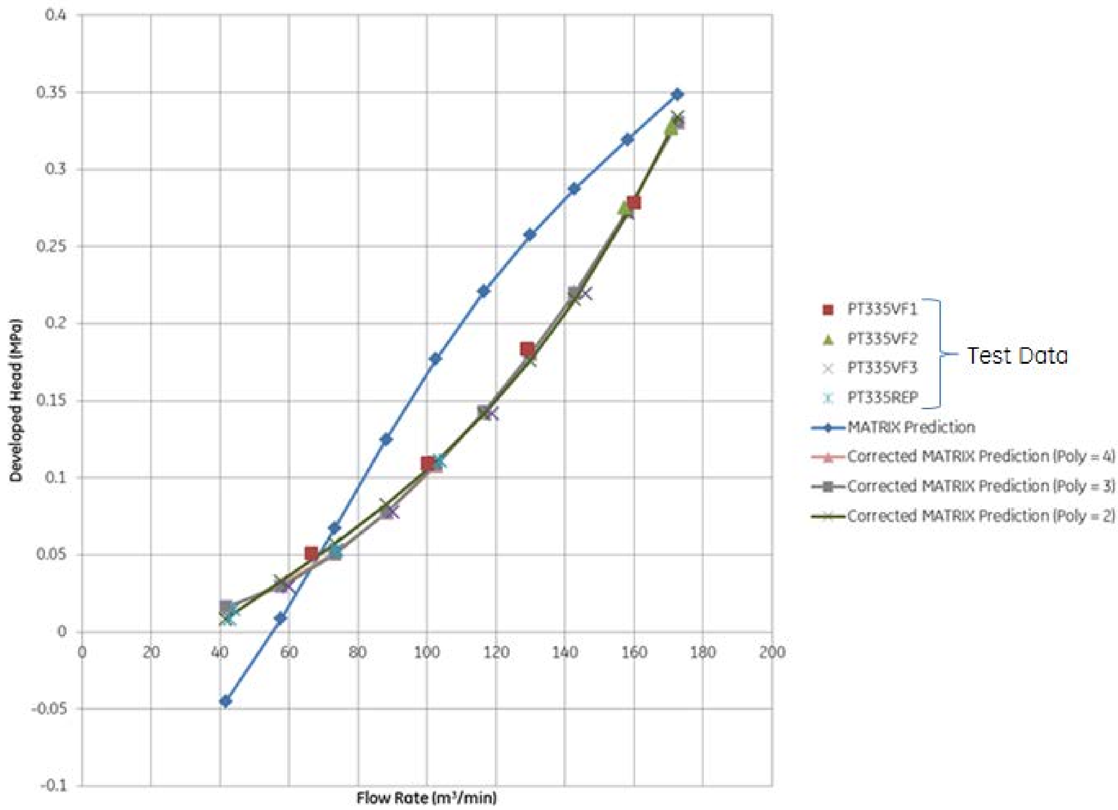

Figure 5-8: Corrected MATRIX Developed Head versus Original Flow Rate

In Figure 5-8, the MATRIX developed head versus flow rate prediction matches the test data with higher order polynomial fits. This improved calculation eliminated the 0.7 multiplier that was employed during the large EM Pump testing, depicted in Figure 3-1, with the 2015 MATRIX model output, more accurately predicting EM Pump characteristics.

The developed pressure using the original (uncorrected), 2nd, 3rd, and 4th order flow correction values were normalized (MATRIX prediction / experimental data). Figure 5-9 shows these results in a normalized format.

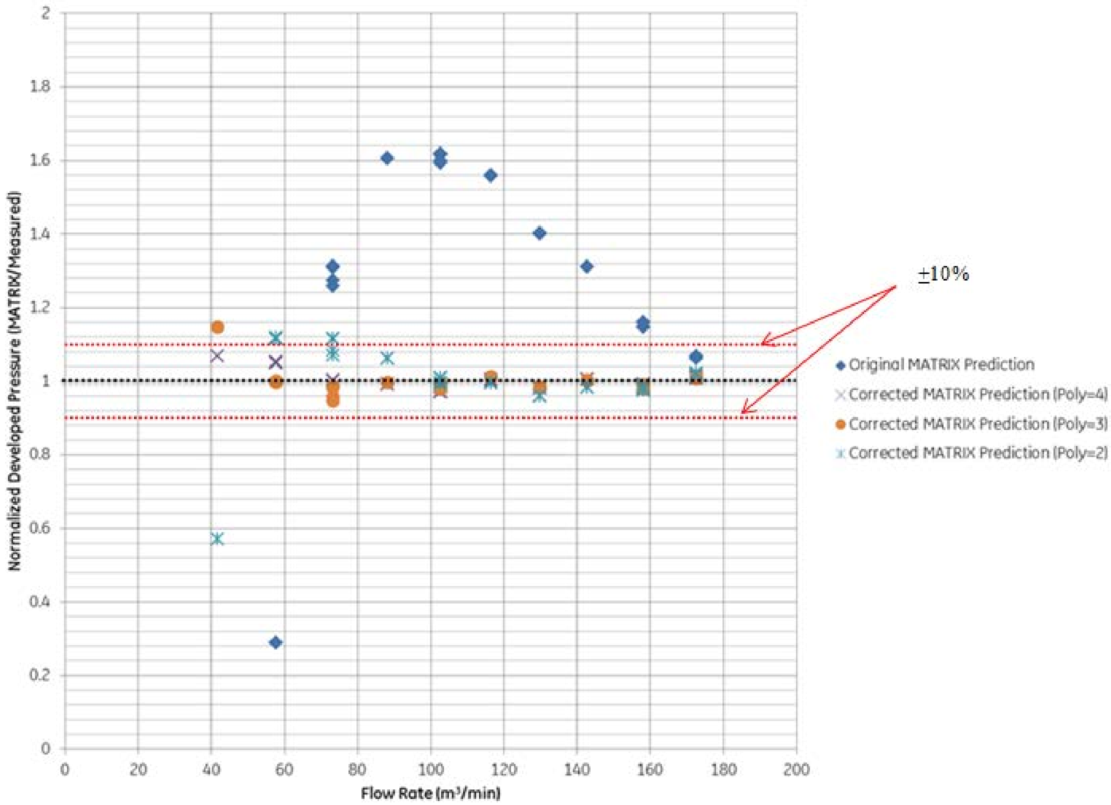

Figure 5-9: Normalized Corrected MATRIX Developed Head versus Original Flow Rate

Figure 5-9 shows that the 4th order polynomial correction equation on the flow rate brings the predicted, developed pressure to be within +10% of the measured data. The lower order flow corrections also provide good overall prediction; however, at the lower flow rates, the 2nd and 3rd order corrections begin to deviate from the normalized +10% band. This is not unexpected since the developed head at lower flow rates is very small, and so the normalized error is magnified.

With the flow correction evaluation complete, Figure 5-10 shows the flow corrected MATRIX pressure-flow map that more accurately depicts conditions for all tested conditions. Additional experimental data could verify that the flow correction is indeed more accurate at different operating points. Figure 5-10 is depicted with the slip values identified.

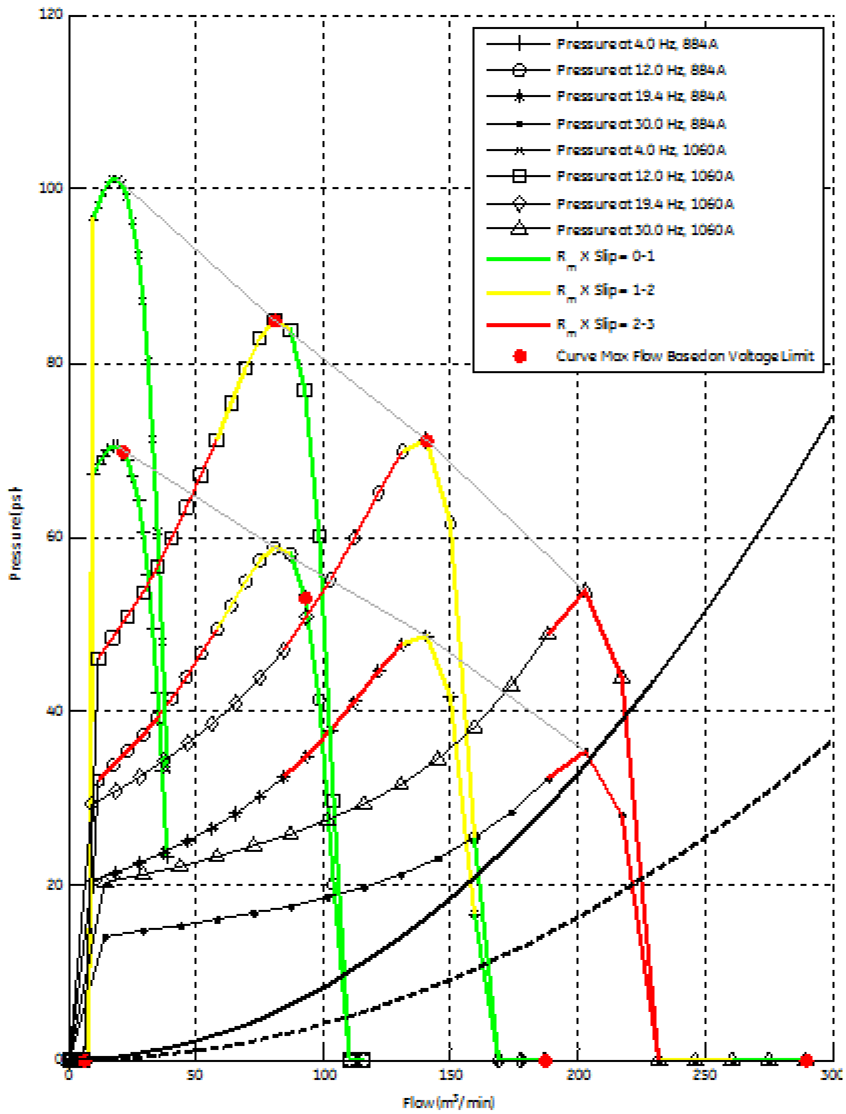

Figure 5-10: 3rd Order Flow Corrected MATRIX Developed Head versus Flow Rate

The green represents where the pump operation is stable. The yellow represents where the pump has the potential for operating without stability issues, and the red represents where the pump may have some flow instabilities, as discussed in Section 3.2.3.

Figure 5-10 shows the main output plot example for the modernized MATRIX software with the flow correction depicting the net developed pressure versus the flow in the EM Pump for eight test cases. Based on these curves, the EM Pump is designed to meet specific pressure and flow requirements of the PRISM reactor system. The dark and dashed curved lines represent the pressure versus flow system curves for the high flow and high flow/bypass loops in the test loop.

5.1.5 Flow Correction Code Improvements

As a result of the successful testing of the flow correction equations, a new variable was added to the DTA structure of the modernized MATRIX code, enabling the user to choose what order of polynomial correction to use. The variable "VDOTCAL" provides the option to turn on/off the flow rate transformation calculation functionality. If this flag is set to "0" then the MATRIX code runs without any correction, but if it is set to be an integer value of 2, 3, or 4, then the corresponding polynomial correction equations are applied to the effective sodium velocity (or "VDOT" in the code), as depicted in Figure 5-11. These flow correction equations adjust the sodium velocity before running through the rest of the MATRIX code. By using a flow correction before running the code, the need for a "0.7" multiplier on the output of the code is eliminated.

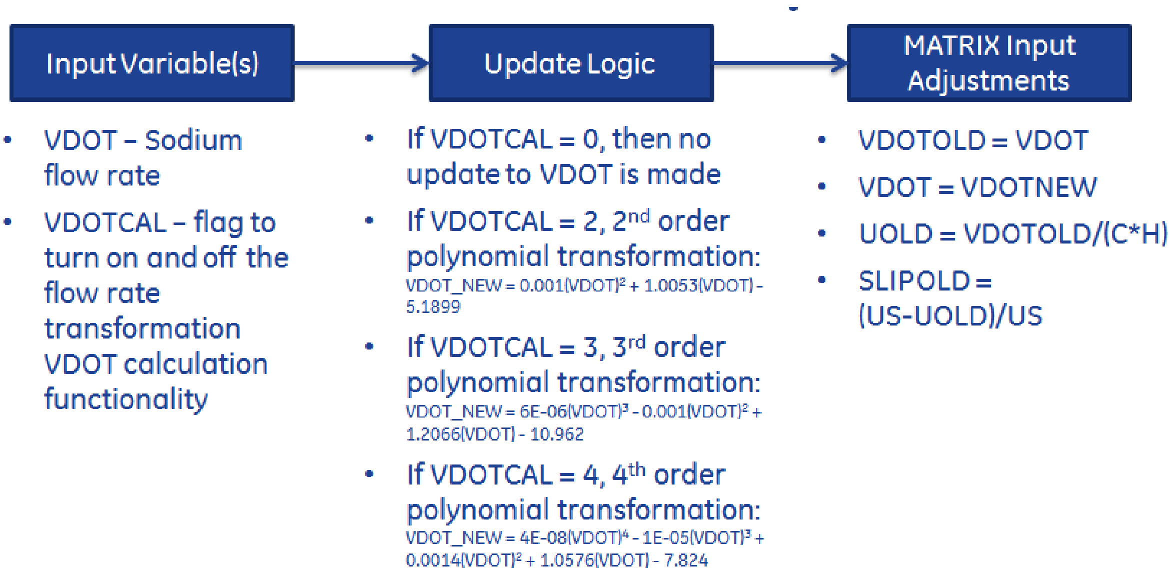

Figure 5-11: MATRIX Flow Correction Options

5.1.6 Flow Correction Improvement Summary

To account for the difference in the "actual" velocity profile and the "flat" velocity profile used in MATRIX, the MATRIX flow inputs were adjusted until the MATRIX predictions matched the experimental test results from the Large EM Pump test data for the range of tests performed. The 2nd, 3rd, and 4th order polynomial fit equations were applied on the original flow data to adjust the input flow values.

This flow correction vastly improves the accuracy of the MATRIX prediction, which now falls within 10% of the experimental pump head values, instead of the more than 30% from the 1999 version. Additional experimental data could improve the accuracy of the prediction.

The impact of flow rate correction on the other functionalities of the modernized MATRIX Code should improve the overall predictive capability of the tool.

The MATRIX code was improved by adjusting the sodium input flow rate value by the VDOTCAL variable, which applies either no correction, or a 2nd, 3rd or 4th polynomial fit to adjust the sodium flow rate. This correction accounts for the differences between the "flat" and the "turbulent" flow velocity profiles expected for high Reynolds numbers in PRISM.

5.2 Material Properties

The materials used, and their physical properties, are important to predict the performance of an EM Pump. During the code modernization, the team discovered the materials and the material properties were built within the code, and could not be easily changed for different pumps or analysis evaluations of material changes. Addition of material properties to the code will allow future EM Pump designers to perform sensitivity and optimization studies on commercial EM Pumps. This addition also allows better thermal analysis optimization to be performed.

The 1999 MATRIX code did not have the ability to update the EM Pump material properties, such as electrical resistivity, thermal expansion, etc., according to the material used for the duct and operating temperatures. Prior to this update or improvement, a pre-processing spreadsheet was used in order to determine changes in dimensions and varying sodium and duct properties (viscosity, resistance, etc.), which depend on operating condition temperatures. These changes then had to be manually entered into the MATRIX input file by the user.

A “MATCAL” variable is added to the MATRIX code which allows the user to turn on/off the material property calculations. The user can choose to calculate the updated duct material properties with the “DUCTMAT” flag, and/or calculate the iron thermal expansion with the “IRONTHE” flag. These flags update the pump material dimensions and properties according to the user input temperatures (TFLUID, TCOPPER, and TIRON).

The added Matrix Code material properties are summarized in Figure 5-12.

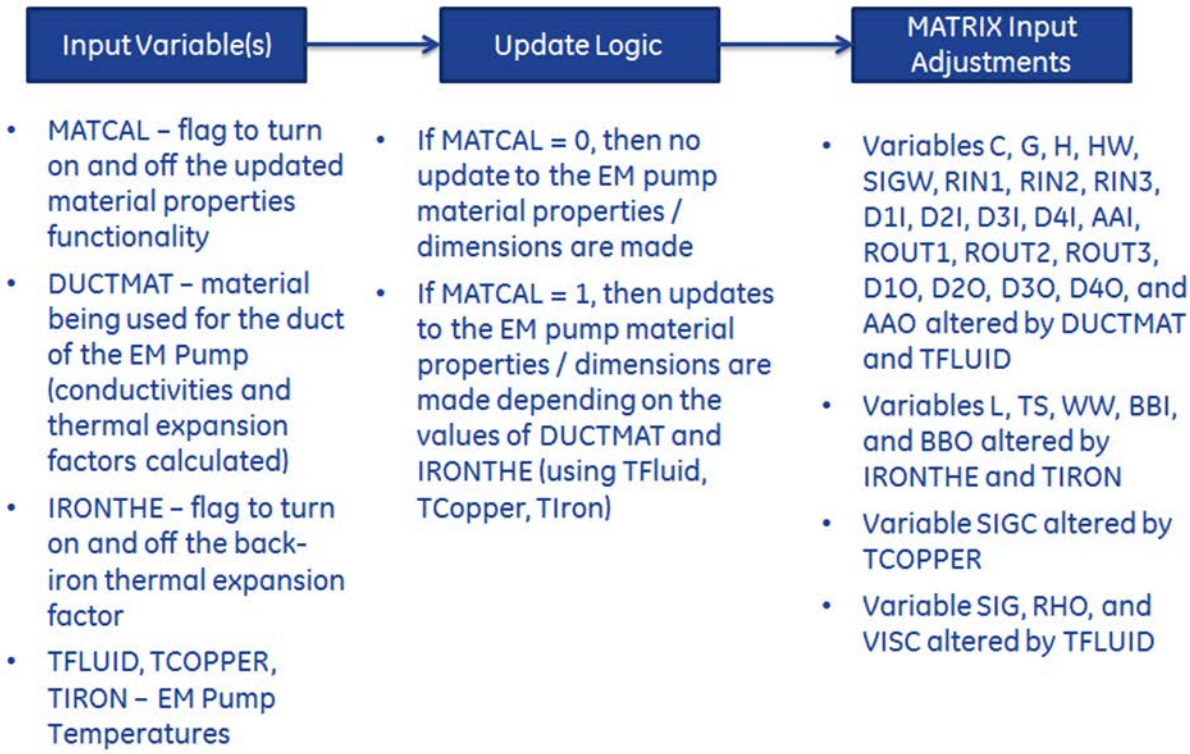

Figure 5-12: MATRIX Material Property Code Improvements

Figure 5-12 shows the variables within MATRIX that can be adjusted due to the material calculations. Figure 5-13 and Figure 5-14 identify the material properties and the equations that were implemented in MATRIX to calculate the properties as a function of temperature.

SIGW →

Duct Material Properties					
Duct Material Resistivity					
Metric Equation Assuming Linear Property Between 400F and 1000F					
EQN:	micro-ohm cm = C0 + C1 x TEMP(°C)				
Matl Index	**1**	**2**	**3**	**4**	**5**
Matl Code	**304 SS**	**316 SS**	**Alloy 625**	**Alloy 718**	**Alloy 600**
C0	70.01256	72.3392	131.4128013	125.2189526	100.3019119
C1	0.066294	0.06858	0.011670823	0.013017456	0.022593516
Duct Thermal Expansion					
EQN:	Mean Thermal Exp. (1/°F) = (A0 + A1 x T + A2 x T^2 + A3 x T^3) x 10^-6				
A0	8.3015	9.05	6.8	6.983333333	7.1
A1	2.63420E-03	-0.001058333	0.001914683	0.001841138	0.001688492
A2	-1.11680E-06	1.5E-06	-2.29167E-06	-1.34325E-06	-7.7381E-07
A3	2.51570E-10	2.08333E-10	1.38889E-09	6.48148E-10	3.47222E-10

Back Iron Thermal Expansion		
EQN:	Mean Thermal Exp. (1/°F) = (A0 + A1 x T + A2 x T^2 + A3 x T^3) x 10^-6	
Matl Index	**1**	**2**
Matl Code	**Iron**	**None**
A0	6.445	
A1	1.25000E-03	
A2	0.00000E+00	
A3	0.00000E+00	

Figure 5-13: Duct and Black Iron Material Property Equations

	Electrical Resistivity of Candidate Conductor Copper Materials			
		Based on 44 m^3/min test pump measurements, reduced by L. Dahl to Siemens/meter		
		Uses inner stator measurements (higher values than outer stator)		
		Conductivity:		
SIGC		Siemens/m = (C0+C1*TF+C2*TF^2) X 1e7 = (1/Ohm-m)		
			C0	4.6180E+00
			C1	-4.1060E-03
			C2	1.0940E-06
	Electrical Resistivity of Sodium			
		Fluid resistivity, micro-ohm-inches		
		Eq'n from Std. FFTF Values..., WHAN-D-3		
SIG		Micro-Ohm-inches = C0+C1*TF+C2*TF^2		
			C0	2.9140E+00
			C1	4.2200E-03
			C2	4.2280E-06
	Density of Sodium			
RHO		lbm/ft^3 = C0+C1*TF+C2*TF^2+C3*TF^3		
			C0	5.9566E+01
			C1	-7.9504E-03
			C2	-2.8720E-07
			C3	6.0350E-11
	Viscosity of Sodium			
VISC		lb/hr-ft = C0*10^(C1/TR) / (TR^C2)		
			C0	1.0479E+01
			C1	3.9717E+02
			C2	4.9250E-01

Figure 5-14: Copper and Sodium Material Property Equations

All temperatures used for the MATRIX input files are entered in Kelvin (K). Temperatures for SIGW and SIGC presented in Figure 5-13 and Figure 5-14 are in degree Celsius, whereas for other variables the temperatures are in degrees Fahrenheit. The code automatically performs the necessary conversions to the proper units prior to other MATRIX calculations.

These material properties' corrections as implemented were validated. EM Pump dimensions can now be entered in the input file, and MATRIX will update them according to the type of material used for the duct and the operating temperatures.

Figure 5-15 shows a comparison of the developed pressure head as a function of flow rate. This compares the previous method of spreadsheet pre-processing (blue line-circles) of materials before running MATRIX to the material correction module added within MATRIX. In this validation, 304 Stainless Steel was used with an outer duct temperature of approximately 600 K. The Figure 5-15 comparison validates the MATRIX Code materials enhancement with minor differences attributed to complier variations.

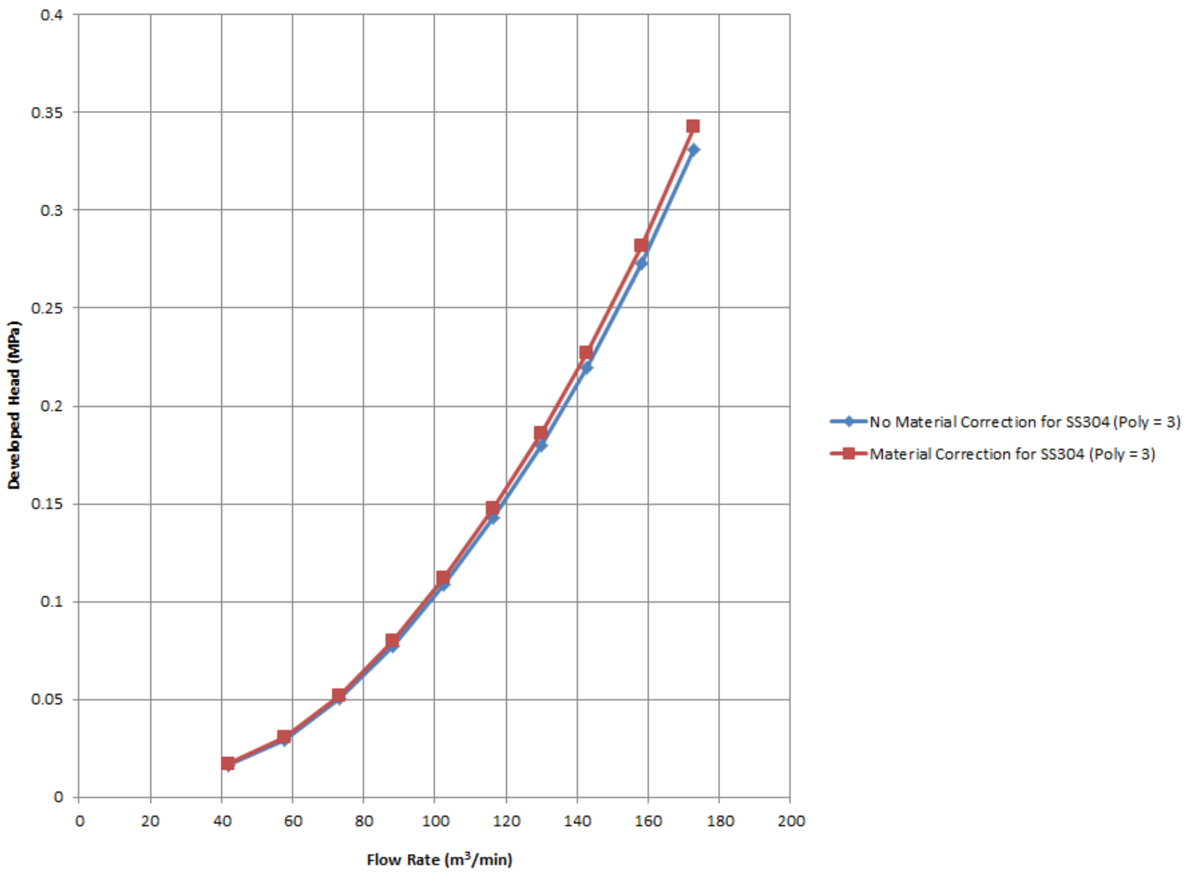

Figure 5-15: Developed Head versus Flow Rate for Material Corrections

5.2.1 Material Properties Summary

The Matrix code updated for material properties includes 1) the thermal expansion of duct and black iron materials, 2) the electrical resistivity of copper conductor materials, duct material, and sodium and 3) the density and viscosity of sodium. The code improvements moved the material properties codes from the input files to variables within the code that can be more easily altered for various materials.

5.3 Thermal Analysis

The MATRIX code was further improved by incorporating an internal thermal analysis tool. The thermal tool calculates the temperature profile within the copper coils (where most of the heat is generated), lamination, and duct. The main goal of developing this thermal analysis MATRIX code upgrade was to obtain the maximum temperature in the copper to better predict the insulation performance as a function of temperature. Such an analysis had never been implemented within the MATRIX code until this project. In the past, heat transfer analysis of the 160 m^3/min EM Pump used for the intermediate heat transfer system (IHTS) was performed using the Advanced General Electric Network Analyzer (AGENA) program (Salamah, *et al*., 1991). AGENA is a general purpose code that uses a thermal network method. AGENA was not created specifically for EM Pump analysis, but could be used for such applications if configured appropriately with nodes and connections for a half-segment inner stator lamination block as shown in Figure 5-16. The nodes have both heat capacitance and heat generation capabilities. The connectors transfer heat between the nodes by conduction and/or by radiation.

5.3.1 AGENA Model

The geometric profile in Figure 5-16 depicts the center of the inner stator on the right and the heat sink (the flowing sodium, Na) on the left. In all subsequent figures, the heat sink is depicted on the right.

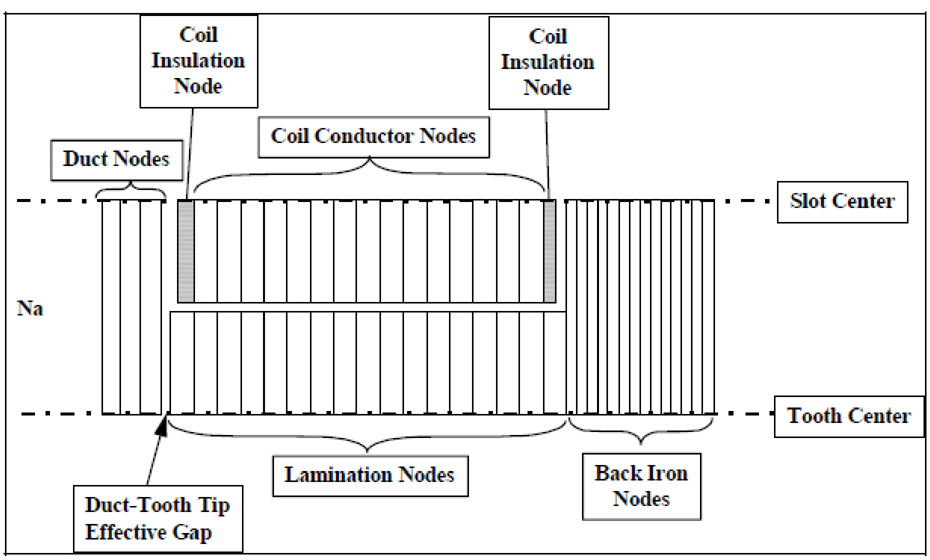

Figure 5-16: AGENA Thermal Model of EM Pump Inner Stator

The temperature profile of the copper block, lamination, and inner duct wall as a function of radius are plotted from the AGENA calculations (Fanning, 2002), as shown in Figure 5-17.

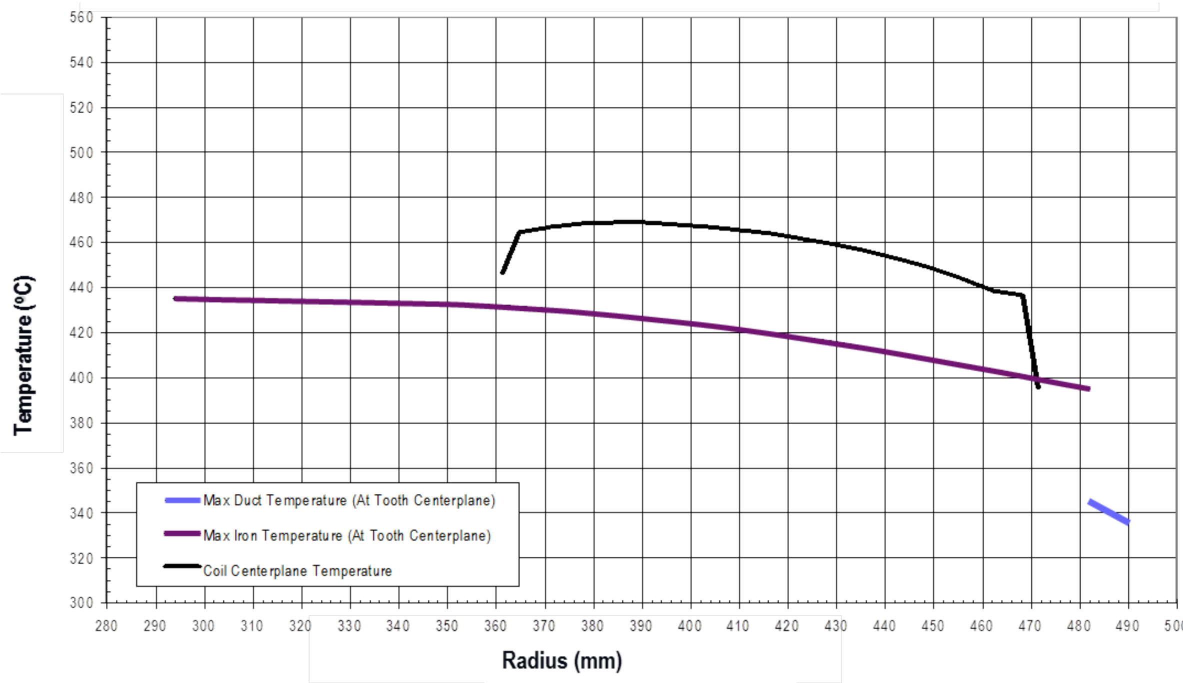

Figure 5-17: AGENA Analysis Results

The temperature profile shows that heat is generated in the copper coils, and the coils are hotter towards the center (left) and cooler toward the sodium heat sink (right). The heat is transferred by conduction from the hotter copper coils to the cooler lamination block, which dissipates the heat across the entire lamination block. The lamination block temperature profile follows the same pattern as the copper coils, hotter towards the center and cooler towards the sodium heat sink. The lamination block maintains the thermal balance between the copper coils and the heat sink. Heat is removed from the lamination block and transferred by conduction through the duct wall to the sodium heat sink.

Although AGENA provides a detailed thermal analysis model, it is a general purpose, transient heat transfer program. The proper values of the effective, thermal resistance, or conductance between the nodes for nodalization, are user-defined inputs. This creates significant uncertainties in the use of the program for direct MATRIX application, and because of its general purpose capabilities, implementing the AGENA program in MATRIX was not considered because of the large scope increase this would cause in the project. Due to these issues, a steady state heat transfer analysis capability within the MATRIX code was developed. MATRIX now provides a single-package EM Pump analysis tool including the capability of thermal analysis.

5.3.2 MATRIX Thermal Analysis Model Development

The MATRIX model developed uses a more fundamental approach and, although it may be simpler than the analysis performed in the past, it provides a better understanding and control of the thermal analysis of the EM Pump. In addition, it provides the opportunity for knowledge capture and transfer from a generation of experienced engineers to the next generation of early career engineers. This is in alignment with technical Objective 3 in the original DOE proposal for the next generation EM Pump users.

Heat transferred in the radial direction assumes conduction. Conduction starts from the back of the stator (represented by the dashed line to the left of N-1 node) and moves outward in the axial direction from the copper block, through the ground insulation, into the lamination. Figure 5-18 shows a diagram of a general radial heat transfer analysis of an interior node N. The term q''' represents the uniform heat generation rate per unit volume in each node; q''_N represents the radial heat flux entering an interior node N; and q''_{N+1} represents the radial heat flux leaving the same interior node N. The radial distance from the center line to node N is represented by R_N , and the length of the node is represented by ΔR.

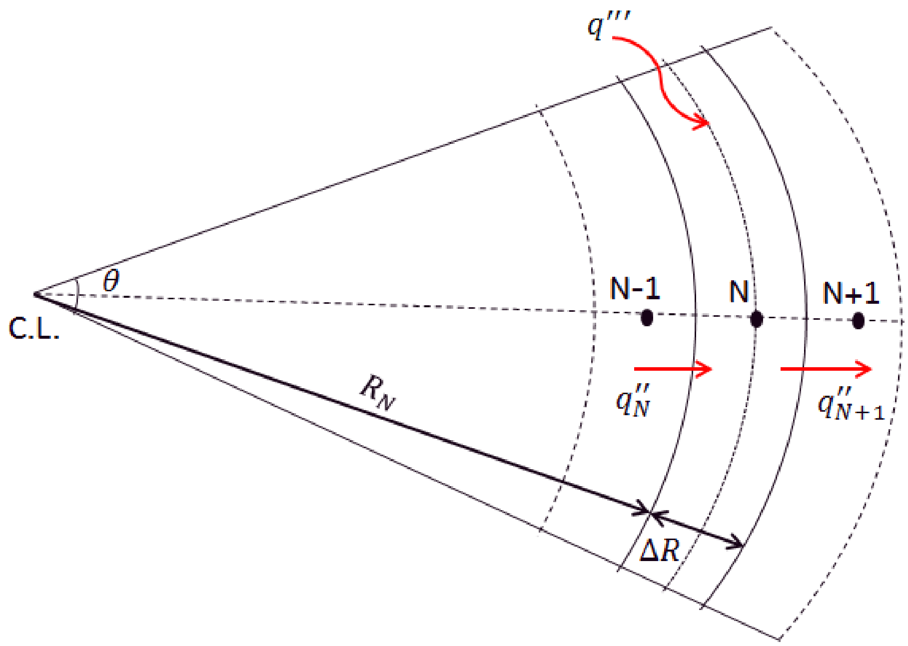

Figure 5-18: Radial Heat Transfer Analysis

A cross-section diagram of the inner stator copper block, the insulation, the iron lamination, and the inner duct used in the steady state heat transfer analysis is shown in Figure 5-19. The centerline (CL) is a gas-filled void where power and instrumentation cables (not shown or modeled) are routed upward out of the pump, and the heat sink (the flowing sodium) is on the right side of the inner duct. Due to the stator's symmetrical characteristics, a Finite Difference heat conduction model was applied at the slot center, indicated by the red boxed region in the diagram. The Finite Difference model calculates the temperature at each node.

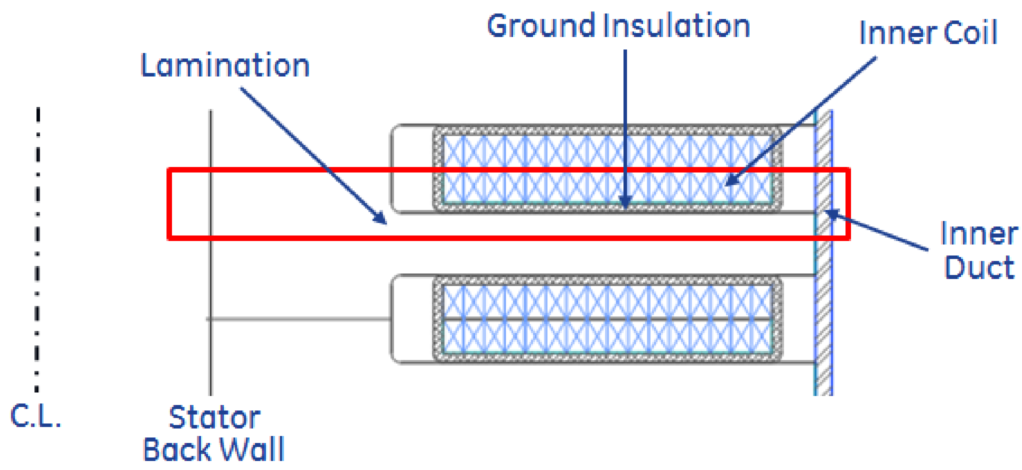

Figure 5-19: Diagram of Inner Stator Coil, Ground Insulation, Lamination, and Duct

The cross-section diagram was divided into Regions A, B, C, and D shown in Figure 5-20 to simplify code development. Each of these regions is covered in subsequent Sections 5.3.3 through 5.3.7.

- Region A – Lamination Yoke: is the back of the lamination where different lamination segments are joined together, allowing the lamination teeth to form the slot into which the copper blocks are set.
- Region B consists of two sections, the Copper Block and the Lamination Block.
  - o Region B – Copper Block: is where the heat is generated due to the large electrical current (I^2R losses) that need to be dissipated.
  - o Region B – Lamination Block: Conducts the heat generated in the copper block through the lamination tooth to the Inner duct wall.
- Region C – Lamination Tooth Tip: Region C is the lamination tooth tip that extends past the copper block, and is in contact with the inner duct wall. This region was considered separate from Region B – Lamination Block because it is not in contact with the copper block.
- Region D – Inner Duct Wall: is the inner duct wall between the lamination tooth tip and the liquid sodium, which is the heat sink. The inner duct wall is the barrier between the sodium and the copper blocks of the pump.

Heat generated in the copper block is transferred via conduction to the lamination tooth through the inner duct wall and to the liquid sodium. Radial gaps between the copper conductor and both the lamination yoke and the inner duct wall are necessary to allow for expansion of the copper block, due to different coefficients of thermal expansion between the copper block and the lamination tooth. Heat transfer across these gaps would be through radiative heat transfer, which is (factors of magnitude) less efficient than conductive heat transfer and currently neglected in the model.

The length and the number of nodes for each region are user inputs. The boundary conditions for the model are the heat generation rates per unit volume in the copper block, lamination, and inner duct wall, and the temperature of the liquid sodium flowing in the duct. The heat generation rates in the copper block, due to the large electric current, and the inner duct wall are calculated by MATRIX whereas the heat generation rate in the lamination is a user input.

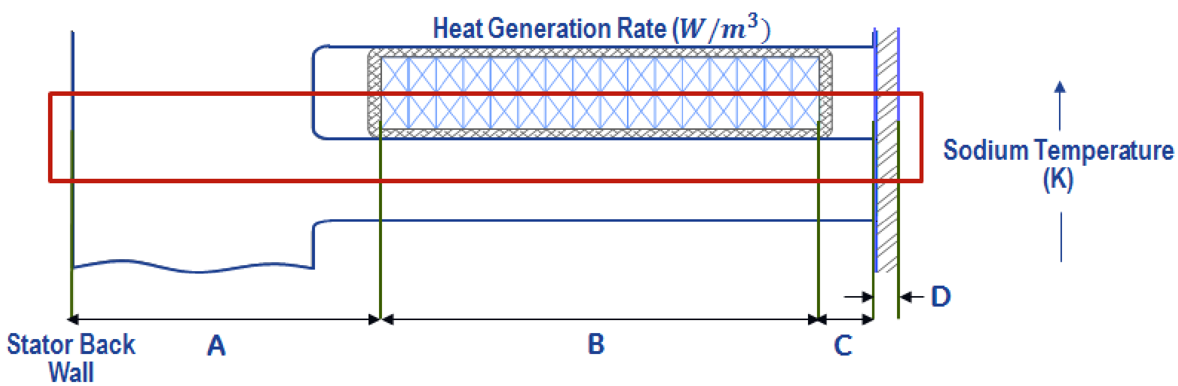

Figure 5-20: Diagram of Different Regions Used in Thermal Analysis

A Finite Difference model was developed for each region so the temperature profiles could be calculated. The following sections describe the heat transfer analysis performed for each region.

5.3.3 Region A – Lamination Yoke: Thermal Analysis Model

Figure 5-21 illustrates the heat transfer model for the first node of the lamination yoke, beginning at the stator back wall indicated by the dotted line. The height, Δz_L, of each node in Region A was assumed to be the same as the height of each lamination node in Regions B and C, providing an approximation of the thermal analysis model for the lamination yoke area. The term R_{NA} is the radial distance from the center line to the node, and ΔR_A is the length of each node in Region A, which is determined by the total length of the lamination in this region, and the number of nodes selected. For this report, Region A was analyzed with 20 nodes.

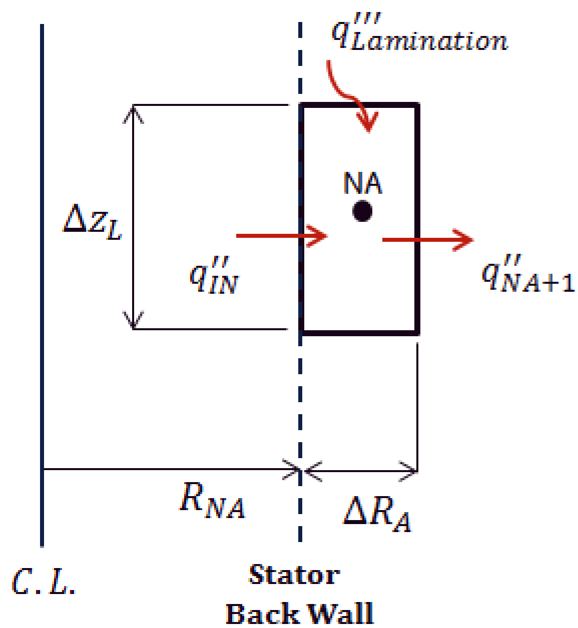

Figure 5-21: Region A – Lamination Yoke: Thermal Analysis for the First Node

Equation 5.3 models the heat transfer in the first node, where the sum of the radial heat flux into the node and the heat generation rate of the lamination, $q'''_{Lamination}$, in the node is equal to the sum of the radial heat flux leaving the node. A similar analysis was performed for the nodes in Regions C and D. The left hand (first node) boundary condition q''_{IN} is set to zero to represent an adiabatic or fully-insulated boundary condition.

$$q''_{IN}\Delta z_L R_{NA} 2\pi\left(\frac{\theta}{360°}\right) + q'''_{Lamination}\Delta z_L \Delta R_A\left(R_{NA} + \frac{\Delta R_A}{2}\right)\left(\frac{\theta}{360°}\right) = q''_{NA+1}\Delta z_L(R_{NA} + \Delta R_A)2\pi\left(\frac{\theta}{360°}\right) \quad (5.3)$$

Using Fourier's law of heat conduction, i.e. $q'' = -k\frac{\partial T}{\partial R}$, a general expression that models the heat transfer in the first node of the lamination in Region A was developed. The term k_I in the general expression in Equation 5.4 is the thermal conductivity of the lamination.

$$-T_{NA}\left[\frac{k_I \Delta z_L (R_{NA}+\Delta R_A)}{\Delta R_A}\right] + T_{NA+1}\left[\frac{k_I \Delta z_L (R_{NA}+\Delta R_A)}{\Delta R_A}\right] = -q'''_{Lamination}\left[\Delta z_L \Delta R_A \left(R_{NA}+\frac{\Delta R_A}{2}\right)\right] \tag{5.4}$$

A similar analysis was performed for the interior and last nodes of the lamination for Region A. Figure 5-22 shows the modelling of the inner nodes of Region A.

.

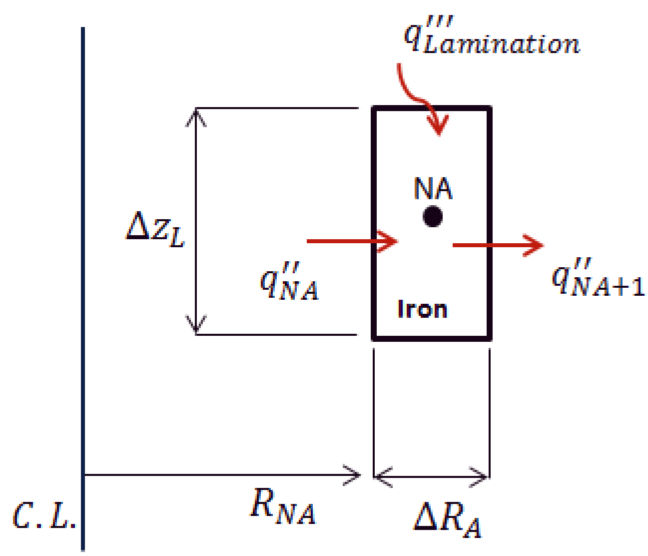

Figure 5-22: Region A – Lamination Yoke: Thermal Analysis for an Interior Node

Equation 5.5 is the heat transfer equation for the interior nodes of the lamination in Region A.

$$T_{NA-1}\left[\frac{k_I \Delta z_L R_{NA}}{\Delta R_A}\right] - T_{NA}\left[\frac{k_I \Delta z_L R_{NA}}{\Delta R_A} + \frac{k_I \Delta z_L (R_{NA}+\Delta R_A)}{\Delta R_A}\right] + T_{NA+1}\left[\frac{k_I \Delta z_L (R_{NA}+\Delta R_A)}{\Delta R_A}\right] = -q'''_{Lamination}\left[\Delta z_L \Delta R_A \left(R_{NA}+\frac{\Delta R_A}{2}\right)\right] \tag{5.5}$$

Figure 5-23 shows the model for the last node in Region A. The heat flux leaving the last node, q''_{OUT}, enters the first node of the lamination in Region B.

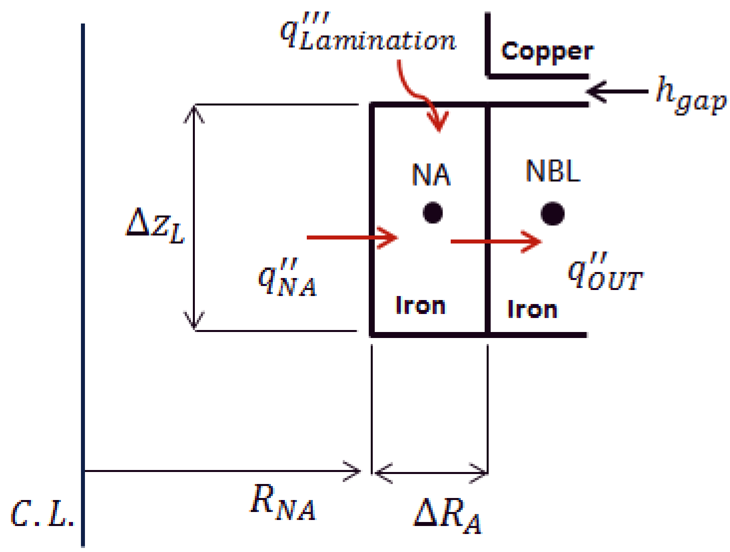

Figure 5-23: Region A – Lamination Yoke: Thermal Analysis for the Last Node

In order to account for non-uniform noding in the lamination between Regions A and B, Equation 5.6 models the heat transfer in the last node of Region A.

$$q''_{OUT} = -k_I \left(\frac{T_{NB(1)} - T_{NA}}{\frac{\Delta R_B}{2} + \frac{\Delta R_A}{2}} \right) = -2k_I \left(\frac{T_{NB(1)} - T_{NA}}{\Delta R_B + \Delta R_A} \right) \tag{5.6}$$

Equation 5.7 represents the general expression for the last node of the lamination yoke in Region A. The term $T_{BL(1)}$ is the temperature in the first node of the lamination in Region B.

$$T_{NA-1}\left[\frac{k_I \Delta z_L R_{NA}}{\Delta R_A}\right] - T_{NA}\left[\frac{k_I \Delta z_L R_{NA}}{\Delta R_A} + \frac{2k_I \Delta z_L (R_{NA} + \Delta R_A)}{\Delta R_B + \Delta R_A}\right] + T_{BL(1)}\left[\frac{2k_I \Delta z_L (R_{NA} + \Delta R_A)}{\Delta R_B + \Delta R_A}\right] = -q'''_{Lamination}\left[\Delta z_L \Delta R_A \left(R_{NA} + \frac{\Delta R_A}{2}\right)\right] \quad (5.7)$$

5.3.4 Region B – Copper Block: Thermal Analysis Model

Figure 5-24 shows the model of the first node of the Region B Copper Block. Heat is transferred in the radial direction, represented by the q''_{NBC+1} and q''_{IN} terms, and in the axial direction into the lamination, represented by the q''_{C-L} term. The q'''_{Copper} term is the heat generation rate per unit volume in the copper block, from the electric current flow. The height of the copper block region is represented by the Δz_C term, and the radial distance from the center line to each node in Region B is represented by R_{NB}. The term ΔR_B is the length of each node, which is the same for both the lamination and copper block in Region B and the user input for the number of nodes. Terms with the subscript NBC represent the copper block, and terms with the subscript NBL represent the lamination in this region.

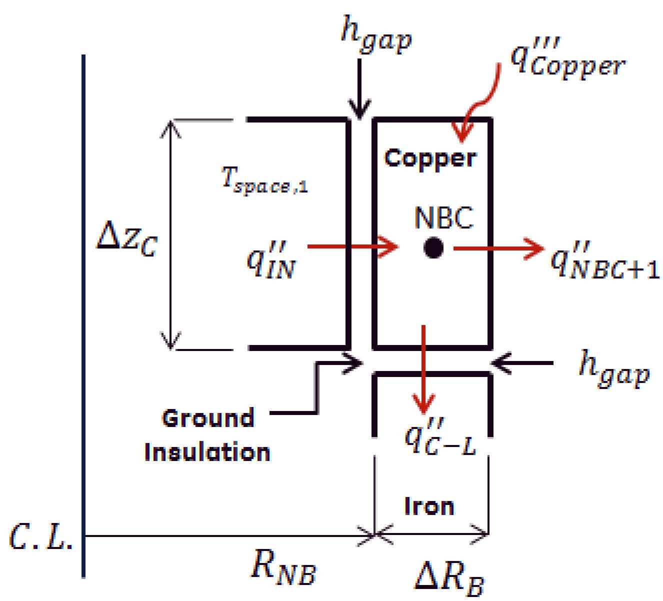

Figure 5-24: Region B – Copper Block: Thermal Analysis for the First Node

As shown in Figure 5-20, the copper coil or block is encased by ground insulation. The ground insulation serves two purposes. The first is to provide electrical insulation between the copper coils and the lamination block. The second is to provide a thermal pathway for the heat generated in the copper coils, due to electrical current, to be dissipated to the lamination block. From the thermal modelling perspective the ground insulation is identified as h_{gap}. The term h_{gap} identified in Figure 5-24 is used for the effective heat transfer coefficient of the ground insulation that surrounds the copper coil or block. The heat transfer coefficient or thermal conductivity is the ability of a material to conduct heat from the copper block to the lamination. The thermal conductivity of several different materials was experimentally determined as part of other tasks in this project at GRC. The results of these experiments are shown in Figure 5-25.

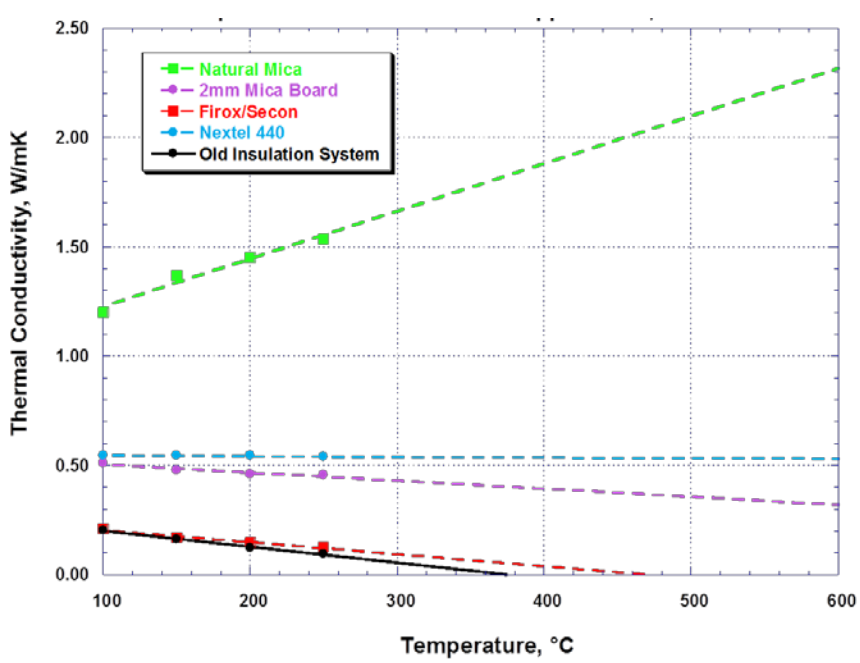

Figure 5-25: Thermal Conductivity of Tested Insulation Materials

Figure 5-25 shows the measured thermal conductivity of various individual insulation components from the prior insulation system. Firox tape and Secon-5 binder were tested together since Secon-5 is the binder used for Firox tape. Nextel 440 tape (no longer commercially available) was salvaged from coils of the large EM Pump test, cleaned and re-used. Data was collected up to the instrument limit (~250°C), but dashed lines are provided to extrapolate the trends out to EM Pump operating hot-spot temperatures of 530-600°C.

The entire benchmark insulation system was tested (shown in black); that system has the lowest thermal conductivity. This was expected since the insulation system consists of many layers, and the multitudes of layers and interfaces are detrimental to good heat flow. It was shown that the Secon-5 binder cracks noticeably after curing due to miss-match in the coefficient of thermal expansion. The Firox/Secon has comparable thermal conductivity and is the rate-limiting factor in the design; again, not unexpected, due to the multitude of interfaces and layers.

The best thermal conductivity was found with the native mica sheets, extrapolating out to about 2 W/mK at EM Pump operating hot spot temperatures. Being in a series path, unfortunately, the component layer with the poorest thermal conductivity or largest thermal resistance dominates the thermal resistance of the entire insulation system. Thus, though native mica has a thermal conductivity that is four times larger, that benefit is never realized.

Shown in purple is the thermal conductivity data for the Silicon Bonded Mica Hard Board (SBMHB), the proposed material in the slot-liner approach. The thermal conductivity of this material, while still low, is at least triple the thermal conductivity of the benchmark Secon-5 insulation system - a beneficial improvement.

The experimental data, identified above, was used to back up the thermal analysis used for MATRIX calculations as explained below in support of Figure 5-24.

The h_{gap} used in the calculations, depicted in Figure 5-24, was 0.18 W/m-K, which is in line with experimental data shown in Figure 5-25. This is more than the benchmark Secon-5 material, but less than the SBMHB, providing a conservative analysis.

The steps are shown in Equations 5.8 through 5.10 for taking into account the different layers of insulation material that makes up the ground insulation. These layers include the strand insulation, inner coil wrap, and primary ground wall insulation. The term $\delta_{GD,layer}$ represents the thickness of an insulation layer and the term $k_{GD,layer}$ represents the thermal conductivity of the insulation material used in a layer. For the model developed, a total ground insulation thickness of 0.003048 m and an effective thermal conductivity of 0.18 W/m-K were used. Note that the effective heat transfer coefficient for the ground insulation is assumed to be the same for all sides of the copper block.

$$h_{gap} = \frac{k_{GD,eff}}{\delta_{GD,total}} \tag{5.8}$$

$$h_{gap} = \frac{\left(\dfrac{\delta_{GD,total}}{\dfrac{\delta_{GD,layer1}}{k_{GD,layer1}} + \dfrac{\delta_{GD,layer2}}{k_{GD,layer2}} + \dfrac{\delta_{GD,layer3}}{k_{GD,layer3}}} \right)}{\delta_{GD,total}} \tag{5.9}$$

$$h_{gap} = \left(\frac{\delta_{GD,layer1}}{k_{GD,layer1}} + \frac{\delta_{GD,layer2}}{k_{GD,layer2}} + \frac{\delta_{GD,layer3}}{k_{GD,layer3}} \right)^{-1} \tag{5.10}$$

Equation 5.11 is written to model the heat transfer in the first node of the copper block, where the sum of the radial heat flux entering the node and the heat generation rate in the copper block is equal to the sum of the radial and axial heat fluxes leaving the node of the copper block.

$$\begin{aligned} q''_{IN} \Delta z_C R_{NB} 2\pi \left(\frac{\theta}{360°} \right) + q'''_{Copper} \Delta z_C \Delta R_B \left(R_{NB} + \frac{\Delta R_B}{2} \right) 2\pi \left(\frac{\theta}{360°} \right) \\ = q''_{C-L} \Delta R_B \left(R_{NB} + \frac{\Delta R_B}{2} \right) 2\pi \left(\frac{\theta}{360°} \right) \\ + q''_{NBC+1} \Delta z_C (R_{NB} + \Delta R_B) 2\pi \left(\frac{\theta}{360°} \right) \end{aligned} \tag{5.11}$$

Equation 5.12 is the general expression for the first node in the copper block, used to obtain the temperature profile of the coil. In the first node, there is heat flux from the space at the lateral sides of the copper block. The $T_{space,1}$ term is the temperature in the space inside the gap at the lateral side of the copper block, and it was implemented in the model as the average of the temperature of the first node in the copper, $T_{NBC(1)}$, and the temperature of the first node in the lamination, $T_{NBL(1)}$, located below the block, as defined in Equation 5.13.

$$-T_{NBC}\left[h_{gap}\Delta z_C R_{NB}+\frac{k_{eff}\Delta z_C(R_{NB}+\Delta R_B)}{\Delta R_B}+h_{gap}\Delta R_B\left(R_{NB}+\frac{\Delta R_B}{2}\right)\right]$$
$$+T_{NBC+1}\left[\frac{k_{eff}\Delta z_C(R_{NB}+\Delta R_B)}{\Delta R_B}\right]+T_{NBL(1)}\left[h_{gap}\left(R_{NB}+\frac{\Delta R_B}{2}\right)\Delta R_B\right] \quad (5.12)$$
$$+T_{space,1}\left[h_{gap}\Delta z_C R_{NB}\right]=-q'''_{Copper}\left[\Delta z_C\left(R_{NB}+\frac{\Delta R_B}{2}\right)\Delta R_B\right]$$

$$T_{space,1}=\frac{\left(T_{NBC(1)}+T_{NBL(1)}\right)}{2} \quad (5.13)$$

The term k_{eff} in the general equation represents the effective thermal conductivity of the copper block, including the insulation between the coil strands, which is determined from Equation 5.14 under the physical law that the resistances are additive.

$$k_{eff}=\frac{\delta_{copper+insulation}}{\frac{\delta_{copper}}{k_{copper}}+\frac{\delta_{insulation}}{k_{insulation}}} \quad (5.14)$$

The radial thickness of a copper strand, δ_{copper}, is 6 mm, the thickness of the insulation between the coil strands, $\delta_{insulation}$, is 0.127 mm and the thermal conductivity of copper, k_{copper}, is 370 W/m-K. The thermal resistance of the insulation that is installed between the coil strands in the copper block was determined from Equation 5.15.

$$R_{th,insulation}=\frac{\delta_{insulation}}{k_{insulation}} \quad (5.15)$$

The thermal conductivity for the insulation was calculated based on the thermal insulation resistance of 0.005 m^2-K/W. In contrast to the thermal conductivity values depicted in Figure 5-25, which are independent of insulation thickness, the thermal resistance, $R_{th,insulation}$, values are thickness dependent. The thermal resistivity of several different materials was experimentally determined as part of other tasks in this project at GRC.

A plot of the thermal resistance of the benchmark insulation materials and materials used for the slot-liner approach is shown in Figure 5-26.

.

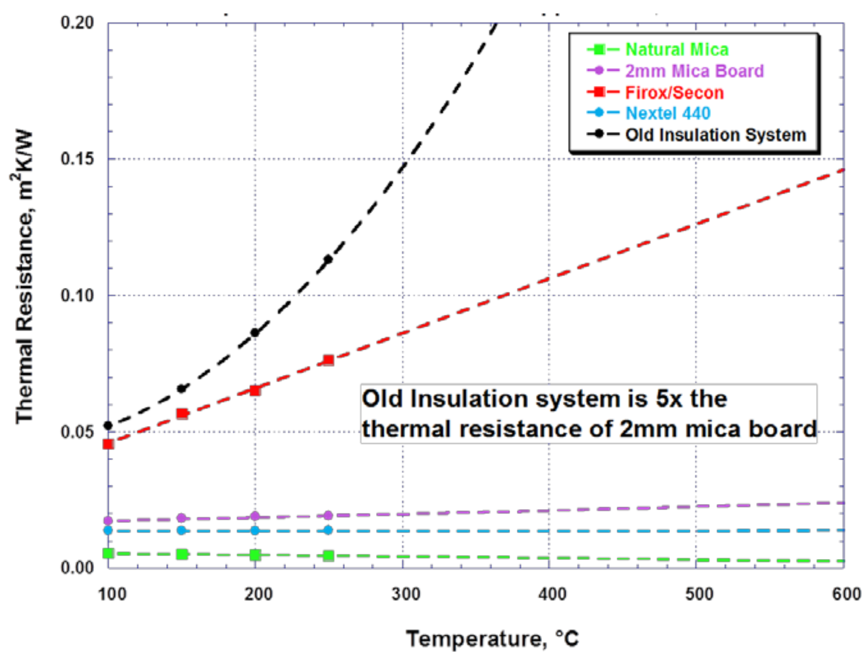

Figure 5-26: Thermal Resistance of Tested Insulation Materials

As with Figure 5-25, the black line in Figure 5-26 represents the benchmark Secon-5 material and the purple the proposed SBMHB slot liner material. Comparing the black to the purple lines, the expected improvement in heat dissipation is appreciable. Specifically, it is expected that the new design would have about five times' better thermal conduction than the original design. The thermal resistance of the slot-liner system is only about 20% of the thermal resistance that the original pump system demonstrated. Since the slot-liner approach employs a material with a much improved dielectric strength, it is anticipated that the total ground wall insulation thickness could be reduced accordingly.

Figure 5-25 and Figure 5-26 were used to obtain the thermal conductivity and resistance values of the insulation material in between the copper strands and used in Equation 5.14 (keff) to find the effective thermal conductivity in the copper block, which has a value of 1.22 W/m^2-K.

A similar heat transfer analysis was performed for the interior and last nodes of the copper block. Figure 5-27 illustrates a diagram of the heat transfer analysis for an interior node.

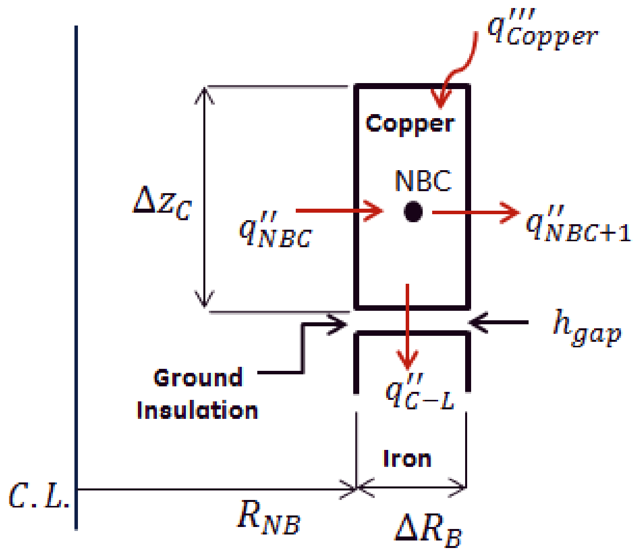

Figure 5-27: Region B – Copper Block: Thermal Analysis for an Interior Node

Equation 5.16 is the general expression for an interior node N_{BC} of the copper block. The term T_{NBL} represents the temperature of the corresponding lamination interior node located below the same copper block interior node.

$$\begin{aligned} & T_{NBC-1}\left[\frac{k_{eff}\Delta z_C R_{NB}}{\Delta R_B}\right] \\ & - T_{NBC}\left[\frac{k_{eff}\Delta z_c R_{NB}}{\Delta R_B} + \frac{k_{eff}\Delta z_C(R_{NB}+\Delta R_B)}{\Delta R_B} + h_{gap}\left(R_{NB}+\frac{\Delta R_B}{2}\right)\Delta R_B\right] \\ & + T_{NBC+1}\left[\frac{k_{eff}\Delta z_C(R_{NB}+\Delta R_B)}{\Delta R_B}\right] + T_{NBL}\left[h_{gap}\left(R_{NB}+\frac{\Delta R_B}{2}\right)\Delta R_B\right] \\ & = -q'''_{Copper}\left[\Delta z_C\left(R_{NB}+\frac{\Delta R_B}{2}\right)\Delta R_B\right] \end{aligned} \tag{5.16}$$

Figure 5-28 shows the model of the last node of the Region B Copper Block.

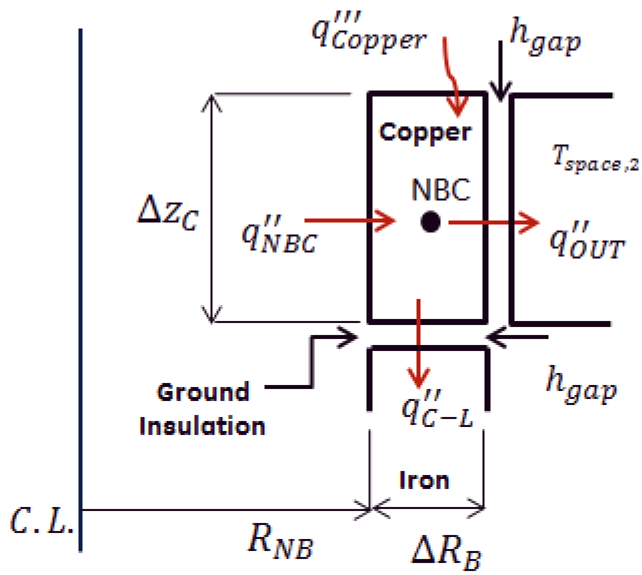

Figure 5-28: Region B – Copper Block: Thermal Analysis for the Last Node

Equation 5.17 is the general expression that models the heat transfer in the last node. As in the first node, there is heat flux from the space at the lateral side of the copper block, and the $T_{space,2}$ term is the temperature in the space next to the end side of the block.

$$T_{NBC-1}\left[\frac{k_{eff}\Delta z_C R_{NB}}{\Delta R_B}\right] - T_{NBC}\left[\frac{k_{eff}\Delta z_C R_{NB}}{\Delta R_B} + h_{gap}\Delta z_C(R_{NB}+\Delta R_B) + h_{gap}\Delta R_B\left(R_{NB}+\frac{\Delta R_B}{2}\right)\right] + T_{NBL(LN)}\left[h_{gap}\left(R_{NB}+\frac{\Delta R_B}{2}\right)\Delta R_B\right] + T_{space,2}\left[h_{gap}\Delta z_C(R_{NB}+\Delta R_B)\right] = -q'''_{Copper}\left[\Delta z_C\left(R_{NB}+\frac{\Delta R_B}{2}\right)\Delta R_B\right] \quad (5.17)$$

$T_{space,2}$ was implemented in the model as the average of the temperature of the last node in the copper block, $T_{NBC(LN)}$, and the temperature of the last node in the lamination, $T_{NBL(LN)}$, as defined in Equation 5.18.

$$T_{space,2} = \frac{(T_{NBC(LN)} + T_{NBL(LN)})}{2} \quad (5.18)$$

5.3.5 Region B – Lamination Block: Thermal Analysis Model

Figure 5-29 shows the model of the first node of the Region B Lamination Block. The term q''_{IN} is the heat flux leaving the last node of the lamination yoke in Region A, and the term q''_{NBL+1} is the heat flux leaving the first node in Region B in the radial direction. As explained above, the heat flux leaving the copper block in the axial direction, going through the ground insulation that surrounds the copper block, and into the lamination below is represented by the term q''_{C-L}.

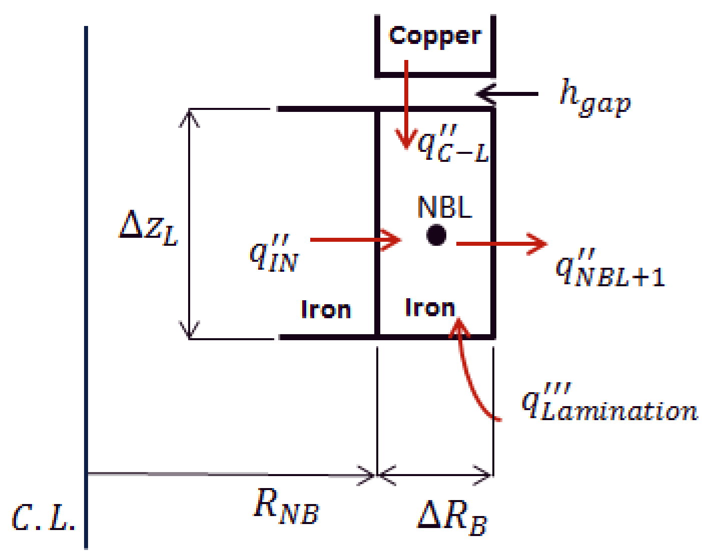

Figure 5-29: Region B – Lamination Block: Thermal Analysis for the First Node

As in the copper block, a similar analysis was developed to obtain the general equation for the heat transfer in the first node of the lamination in this region, as defined in Equation 5.19. The term $T_{NA(LN)}$ represents the temperature at the last node of the lamination yoke in Region A, and the term $T_{NBC(1)}$ represents the temperature at the first node of the copper block. As in Region A, non-uniform noding was accounted for in the first node.

$$-T_{NBL}\left[\frac{2k_I\Delta z_L R_{NB}}{\Delta R_A+\Delta R_B}+h_{gap}\Delta R_B\left(R_{NB}+\frac{\Delta R_B}{2}\right)+\frac{k_I\Delta z_L(R_{NB}+\Delta R_B)}{\Delta R_B}\right]$$
$$+T_{NBL+1}\left[\frac{k_I\Delta z_L(R_{NB}+\Delta R_B)}{\Delta R_B}\right]+T_{NA(LN)}\left[\frac{2k_I\Delta z_L R_{NB}}{\Delta R_A+\Delta R_B}\right]$$
$$+T_{NBC(1)}\left[h_{gap}\Delta R_B\left(R_{NB}+\frac{\Delta R_B}{2}\right)\right]$$
$$=-q'''_{Lamination}\left[\Delta z_L\Delta R_B\left(R_{NB}+\frac{\Delta R_B}{2}\right)\right] \quad (5.19)$$

General expressions for the interior and last nodes of the lamination in Region B were also developed in a similar way. Figure 5-30 shows the model of an interior node of the Region B Lamination Block.

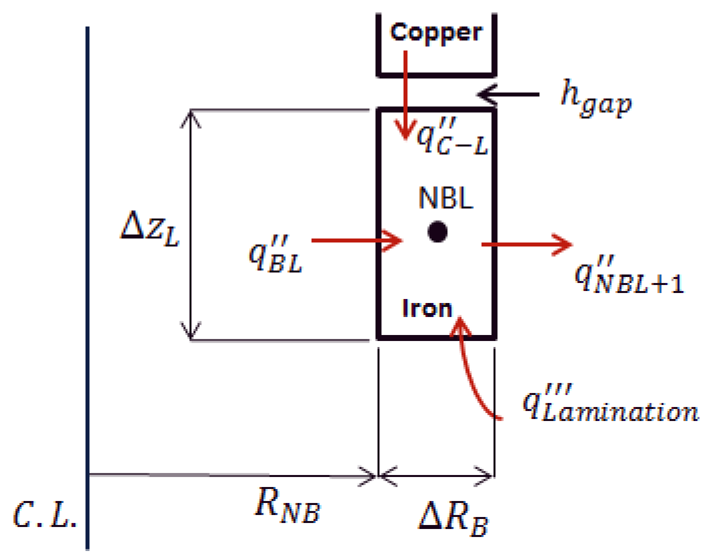

Figure 5-30: Region B – Lamination Block: Thermal Analysis for an Interior Node

Equation 5.20 is the general expression for the heat transfer for a Region B interior node. The temperature at each corresponding interior node of the copper block is represented by the T_{NBC} term.

$$T_{NBL-1}\left[\frac{k_I\Delta z_L R_{NB}}{\Delta R_B}\right] - T_{NBL}\left[\frac{k_I\Delta z_L R_{NB}}{\Delta R_B} + h_{gap}\Delta R_B\left(R_{NB}+\frac{\Delta R_B}{2}\right) + \frac{k_I\Delta z_L(R_{NB}+\Delta R_B)}{\Delta R_B}\right] + T_{NBL+1}\left[\frac{k_I\Delta z_L(R_{NB}+\Delta R_B)}{\Delta R_B}\right] + T_{NBC}\left[h_{gap}\Delta R_B\left(R_{NB}+\frac{\Delta R_B}{2}\right)\right] = -q'''_{Lamination}\left[\Delta z_L\Delta R_B\left(R_{NB}+\frac{\Delta R_B}{2}\right)\right] \quad (5.20)$$

Figure 5-31 shows the model of the last node of the Region B Lamination Block. The term $q''_{NC(1)}$ is the heat flux leaving the last node of Region B and entering the first node of the lamination in Region C.

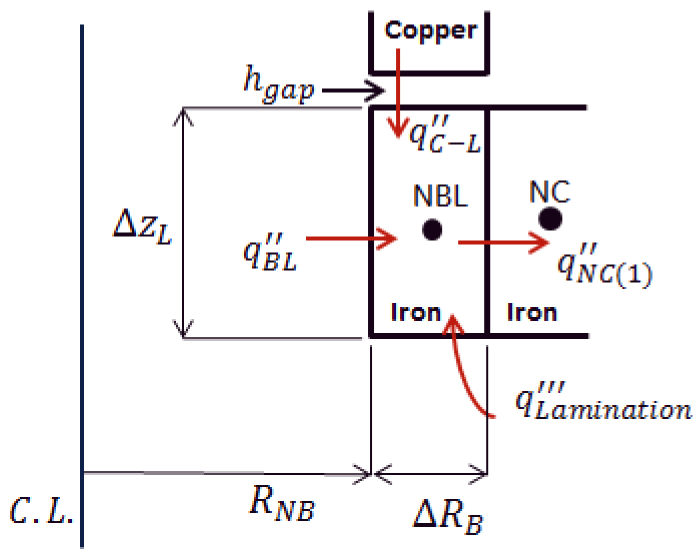

Figure 5-31: Region B – Lamination Block: Thermal Analysis for the Last Node

Equation 5.21 is the general expression for the heat transfer in the last node of the lamination tooth in this region. The temperature at the last node of the copper block is represented by the $T_{NBC(LN)}$ term, and the temperature at the first node of the lamination tooth in Region C is represented by the $T_{NC(1)}$ term. Non-uniform noding between Regions B and C was also accounted for in the general expression.

$$
\begin{aligned}
&T_{NBL-1}\left[\frac{k_I \Delta z_L R_{NB}}{\Delta R_B}\right] \\
&- T_{NBL}\left[\frac{k_I \Delta z_L R_{NB}}{\Delta R_B} + h_{gap}\Delta R_B\left(R_{NB} + \frac{\Delta R_B}{2}\right) + \frac{2k_I \Delta z_L (R_{NB} + \Delta R_B)}{\Delta R_B + \Delta R_C}\right] \\
&+ T_{NC(1)}\left[\frac{2k_I \Delta z_L (R_{NB} + \Delta R_B)}{\Delta R_B + \Delta R_C}\right] + T_{NBC(LN)}\left[h_{gap}\Delta R_B\left(R_{NB} + \frac{\Delta R_B}{2}\right)\right] \\
&= -q'''_{Lamination}\left[\Delta z_L \Delta R_B\left(R_{NB} + \frac{\Delta R_B}{2}\right)\right]
\end{aligned}
\tag{5.21}
$$

5.3.6 Region C – Lamination Tooth Tip: Thermal Analysis Model

Figure 5-32 shows the model of the first node of the Region C Lamination Tooth Tip. In this region, heat is transferred in the radial direction towards the inner duct wall between the lamination and the liquid sodium. The term q''_{IN} represents the heat flux leaving the last node of the lamination in Region B, and entering the first node of the lamination in Region C. R_{NC} is the radial distance from the center line to each node in this region, and ΔR_C is the length of a node. For this report, 15 nodes were used in Region C.

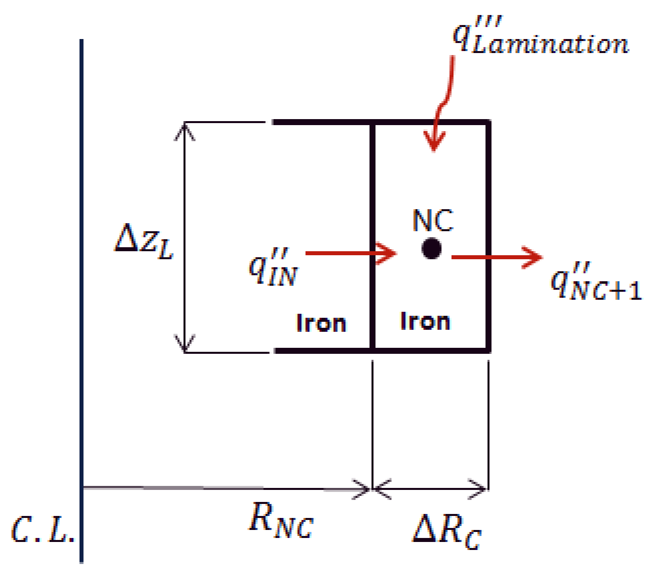

Figure 5-32: Region C – Lamination Tooth Tip: Thermal Analysis for the First Node

Equation 5.22 is the general expression for the heat transfer in the first node of Region C. The temperature in the last node of the lamination tooth in Region B is represented by the $T_{NBL(LN)}$ term. As in the analysis developed for the lamination in Regions A and B, a similar method was applied to account for non-uniform noding.

$$-T_{NC}\left[\frac{2k_I\Delta z_L R_{NC}}{\Delta R_C+\Delta R_B}+\frac{k_I\Delta z_L(R_{NC}+\Delta R_C)}{\Delta R_C}\right]+T_{NC+1}\left[\frac{k_I\Delta z_L(R_{NC}+\Delta R_C)}{\Delta R_C}\right]$$
$$+T_{NBL(LN)}\left[\frac{2k_I\Delta z_L R_{NC}}{\Delta R_C+\Delta R_B}\right]=-q'''_{Lamination}\left[\Delta z_L\Delta R_C\left(R_{NC}+\frac{\Delta R_C}{2}\right)\right] \quad (5.22)$$

Figure 5-33 shows the model of an interior node of the Region C Lamination Tooth Tip.

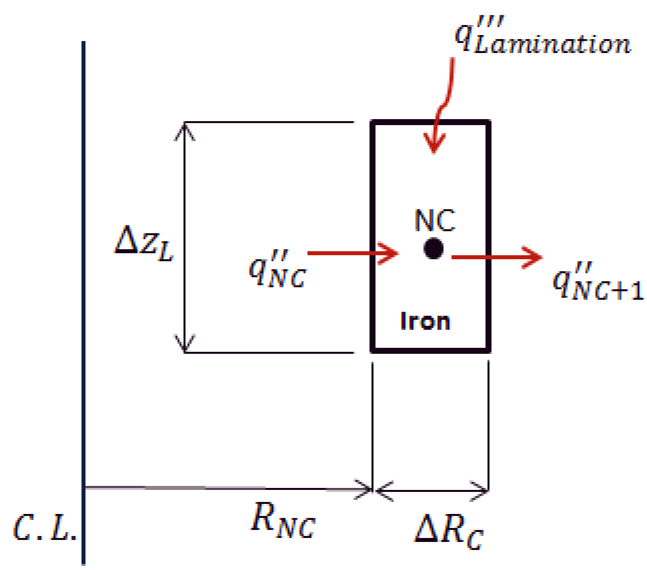

Figure 5-33: Region C – Lamination Tooth Tip: Thermal Analysis for an Interior Node

Equation 5.23 is the general expression for the heat transfer for a Region C interior node.

$$T_{NC-1}\left[\frac{k_I \Delta z_L R_{NC}}{\Delta R_C}\right] - T_{NC}\left[\frac{k_I \Delta z_L R_{NC}}{\Delta R_C} + \frac{k_I \Delta z_L (R_{NC} + \Delta R_C)}{\Delta R_C}\right] + T_{NC+1}\left[\frac{k_I \Delta z_L (R_{NC} + \Delta R_C)}{\Delta R_C}\right] = -q'''_{Lamination}\left[\Delta z_L \Delta R_C \left(R_{NC} + \frac{\Delta R_C}{2}\right)\right] \tag{5.23}$$

Figure 5-34 shows the model of the last node of the Region C Lamination Tooth Tip. The term q''_{L-D} is the heat flux leaving the last node of the lamination tooth tip, and entering the first node of the inner duct wall. It is assumed complete tooth-to-duct contact is maintained between the lamination and the inner duct wall.

The term $h_{conductance}$ represents the heat transfer coefficient in the lamination and inner duct wall contact area. The value for $h_{conductance}$ was obtained by first comparing the data obtained from the AGENA analysis, shown in Figure 5-17, and then adjusting the $h_{conductance}$ value through a sensitivity study as explained in Section 5.3.9, with the final comparison shown in Figure 5-39. The value for $h_{conductance}$ was verified with test data reported for the lamination (Fanning, 2002) as explained in Section 5.3.10 and compared in Figure 5-40. The verified $h_{conductance}$ value of 1,100 W/m²-K was used for further analyses.

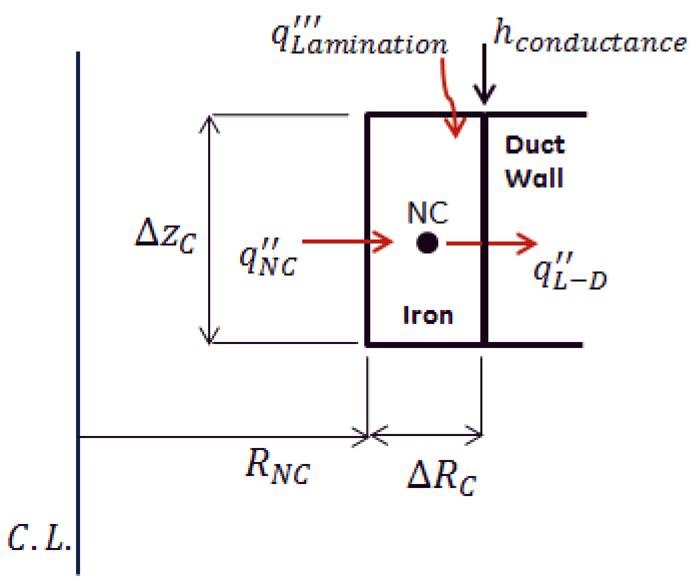

Figure 5-34: Region C – Lamination Tooth Tip: Thermal Analysis for the Last Node

Equation 5.24 is the general expression for the heat transfer in the last node of the lamination tooth tip in Region C. The term $T_{ND(1)}$ is the temperature at the first node of the inner duct wall.

$$T_{NC-1}\left[\frac{k_I \Delta z_L R_{NC}}{\Delta R_C}\right] - T_{NC}\left[\frac{k_I \Delta z_L R_{NC}}{\Delta R_C} + h_{conductace}\Delta z_L (R_{NC} + \Delta R_C)\right] + T_{ND(1)}[h_{conductance}\Delta z_L (R_{NC} + \Delta R_C)] = -q'''_{Lamination}\left[\Delta z_L \Delta R_C \left(R_{NC} + \frac{\Delta R_C}{2}\right)\right] \quad (5.24)$$

5.3.7 Region D – Inner Duct Wall: Thermal Analysis Model

Figure 5-35 shows the model of the first node of the Region D – Inner Duct Wall. The term q'''_{Duct} is the heat generation rate per unit volume in the inner duct wall, generated from the current flowing through the duct wall, caused by the current distributed within the liquid sodium in the duct. The term q''_{L-D} represents the heat flux transferred in the radial direction from the lamination tooth tip and into the first node of the duct wall. The heat flux flowing from Region C to Region D is calculated with the heat transfer coefficient, $h_{conductance}$. The height, Δz_D, of each node in this region is the same as the height of the lamination in Regions A, B and C. The term R_{ND} is the radial distance from the center line to each node in Region D, and ΔR_D is the length of each node in the duct wall. Region D was analyzed with 5 nodes.

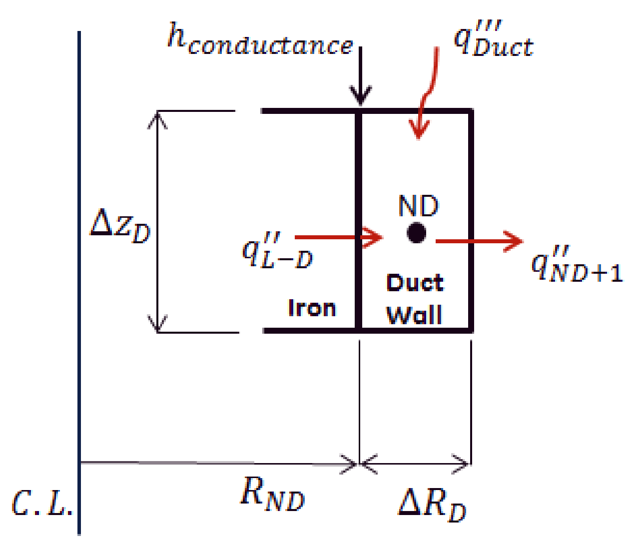

Figure 5-35: Region D – Inner Duct Wall: Thermal Analysis for the First Node

Equation 5.25 is the general expression for the heat transfer in the first node of the Region D inner duct wall. The term $T_{NC(LN)}$ represents the temperature at the last node of the lamination tooth in Region C. The term k_D is the thermal conductivity of the material used in the duct wall. The analysis presented in this report used 304 stainless steel.

$$
\begin{aligned}
&-T_{ND}\left[h_{conductance}\Delta z_D R_{ND} + \frac{k_D \Delta z_D (R_{ND} + \Delta R_D)}{\Delta R_D}\right] \\
&+ T_{ND+1}\left[\frac{k_D \Delta z_D (R_{ND} + \Delta R_D)}{\Delta R_D}\right] \\
&+ T_{NC(LN)}\left[h_{conductance}\Delta z_D R_{ND}\right] \\
&= -q'''_{Duct}\left[\Delta z_D \Delta R_D \left(R_{ND} + \frac{\Delta R_D}{2}\right)\right]
\end{aligned}
\quad (5.25)
$$

Figure 5-36 shows the model of an interior node of the Region D – Inner Duct Wall.

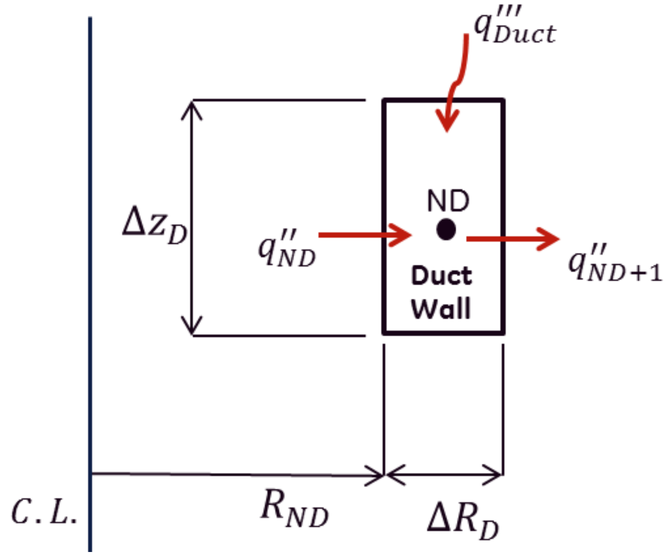

Figure 5-36: Region D – Inner Duct Wall: Thermal Analysis for an Interior Node

Equation 5.26 is the general expression for the heat transfer for Region D interior nodes.

$$T_{ND-1}\left[\frac{k_D \Delta z_D R_{ND}}{\Delta R_D}\right] - T_{ND}\left[\frac{k_D \Delta z_D R_{ND}}{\Delta R_D} + \frac{k_D \Delta z_D (R_{ND} + \Delta R_D)}{\Delta R_D}\right] + T_{ND+1}\left[\frac{k_D \Delta z_D (R_{ND} + \Delta R_D)}{\Delta R_D}\right] = -q'''_{Duct}\left[\Delta z_D \Delta R_D \left(R_{ND} + \frac{\Delta R_D}{2}\right)\right] \quad (5.26)$$

Figure 5-37 shows the model of the last node of the Region D – Inner Duct Wall. The term q''_{D-S} is the heat flux leaving the duct wall and entering the liquid sodium flowing in the duct.

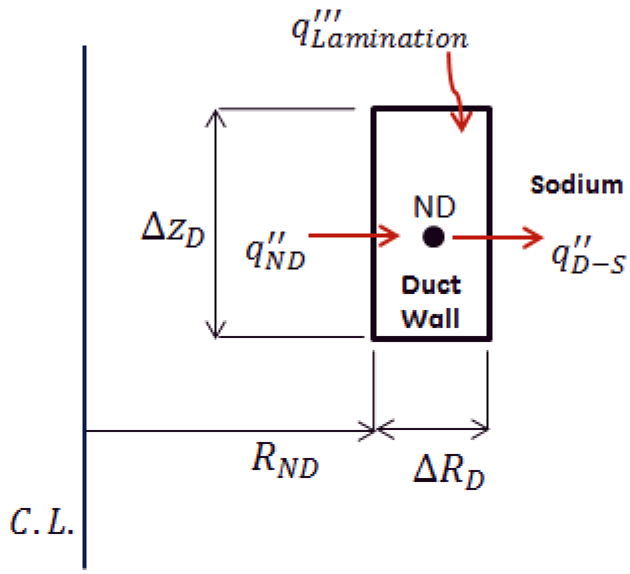

Figure 5-37: Region D – Inner Duct Wall: Thermal Analysis for the Last Node

Equation 5.27 is the general expression for the heat transfer in the last node of the inner duct wall.

$$T_{ND-1}\left[\frac{k_D \Delta z_D R_{ND}}{\Delta R_D}\right] - T_{ND}\left[\frac{k_D \Delta z_D R_{ND}}{\Delta R_D} + h_{Na} \Delta z_D (R_{ND} + \Delta R_D)\right] = -T_{Na}[h_{Na} \Delta z_D (R_{ND} + \Delta R_D)] - q'''_{Duct}\left[\Delta z_D \Delta R_D \left(R_{ND} + \frac{\Delta R_D}{2}\right)\right] \quad (5.27)$$

The heat transfer coefficient of liquid sodium, h_{Na}, was obtained from:

$$h_{Na} = \frac{Nu\, k_{Na}}{D_h} \qquad (5.28)$$

Where Nu is Nusselt number, k_{Na} is the thermal conductivity for sodium and D_h is the hydraulic diameter of the duct.

The Nusselt number was calculated through the correlation Equation 5.29, proposed by Sleicher and Rouse (Kays *et al.*, 1993). This equation is used for liquid metals with very low Prandtl number, which is a characteristic of metal fluids with high thermal conductivity.

$$Nu = 6.3 + 0.0167 Re^{0.85} Pr^{0.93} \qquad (5.29)$$

The Reynolds number was calculated from Equation 5.30, using the density, ρ, and viscosity, μ, of liquid sodium, the velocity, V, and the hydraulic diameter of the duct, D_h. A typical value for the Reynolds number in this application has an order of magnitude of 10^6.

$$Re = \frac{\rho V D_h}{\mu} \qquad (5.30)$$

The Prandtl number was calculated from Equation 5.31, where the specific heat, C_p, and the thermal conductivity, k_{Na}, of liquid sodium were used. The Prandtl number for liquid sodium is a value of approximately 0.005, a small value due to its high thermal conductivity.

$$Pr = \frac{\mu C_p}{k_{Na}} \qquad (5.31)$$

5.3.8 System of Equations and Implementation in MATRIX

The general expressions for each of the nodes of the copper block, inner duct wall, and lamination in each region were combined into a system of equations. The equations were arranged into the MATRIX format:

$$[A][T] = [D] \qquad (5.32)$$

The sizes of the matrices are dependent on the number of nodes selected for each region in the analysis. The temperatures at each node, represented by vector T, are the unknown values in the system of equations. Vector T was solved by multiplying both sides by the inverse of MATRIX A, as shown in Equations 5.33 and 5.34.

$$[A]^{-1}[A][T] = [A]^{-1}[D] \tag{5.33}$$

$$[T] = [A]^{-1}[D] \tag{5.34}$$

Matrix A has the format shown in Equation 5.35, where M is the number of nodes selected for Region A; N is the number of nodes for Region B; O is the number of nodes for Region C; and P is the number of nodes for Region D.

$$A = \begin{bmatrix}
b_{NA(1)} & c_{NA(1)} & 0 & 0 & 0 & 0 & 0 & 0 & 0 & 0 & 0 & 0 & 0 & 0 & 0 \\
a_{NA(2)} & b_{NA(2)} & c_{NA(2)} & \vdots & \vdots & \vdots & \vdots & \vdots & \vdots & \vdots & \vdots & \vdots & \vdots & \vdots & \vdots \\
0 & \ddots & \vdots & \vdots & \vdots & \vdots & 0 & \vdots & \vdots & \vdots & \vdots & \vdots & \vdots & \vdots & \vdots \\
\vdots & a_{NA(M)} & b_{NA(M)} & 0 & 0 & \vdots & u_{NA(M)} & \vdots & \vdots & \vdots & \vdots & \vdots & \vdots & \vdots & \vdots \\
\vdots & 0 & 0 & b_{NBC(1)} & c_{NBC(1)} & 0 & x_{NBC(1)} & 0 & \vdots & \vdots & \vdots & \vdots & \vdots & \vdots & \vdots \\
\vdots & \vdots & 0 & a_{NBC(2)} & b_{NBC(2)} & c_{NBC(2)} & 0 & \ddots & \vdots & \vdots & \vdots & \vdots & \vdots & \vdots & \vdots \\
\vdots & \vdots & 0 & 0 & \ddots & \vdots & 0 & 0 & 0 & \vdots & \vdots & \vdots & \vdots & \vdots & \vdots \\
\vdots & \vdots & 0 & 0 & a_{NBC(N)} & b_{NBC(N)} & 0 & 0 & x_{NBC(N)} & \vdots & \vdots & \vdots & \vdots & \vdots & \vdots \\
\vdots & \vdots & x_{NBL(1)} & y_{NBL(1)} & 0 & 0 & b_{NBL(1)} & c_{NBL(1)} & 0 & \vdots & \vdots & \vdots & \vdots & \vdots & \vdots \\
\vdots & \vdots & 0 & 0 & \ddots & 0 & a_{NBL(2)} & b_{NBL(2)} & c_{NBL(2)} & \vdots & \vdots & \vdots & \vdots & \vdots & \vdots \\
\vdots & \vdots & \vdots & \vdots & 0 & 0 & 0 & \ddots & \vdots & 0 & \vdots & \vdots & \vdots & \vdots & \vdots \\
\vdots & \vdots & \vdots & \vdots & \vdots & y_{NBL(N)} & \vdots & a_{NBL(N)} & b_{NBL(N)} & z_{NBL(N)} & 0 & \vdots & \vdots & \vdots & \vdots \\
\vdots & \vdots & \vdots & \vdots & \vdots & 0 & \vdots & 0 & u_{NC(1)} & b_{NC(1)} & c_{NC(1)} & 0 & \vdots & \vdots & \vdots \\
\vdots & \vdots & \vdots & \vdots & \vdots & \vdots & \vdots & \vdots & 0 & a_{NC(2)} & b_{NC(2)} & c_{NC(2)} & \vdots & \vdots & \vdots \\
\vdots & \vdots & \vdots & \vdots & \vdots & \vdots & \vdots & \vdots & \vdots & 0 & \ddots & \vdots & 0 & \vdots & \vdots \\
\vdots & \vdots & \vdots & \vdots & \vdots & \vdots & \vdots & \vdots & \vdots & \vdots & a_{NC(O)} & b_{NC(O)} & z_{NC(O)} & 0 & \vdots \\
\vdots & \vdots & \vdots & \vdots & \vdots & \vdots & \vdots & \vdots & \vdots & \vdots & 0 & z_{ND(1)} & b_{ND(1)} & c_{ND(1)} & 0 \\
\vdots & \vdots & \vdots & \vdots & \vdots & \vdots & \vdots & \vdots & \vdots & \vdots & \vdots & 0 & a_{ND(2)} & b_{ND(2)} & c_{ND(2)} \\
\vdots & \vdots & \vdots & \vdots & \vdots & \vdots & \vdots & \vdots & \vdots & \vdots & \vdots & \vdots & 0 & \ddots & \vdots \\
0 & 0 & 0 & 0 & 0 & 0 & 0 & 0 & 0 & 0 & 0 & 0 & 0 & a_{ND(P)} & b_{ND(P)}
\end{bmatrix} \tag{5.35}$$

Vector T has the format shown in Equation 5.36 and Vector D has the format shown in Equation 5.37.

$$T = \begin{bmatrix} T_{NA(1)} \\ T_{NA(2)} \\ \vdots \\ T_{NA(M)} \\ T_{NBC(1)} \\ T_{NBC(2)} \\ \vdots \\ T_{NBC(N)} \\ T_{NBL(1)} \\ T_{NBL(2)} \\ \vdots \\ T_{NBL(N)} \\ T_{NC(1)} \\ T_{NC(2)} \\ \vdots \\ T_{NC(O)} \\ T_{ND(1)} \\ T_{ND(2)} \\ \vdots \\ T_{ND(P)} \end{bmatrix} \quad (5.36)$$

$$D = \begin{bmatrix} d_{NA(1)} \\ d_{NA(2)} \\ \vdots \\ d_{NA(M)} \\ d_{NBC(1)} \\ d_{NBC(2)} \\ \vdots \\ d_{NBC(N)} \\ d_{NBL(1)} \\ d_{NBL(2)} \\ \vdots \\ d_{NBL(N)} \\ d_{NC(1)} \\ d_{NC(2)} \\ \vdots \\ d_{NC(O)} \\ d_{ND(1)} \\ d_{ND(2)} \\ \vdots \\ d_{ND(P)} \end{bmatrix} \qquad (5.37)$$

An algorithm solved the system of equations at a chosen number of nodes for each region, and calculated the temperature profile in the copper block, the lamination, and the inner duct wall. This thermal analysis algorithm was named THERMAL_MOD. The code first builds the matrices and vectors shown in Equations 5.35, 5.36, and 5.37 using the general expressions developed for each node in each of the defined regions of the stator. The sizes of the matrices built by the program are adjusted according to the total number of nodes selected by the user in each region. In order to solve the T vector for the temperatures, as shown in Equation 5.34, an existing MATRIX inversion subroutine algorithm created by Ashwith J. Rego, Indian Institute of Technology Bombay (Rego, 2014), was implemented in the code to obtain the inverse of MATRIX A. The multiplication operation between vector D and the inverted MATRIX A was achieved by the Fortran command MATMUL, resulting in the temperature profile at each region.

After the flow correction and material update code were developed, the THERMAL_MOD algorithm for the thermal analysis was integrated into MATRIX as a separate module that is called by the main program when MATRIX is run. The module uses the heat generation rate per unit volume in the copper block, in the inner duct wall, and the velocity in the inner duct calculated in the MATRIX main code. A series of input entries were added to the DTA1 input block in the main program that allow the user to enter data that defines the system being analyzed. The user inputs for the thermal analysis are: the number of nodes for each defined region of the stator; the geometric parameters that are used in the model, such as the length and height of each region, as shown in Figure 5-20; the thermal conductivities of the copper block, lamination and the materials used for the insulation in between and surrounding the coil and the inner duct wall; the liquid sodium temperature; the heat generation rate in the lamination yoke and tooth; and the heat transfer coefficient or conductance between the lamination and the inner duct wall. Figure 5-38 shows from the actual lines of code and the list of inputs that are provided by the user for the thermal analysis.

```
DUCTMAT=304        $ DUCT MATERIAL ('304' FOR SS304, '316' FOR SS316, '625' FOR ALLOY 625, '718' FOR ALLOY 718, '600' FOR ALLOY 600)
IRONTHE=1          $ BACK IRON THERMAL EXPANSION CALCULATION ('1' UPDATE IRON DIMENSIONS WITH THERMAL EXPANSION FACTOR, '0' OTHERWISE)
TFLUID=608         $ FLUID AND DUCT TEMPERATURES (K)
TCOPPER=706        $ COPPER TEMPERATURE (K)
TIRON=713          $ BACK IRON TEMPERATURE (K)
HTRANS=1           $ STEADY STATE THERMAL ANALYSIS ('1' PERFORM THERMAL ANALYSIS, '0' NO THERMAL ANALYSIS)
STATOR=1           $ CHOOSE WHICH STATOR TO PERFORM STEADY STATE THERMAL ANALYSIS ON ('1' INNER STATOR, '2'OUTER STATOR)
NA=20              $ NUMBER OF NODES FOR REGION A - LAMINATION (THERMAL ANALYSIS)
NB=48              $ NUMBER OF NODES FOR REGION B - COPPER BLOCK AND LAMINATION (THERMAL ANALYSIS)
NCRE=15            $ NUMBER OF NODES FOR REGION C - LAMINATION (THERMAL ANALYSIS)
NDUCT=5            $ NUMBER OF NODES FOR REGION D (ND) - INNER DUCT WALL (THERMAL ANALYSIS)
LLA=0.074          $ LENGTH OF LAMINATION IN REGION A, METER
RNAIN=0.293        $ RADIAL DISTANCE FROM CENTER OF STATOR TO THE EDGE OF THE BACK IRON, METER
DELTAZA=0.01215    $ HEIGHT OF REGION A, METER
LBC=0.102          $ LENGTH OF COPPER BLOCK, METER
DELTACS=0.006      $ LENGTH OF A SINGLE COPPER STRAND, METER
LLC=0.014          $ LENGTH OF LAMINATION IN REGION C, METER
LD=0.00508         $ LENGTH OF INNER DUCT WALL FOR REGION D, METER
DID=0.9743         $ INNER DIAMETER OF DUCT, METERS
DOD=1.12799        $ OUTER DIAMETER OF DUCT, METERS
KI=46.73           $ THERMAL CONDUCTIVITY OF IRON, WATTS PER METER KELVIN
KC=370             $ THERMAL CONDUCTIVITY OF COPPER, WATTS PER METER KELVIN
KDUCT=19.18        $ THERMAL CONDUCTIVITY OF INNER DUCT WALL MATERIAL, WATTS PER METER KELVIN
KGD1=1.0742        $ THERMAL CONDUCTIVITY OF LAYER 1 OF GROUND INSULATION SURROUNDING COPPER BLOCK, WATTS PER METER KELVIN
GDIT1=0.000254     $ THICKNESS OF LAYER 1 OF GROUND INSULATION, METER
KGD2 = 1.29        $ THERMAL CONDUCTIVITY OF LAYER 2 OF GROUND INSULATION SURROUNDING COPPER BLOCK, WATTS PER METER KELVIN
GDIT2 = 0.000914 $ THICKNESS OF LAYER 2 OF GROUND INSULATION, METER
KGD3 = 0.6         $ THERMAL CONDUCTIVITY OF LAYER 3 OF GROUND INSULATION SURROUNDING COPPER BLOCK, WATTS PER METER KELVIN
GDIT3 = 0.001      $ THICKNESS OF LAYER 3 OF GROUND INSULATION, METER
RINS=0.005         $ THERMAL RESISTANCE OF INSULATION BETWEEN COIL STRANDS, WATTS PER METER KELVIN
INST=0.000127      $ THICKNESS OF INSULATION BETWEEN COIL STRANDS, METER
TSODIUM=633.15     $ TEMPERATURE OF LIQUID SODIUM, KELVIN
HGRLY=9365.5       $ HEAT GENERATION RATE IN LAMINATION YOKE (REGION A), WATTS PER CUBIC METER
HGRLT=9365.5       $ HEAT GENERATION RATE IN LAMINATION TOOTH (REGIONS B AND C), WATTS PER CUBIC METER
DZBC=0.01          $ HEIGHT OF REGION BC (COPPER BLOCK), METER
HSTAT=4.3918       $ HEIGHT OF STATOR (INNER STATOR IF 'STATOR'=1, OUTER STATOR IF 'STATOR'=2), M
INNST=0.482        $ INNER DUCT WALL INNER RADIUS (INNER STATOR IF 'STATOR'=1, OUTER STATOR IF 'STATOR'=2), M
OUTST=0.4871       $ OUTER DUCT WALL INNER RADIUS (INNER STATOR IF 'STATOR'=1, OUTER STATOR IF 'STATOR'=2), M
HCOND=1100         $ HEAT TRANSFER COEFFICIENT BETWEEN LAMINATION AND INNER DUCT WALL, WATTS PER METER SQUARE KELVIN
$$
```

Figure 5-38: Inputs Provided by the User for Thermal Analysis

Table 5-2 provides a list of physical parameters that can be changed in the thermal analysis module along with their units and typical parameter ranges.

Table 5-2: Key Thermal Module Inputs

Inputs	Units	Typical Ranges
Number of nodes in Region A	--	15-25
Number of nodes in Region B	--	40-60
Number of nodes in Region C	--	10-15
Number of nodes in Region D	--	5-10
Thermal conductivity of iron	W/m-K	46.73
Thermal conductivity of copper	W/m-K	370
Thermal conductivity of the inner duct wall material	W/m-K	19.18
Thermal conductivity of the first layer of the ground insulation	W/m-K	1.0742
Thermal conductivity of the second layer of the ground insulation	W/m-K	0.000914
Thermal conductivity of the third layer of the ground insulation	W/m-K	0.001
Thermal resistance of insulation between coil strands	m^2-K/W	0.005
Temperature of liquid sodium (depends upon operating condition)	K	633.15
Heat generation rate in lamination	W/m^3	4032.8-11301.2
Heat transfer coefficient or conductance between the lamination and the inner duct wall	W/m^2-K	1100

Geometric parameters are dependent on stator design. The number of nodes used in each region to build the finite difference model should stay within the ranges defined. The thermal conductivity, thermal resistance, heat generation rate, and heat transfer coefficient are parameters used in the general equations for the thermal model and affect the temperature profiles calculation. The temperature of liquid sodium is used as a boundary condition for the thermal analysis. An appropriate range for the heat transfer coefficient or conductance between the lamination and inner duct wall would be determined from further analysis

By integrating the thermal analysis algorithm in MATRIX, and providing the user with the option of adjusting the parameters that define the stator design being analyzed, this latest improvement to the EM Pump legacy code is able to predict the temperature levels in different areas of the stator at various operating conditions, based on insulation material used in the copper block.

5.3.9 Validation of the MATRIX Model with AGENA

Figure 5-39 shows a comparison between the results from the AGENA analysis and the results from the analysis performed by the present MATRIX program using a sodium temperature of 335°C with the benchmark insulation system. Some differences are noted in the temperature profile at the lamination yoke between the two models. This is because of different height of the back lamination yoke in the two models. Since the main focus of the thermal analysis is to determine the temperature profile in the copper block, this approximation of the heat transfer model in the lamination yoke in MATRIX is acceptable for insulation evaluations.

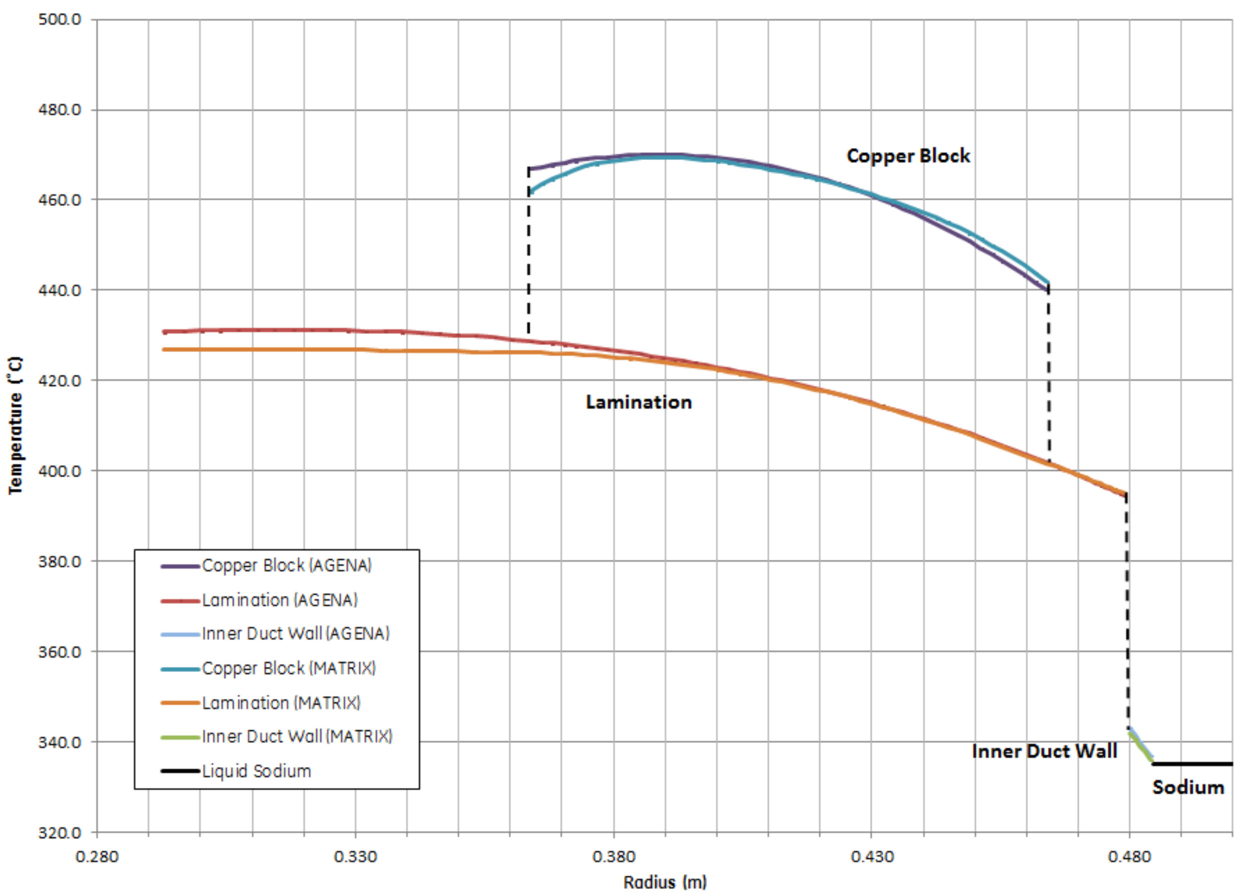

Figure 5-39: Comparison of Thermal Analysis Results from AGENA and MATRIX

5.3.10 Validation of the MATRIX Model with 160 m^3/min EM Pump Test Data

The heat transfer coefficient or conductance for the contact area between the lamination tooth tip and the inner duct wall was determined through a sensitivity study of the MATRIX results. The temperature profile of the lamination obtained from the present MATRIX was compared to previously reported test data (Fanning, 2002), represented on the graph in Figure 5-40 by the blue-colored points. Different values for the heat transfer coefficient, $h_{conductance}$, in the contact conductance area were tested until the lamination temperature profile was an appropriate match for the test data. The temperatures for the copper block, lamination, and inner duct wall in the graph in Figure 5-40 are the result from MATRIX analysis using a heat transfer coefficient, $h_{conductance}$, of 1,100 W/m^2-K.

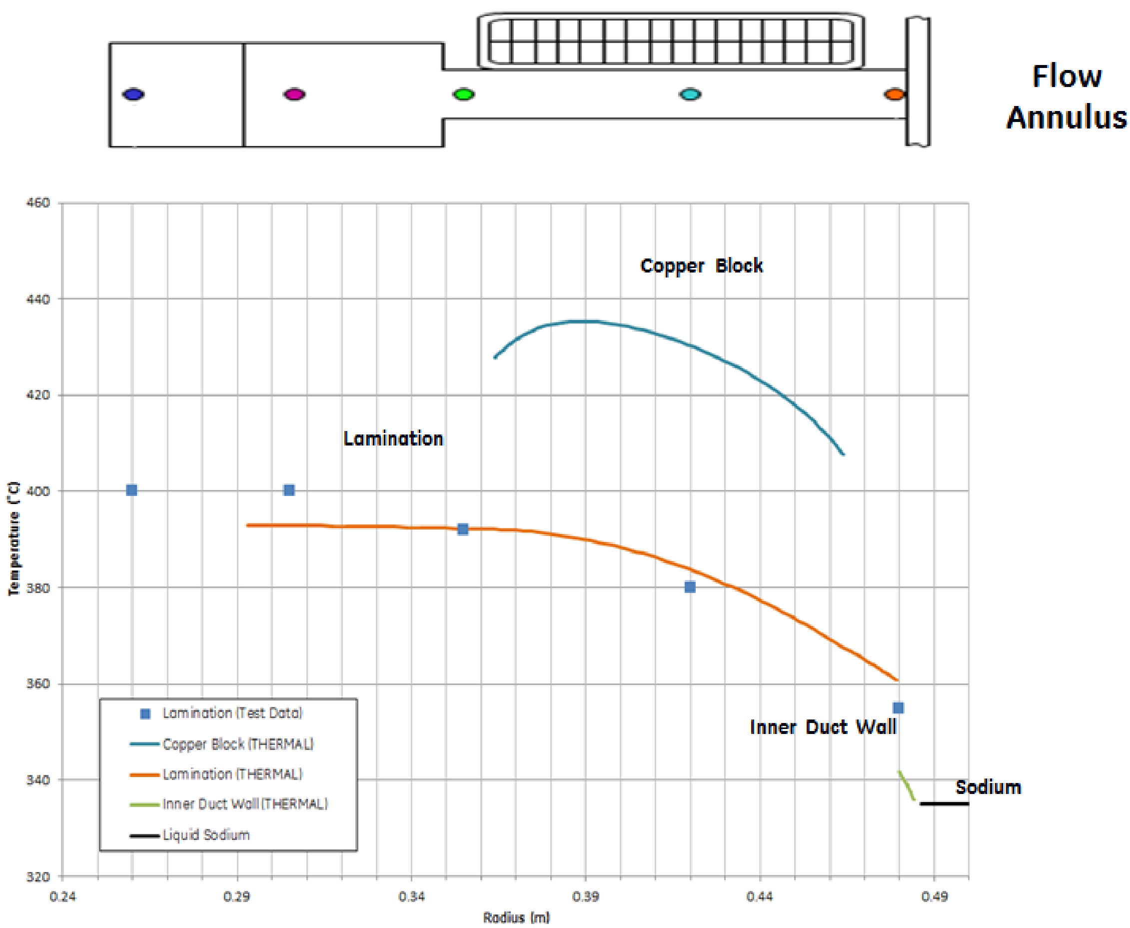

Figure 5-40: Sensitivity Study Based on Test Lamination Data

5.3.11 Parametric Studies Using the MATRIX Model

Parametric studies were performed in order to obtain the temperature profiles at different operating conditions. The temperature of the liquid sodium was changed from 335˚C to 360˚C, the nominal primary sodium inlet temperature for PRISM (Triplett, *et al., 2012*). As expected, the temperature of the lamination and the copper block increased with increased sodium or heat sink temperature.

Figure 5-41 shows a comparison of results from MATRIX analysis at operating frequencies of 6 Hz and 12 Hz. As expected the maximum temperature in the copper block increased with increasing frequency, from 387˚C at 6 Hz to approximately 396˚C at 12 Hz.

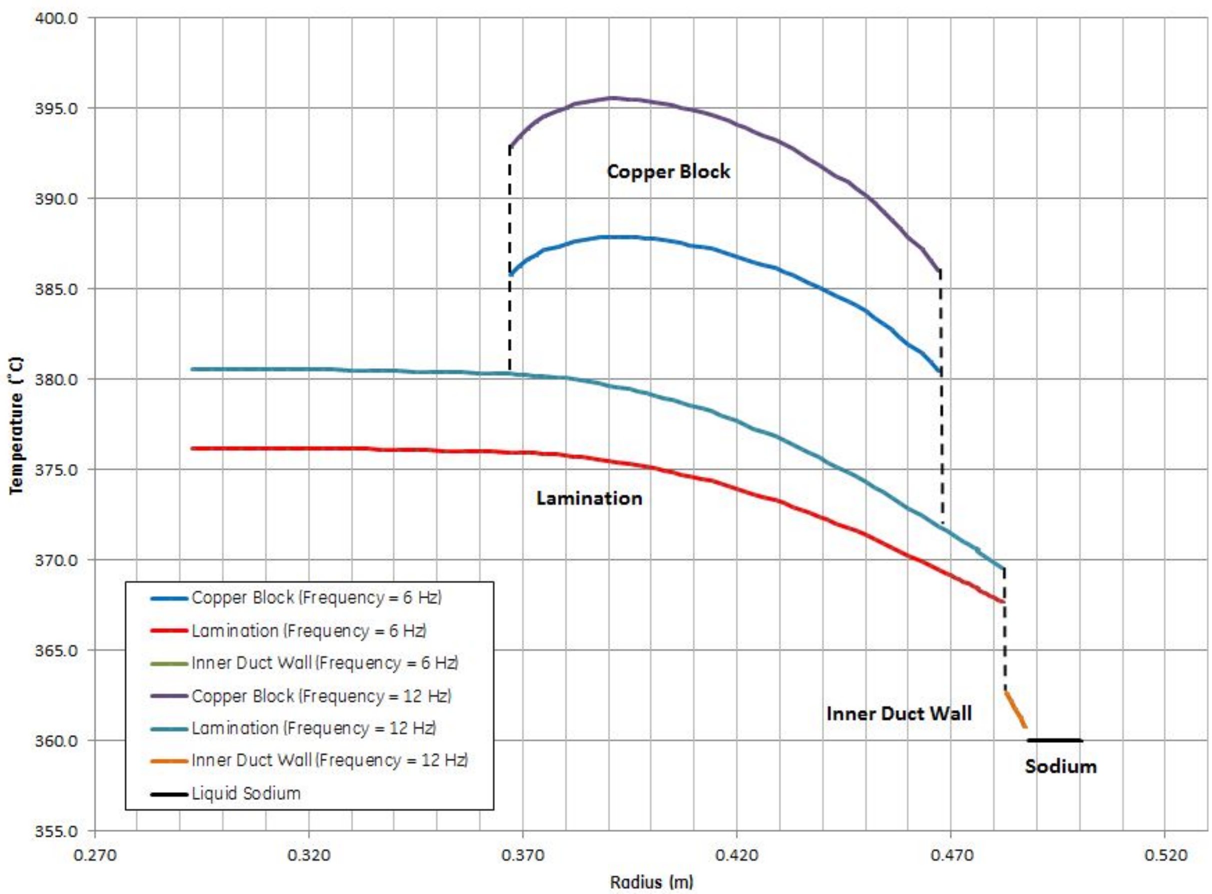

Figure 5-41: Temperature Profiles at 6 Hz and 12 Hz

The same parametric study was performed for operating frequencies of 20.5 Hz and 23 Hz. Figure 5-42 shows a comparison of the temperature profiles obtained from MATRIX analysis for the two operating conditions. The maximum temperature in the copper block increased from 422˚C at 20.5 Hz to 435˚C at 23 Hz, as expected.

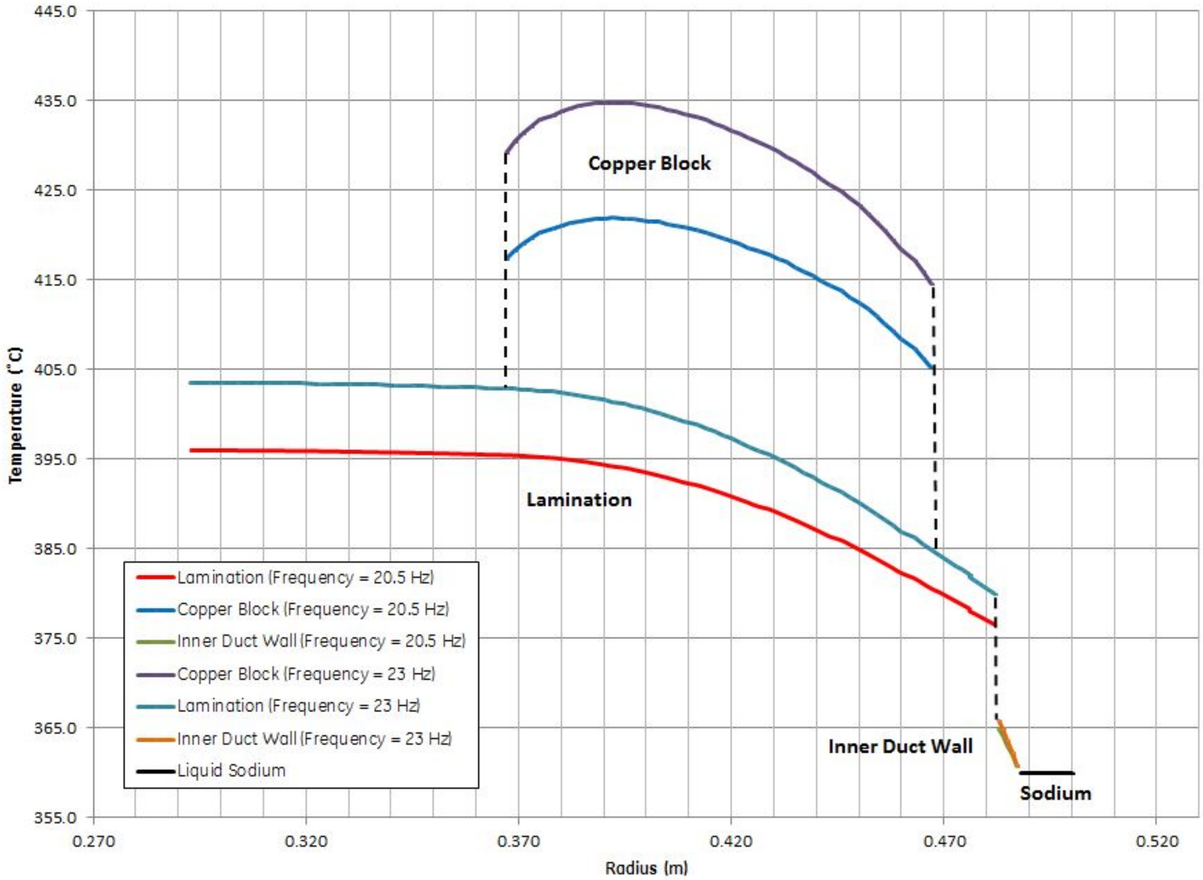

Figure 5-42: Temperature Profiles at 20.5 Hz and 23 Hz

Table 5-3 lists the EM Pump operating conditions that were used in the parametric study. As previously stated, the heat generation rate per unit volume in the copper block and in the inner duct wall are calculated by MATRIX. The heat generation rate in the lamination is provided as input to the code, and it was estimated for this study based on the ratio between the values of the heat generation rates in the copper block and in the lamination that were previously reported for the same EM Pump design (Kwant, *et al., 1998*). From the temperatures obtained in each study, it is estimated that about 8% of the heat generated in the coil is transferred or lost through the lateral sides of the copper block.

Table 5-3: 160 m3/min EM Pump Operating Conditions Used in Parametric Studies

Frequency (Hz)	Input Current (A)	Net Power (kW)	Heat Generation Rate in the Copper Block (W/m3)	Heat Generation Rate in the Lamination (W/m3)	Heat Generation Rate in the Inner Duct Wall (W/m3)
6	607	28.5	78,360	4,216	1,230,192
12	682	203.6	100,260	5,394	1,573,561
20.5	884	842.3	174,080	9,365.5	2,732,117
23	965	1,137.2	210,080	11,302.3	3,297,170

The results in Figure 5-39 through Figure 5-42 were obtained for the EM Pump with the benchmark insulation system that is composed of the following material: two layers of half-lapped Firox tape for the strand insulation; approximately eleven layers of half-lapped Firox tape with Secon-5 binder for the primary ground wall; one layer of half-lapped NEXTEL 440 ceramic fiber tape for the outer wrap; and a crystalline mica sheet. It is important to note that the small increase observed in the temperature profiles between different operating conditions with large difference in heat generation rate is mainly attributed to the good tooth-to-duct thermal contact maintained between the lamination tooth tip and inner duct wall. Results from the MATRIX analysis show that maintaining full and good contact in this area is the key to achieving low stator temperatures.

The 2015 MATRIX version allows the user to change the heat transfer coefficient or conductance between the lamination tooth tip and the inner duct wall, so tests can be run with a different value of $h_{conductance}$, which allows modelling with variable contact.

With the proposal of new insulation material from research conducted in this project, studies were performed in MATRIX to obtain predicted temperature profiles when using a proposed insulation system. As described in Section 5.3.4, an equation for calculating the effective heat transfer coefficient for the ground insulation was implemented in the thermal analysis algorithm, and input entries were added to MATRIX that allow the user to provide the thermal conductivity and thickness of each layer of insulation that make up the ground insulation surrounding the copper block. The proposed insulation uses two layers of Firox tape for the strand insulation (no change from original), one layer of half-lapped NEXTEL 440 ceramic fiber tape with BNLC (Boron Nitride LubriCoat) for the inner coil wrap, and a layer of SBMHB (Silicon Bonded Mica Hard Board) for the primary ground wall. Two different thicknesses for the SBMHB were used for the studies performed, 0.5 mm and 1mm. The graph in Figure 5-43 compares the predicted temperatures obtained from MATRIX between the benchmark insulation system, and the two different SBMHB thicknesses at an operating frequency of 20.5 Hz.

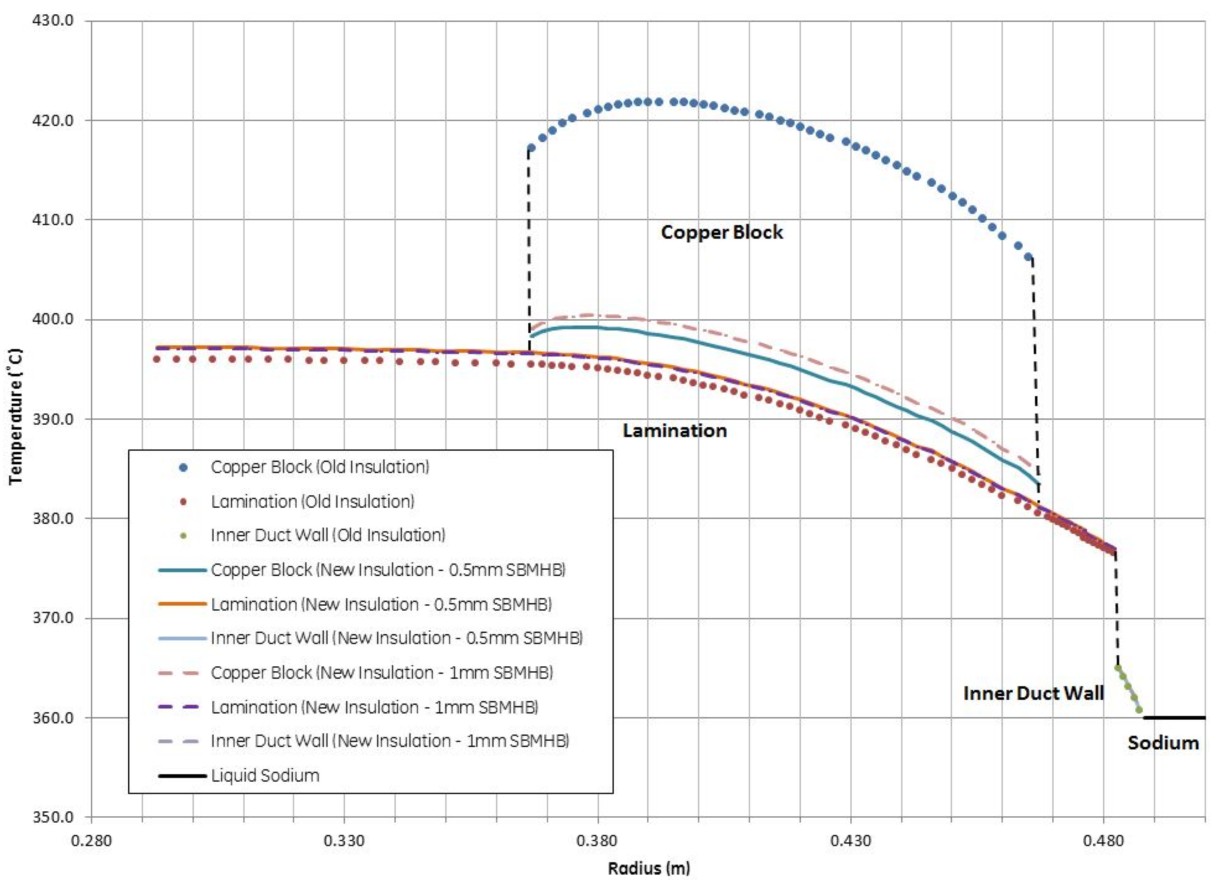

Figure 5-43: Temperature Profiles for the Proposed Insulation System at 20.5 Hz

The same analysis was performed with the proposed insulation system at an operating frequency of 23 Hz. The results are provided in Figure 5-44.

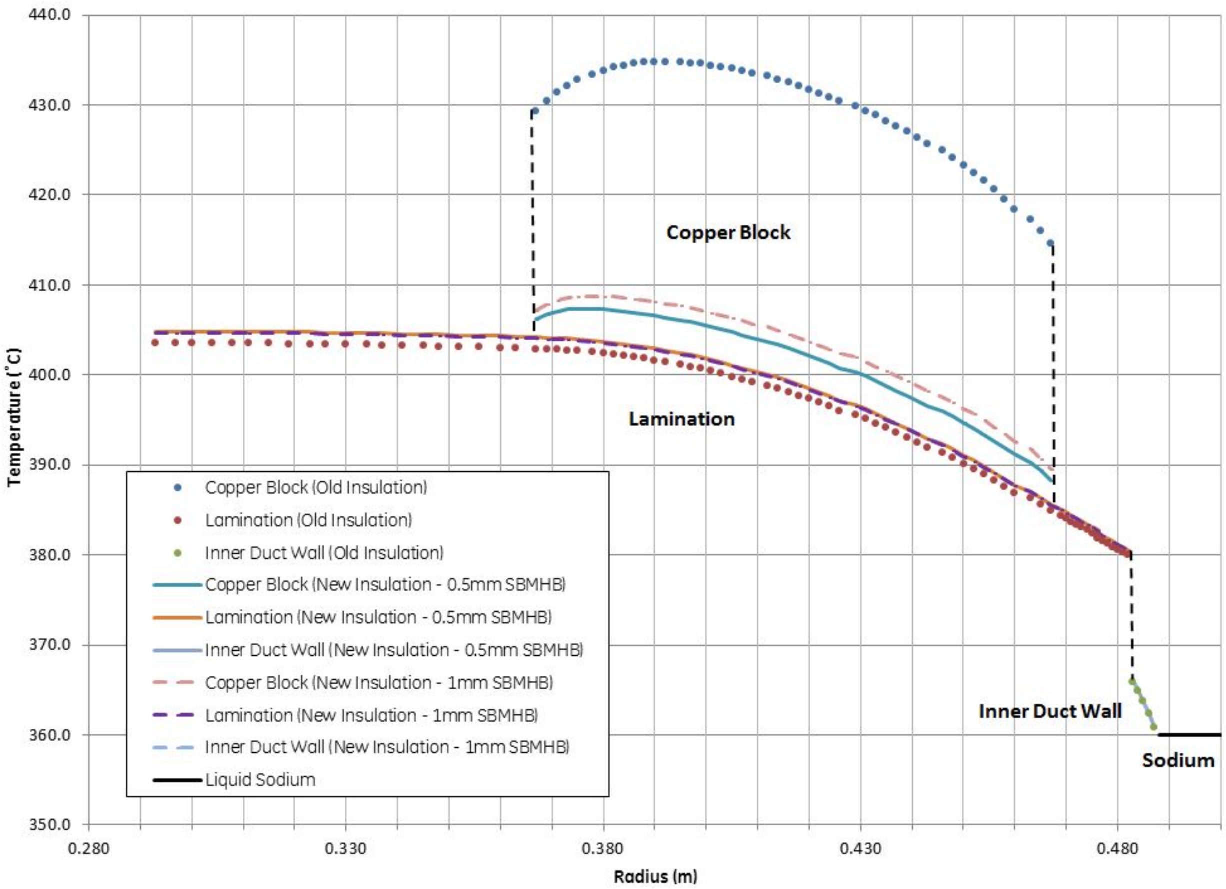

Figure 5-44: Temperature Profiles for the Proposed Insulation System at 23 Hz

With the proposed insulation, the temperature profile in the copper block drops approximately 20˚C, from the benchmark insulation at both 20.5 and 23 Hz. The thicker SBMHB material has a slightly higher temperature profile than the thinner SBMHB material, as would be expected.

From the temperatures obtained in these two analyses, it is predicted that about 6.5% of the heat generated in the coil is lost through the lateral sides of the copper block with the new insulation. The increase of approximately 1˚C in the lamination temperature observed in Figure 5-43 and Figure 5-44 is attributed to the lower percentage of heat lost through the sides of the copper block with the proposed insulation.

5.3.12 Thermal Analysis Model Summary

The MATRIX code was improved by the addition of a thermal analysis module. This module was patterned after the AGENA code, but was implemented from a more fundamental approach using conductive heat transfer through radial nodes. The model was divided into four Regions, A, B, C, and D, with each region consisting of an input node, internal nodes, and an output node. The internal nodes varied per Regions A, B, C, and D, with the recommended total nodes per region of 20, 48, 15, and 5 used for this report, respectively; but the number and length of the nodes can be adjusted as inputs to the model.

Physical testing of benchmark and proposed insulation materials suggested at GRC provides some physical constants for thermal conductivity and thermal resistance, which were used in the model. These physical tests showed that the proposed SBMHB material was thermally beneficial. Full and good contact between the lamination and the inner duct wall was necessary to keep the copper conductor temperatures low. The MATRIX code was verified against the AGENA model and with test data from the 160 m^3/min large EM Pump test data, which provided a good estimate of the thermal conductance between the lamination and the inner duct wall. Parametric studies were done to compare copper and lamination block temperature profiles at different EM Pump operating frequency, which, as expected, showed a corresponding increase in copper conductor temperatures with increasing frequency.

The MATRIX code was also used to model the benchmark insulation and the proposed SBMHB materials, which did indeed show that the SBMHB insulation reduced the copper block temperatures by approximately 20˚C.

This page intentionally left blank

6.0 Overall Summary

In summary, this report sought to provide information in these three broad areas:

- Status of analysis model development
- Improvements made to older simulations
- Comparison to experimental data

This section provides a summary of these three areas.

Status of analysis model development

The 1999 MATRIX code was updated to the modernized 2015 MATRIX version to operate on a computer platform that will be supported in the foreseeable future. The MATRIX code was improved to address the 0.7 multiplier used in the 1999 code that improved the prediction accuracy. The modernization improved simulation run time and increased ability to incorporate modifications in the future. Code modernization also improved the accuracy of the predictions, increasing the number of meshes per slot in the user-defined input. Materials and thermal analysis sections were added and verified using comparative experimental data and/or external models, such as AGENA. Post-processing tools were added to MATRIX which simplified data processing, allowing the user to evaluate the data more effectively.

Improvements made to older simulations

The methodology and results of modernizing the MATRIX analysis code to current GEH code standards is complete. By restructuring the code into the GE DTA format, not only was the data transfer and running efficiency of the code immensely improved, but the maintenance and the ability for future modification of MATRIX was also enhanced. The updated code output results matched the results seen from the legacy MATRIX code within $\pm$5%. In an attempt to improve the predictability of the code, a mesh number per slot (NMS) analysis was executed. The use of more calculation meshes (25 instead of 10 per slot) improved the prediction of the MATRIX data when compared to the measured data; however, there was still a large inconsistency (much greater than $\pm$5% when normalized) in a majority of the data points. Through the addition of flow rate correction equations within the code (2nd, 3rd, or 4th order polynomial), it was seen that the effective sodium velocity could be adjusted, thus improving the overall predictability of the MATRIX code for developed pressure head. Using a 4th order polynomial correction equation on the flow rate allows the predicted, developed pressure to be within $\pm$10% of the measured data taken from a 160 m^3/min EM Pump. Further verification of this flow velocity correction should be performed using measured data from various EM Pumps, if and when available. This report shows that appropriate flow correction to the effective sodium velocity through the EM Pump allows the removal of the 0.7 factor needed to line up the earlier simulation results to the actual pump data, and helps to improve the predictability of future EM Pump's performance.

The materials section replaced cumbersome, data input file structure with the GE DTA format, which improves prediction capabilities and allows for increased materials evaluations. Code comparisons with earlier simulations validated the improvements.

The code for thermal analysis completed the code modernization and improvement with a simplified, radial heat transfer model that was verified against both previous AGENA model and large EM Pump test data. Experimental data obtained during this project, as summarized within this report and fully documented in the Technical Report: Insulation Materials Development and Testing (PLM DOC-0005-2465), was used to verify some of the parameters used in thermal analysis.

Parametric studies were performed to compare copper and lamination block temperature profiles at different EM Pump operating frequencies, which showed a corresponding increase in copper conductor temperatures with increasing frequency, as expected.

The MATRIX code was also used to model the benchmark insulation and the proposed SBMHB materials, which did indeed show that the SBMHB insulation reduced the copper block temperatures by approximately 20˚C.

Comparison to experimental data

The improved MATRIX code with the flow correction applied was used to predict a series of 160 m^3/min EM Pump operational conditions that was compared to the pump experimental data. This was the world's largest EM Pump build to date, and the most recent operational data available. Throughout this comparison process, investigations were made to see what improvements could be made to the code in order to have the MATRIX results agree with the experimental values.

Operating temperature data was also used for thermal conductivity and thermal resistance verifications in the thermal analysis module. After validation, a comparison between the previous benchmark insulation system and the project proposed SBMHB insulation system was made. This comparative analysis showed a lower (better) temperature profile in the copper block for the proposed insulation system.

Independent force calculations verified the thrust or axial force calculated by MATRIX where experimental data was unavailable, although the distribution of the thrust to various EM Pump components is not well defined by MATRIX. Separate analysis could not verify MATRIX attraction or radial force calculations and requires further analysis and evaluation. However, it was concluded that the attraction or radial forces would not cause any appreciable movement of the insulation.

This page intentionally left blank

7.0 Project Products/Deliverables

7.1 Project Publications

Modernization and Capability Investigation of the MATRIX Electromagnetic Pump Analysis Code. Seth Strege, Serkan Yilmaz, Pradip Saha, and Eric P. Loewen. (Submitted to Nuclear Technology: 2015)

Capability Enhancement of MATRIX EM Pump Analysis Code by Including Thermal Analysis. Ana Da Silva, Pradip Saha and Eric P. Loewen. (Drafted for Internal Review, submittal planned in fourth quarter 2015).

7.2 Project Presentations

- Q4 2013 GEH Funding Opportunity Announcement Scope of Work for ANL
- Q4 2013 Annular Linear Induction Pump Insulation Testing at ANL
- 2013 American Nuclear Society National Winter Meeting, SMR Session, Department of Energy Investments in Advance Nuclear Power, Session Chair: Craig D. Welling
- Colloquium titled "PRISM Fast Reactor and Clean Nuclear Fuel Cycle" at University of Nevada, Los Vegas on April 14, 2015 by Dr. E.P. Loewen. A portion of the presentation discussed the project deliverable to students and faculty.

7.3 Project Patents/Other Technologies

Invention disclosure letter for GE patent docket 279303 was submitted to DOE on April 9, 2015 covering the insulation design employing silicon-bonded mica hard board in a slot-liner approach to provide ground wall insulation.

Patent Application, Confirmatory License, and associated documents for GE patent docket 279303 were submitted to DOE on September 17, 2015.

This page intentionally left blank

8.0 Conclusions

8.1 Engineering Disciplines

Understanding the need for better electrical insulation, thermal hydraulics and operation of the plant in general proved a difficult technical problem for the project that required many engineering disciplines for project success. Table 1-1 provided a listing of the key personnel and their technical disciplines. The six different technical disciplines listed (nuclear, electrical, mechanical, materials science, thermal hydraulics and electromagnetic) provided an interesting confluence of EM Pump technical areas:

- High voltage that needs separation by insulation
- Frequency and current that produces heat and forces
- An electrical insulation that must transfer heat
- Duct sodium flow altered by the magnetic field
- Variety of materials from metals (steels and iron) to non-metals (glass and ceramics)

During the bi-weekly project meetings, team members from these engineering disciplines shared information and learned from each other.

8.2 Engineers

Engineers are learning about electricity, magnetism and magnetohydrodynamics. They are re-discovering a suitable high temperature electrical insulation material that will enable sodium-cooled fast reactor plants performance and reliability improvements in addition to the continued development of performance analysis tools in order to better predict EM Pump operation.

The world needs engineers coming together and working on these sorts of co-discipline problems. In the advanced reactor engineering community, there is an acceptance for the need/use of EM Pumps. However, the current nuclear generation community has a 'pathological fear' of EM Pumps. This fear leads not only to opposition of advanced reactor concepts in the nuclear generation community, but also results in 'political' engineering decisions that do more harm than good.

This project is important as it taught more engineers about the possibilities of EM Pumps. It was the unique nature of this project, with a broad spectrum of engineers; that makes EM Pumps positioned for commercial adaptation in the future.

During the opening stages of this project while creating the databank, current engineers came to appreciate the excellent engineering previously accomplished with EM Pumps.

At several venues, this project's technical accomplishments were shared to other engineers.

The value of engineered testing should never be underestimated. Testing and test set up is always threatened by the unknowns in the ability to collect worthwhile data. While progress was made towards an improved, replacement insulation system for EM Pumps, unfortunately, not all of the multi-stress testing objectives were completed. To support advanced liquid-metal cooled reactor engineering and research, the engineering completed and the lessons learned during this project need to be widely distributed.

8.3 Human Resources

The project re-established the relevant technical expertise in the current generation of scientists and engineers at GEH, GRC and ANL.

Past insulation systems are not available in the market today, therefore development of 21st century versions of the laboratory equipment needed to perform high temperature insulation material testing.

The MATRIX Code was updated by two current generation GE electrical engineers for both code enhancements, post processing tools, and mechanical and thermal properties, as supervised by senior Ph.D. engineers. The MATRIX outputs were compared with other calculations from other organizations (GRC, ANL) with the next generation of scientists providing a broad increase in relevant technical expertise.

As the project lead organization, GEH sought to capture knowledge and support this project with early career engineers in GE's best company leadership program, Edison Engineer Development Program (EEDP). During the conduct of this project, four EEDP engineers (mechanical, chemical and two electrical) worked on the project. This grew the Human Resource capital within GEH for the future commercialization of advanced reactors. Members of the EEDP program today are the engineer leaders of tomorrow.

8.4 Physical, Institutional, and Information Resources

The EM Pump databank developed as part of this work will serve as a single-point source of information to the future designers/researchers of EM Pumps.

The legacy MATRIX code for EM Pump analysis has been converted to modern computing platform for easier and more efficient operation. The code has also been improved so that the earlier factor of 0.7 need not be applied to the code results and the copper/insulation/lamination/duct temperatures are calculated as integral part of the improved MATRIX. No separate AGENA type code needs to be run for thermal analysis.

8.4.1 Training and Professional Development Opportunities

Over the course of the project, GEH captured and stored all of the documentation related to the modernization and improvement efforts completed on the MATRIX EM Pump analysis code. These documents will be stored in the Product Lifecycle Management (PLM) System in addition to the EM Pump design databank (supporting GEH Objective 1).

The EM Pump performance analysis tool, MATRIX, has been stored in the Team Foundation Server so it is accessible for future improvements and studies.

Project performance bi-weekly updates, quarterly reports, detailed investigations, and these two final project reports, Technical Report: Insulation Materials Development and Testing (PLM DOC-0005-2465) and Final Technical Report – Next-Generation Electromagnetic Pump Analysis Tools (PLM DOC-0005-2188) are also stored in the Product Lifecycle Management (PLM) System in addition to the EM Pump design databank (supporting GEH Objective 1). These reports along with the EM Pump databank will provide current and future engineers with the basis and foundation of EM Pump insulation and MATRIX code fundamental and starting point for future activities.

This page intentionally left blank

9.0 References

Cook, D.P., "Modeling and Design Algorithms for Electromagnetic Pumps", University of Nevada, Los Vegas, (2007)

Davis, J.R., Deegan, G.E., Leman, J.D. and Perry, W.H, "Operating Experience with Sodium Pumps at EBR-II" (1970)

DePuy, T., "Fluid Dynamics and Heat Transfer in a Hartmann Flow", Rensselaer Polytechnic Institute, Master of Engineering in Mechanical Engineering Thesis, (2010).

Eckert, S. and Gerbeth, G., "Velocity measurements in liquid sodium by means of Ultrasound Doppler Velocimetry", Forschungszentrum Rossendorf (FZR), Institute of Safety Research, (2002)

Elliott, D.G., "MATRIX Analysis of Linear Induction Machines", Final Report FRA-OR&D-75/77, Jet Propulsion Lab, California Inst. of Tech., Pasadena, (1975)

Fanning, A.W., "160 m^3/Min. Electromagnetic Pump Design and Test Results", GE Nuclear Energy, (2002)

Fanning, A. and Kliman, G.B., "160 m^3/min Electromagnetic Pump for Sodium Cooled Reactor Applications", Electric Machines and Drives Conference, IEMDC'03. IEEE International, vol. 1, pp. 477-482, (2003)

Fanning, A., *et al.*, "*Giant Electromagnetic Pump for Sodium Cooled Reactor Applications*", Electric Machines and Drives Conference, IEMDC'03: IEEE International, vol 1. (2003)

Fanning, A., Spreadsheet from 2000_MAP_Summary_3.xls (2009).

Jaross, R.A., "*GE/PRISM EM Pump Coil Development: Construction and Test of First Model Coil*", May 1985, Argonne National Laboratory, Argonne, Illinois.

Kane JJ. "Application Data for Induction EM Pumps" (1964)

Kays, W.M and Crawford, M.E., "Convective Heat and Mass Transfer", McGraw-Hill (3rd Edition), Chapter 14, (1993)

Krasnov, D., Zikanov, O., and Boeck, T., "Numerical Study of Magnetohydrodynamics Duct Flow at High Reynolds and Hartmann numbers", Fluid Mechanics, Vol. 704, pp.421-446, (2012)

Kliman, G.B. and Elliott, D.G., "Linear Induction Motor Experiments in Comparison with Mesh/MATRIX Analysis", IEEE Transactions on Power Apparatus and Systems, vol. PAS-93 (Issue 5), pp. 1624-1633, (1974) Kwant, W., Dahl, L.R., Fanning, A.W. and Dubberley, A., "Development Study of Sodium Immersed Electromagnetic Pump (Part 2) – Design and Fabrication of Inner Stator and Support Structures", General Electric Company, (1998)

Lipo Thomas A., "Introduction to AC Machine Design", Wisconsin Power Electronics Research Center, University of Wisconsin (1979)

Ota, H., *et al.*, "*Development of 160 m³/min Large Capacity Sodium-Immersed Self-Cooled Electromagnetic Pump*", Journal of Nuclear Science and Technology, 41:4, pages 511-ff. (2004)

Rego, A.J., "Subroutine to Find the Inverse of a Square Matrix", Indian Institute of Technology Bombay, (2014) URL: https://svn.ssec.wisc.edu/repos/cloud_team_clavrx/branches/new_cloud_height/dcomp/dcomp_tools.f90

Salamah, S.A., Lunsford, D.W. and Yahalom, R., "AGENA – Advanced General Electric Network Analyzer User's Manual", General Electric Company, (1991)

Sadiku, M.N.O., "Elements of Electromagnetics", Oxford University Press (5th Edition), (2009).

Triplett, B.S., Loewen, E.P., and Dooies, B.J., "PRISM: A Competitive Small Modular Sodium-Cooled Reactor", Nuclear Technology, vol. 178 (Number 2), pp. 186-200, (2012)

10.0 Appendices

This page intentionally left blank

Appendix A - Files in the EM Pump Databank

Document Title	Entity	Page Count	Size (MB)
Collection of calculations regarding large EM Pump development	GE	433	149
Design and Analysis Presentations of Large EM Pump	GE	14	108
Double Stator EM Pump Peer Review	GE	24	266
Duct and Ring Metal Combination Assessments 1998	GE	181	<1
EM Pump Hydraulic and Stress Analyses - Byron Jackson	Byron	69	2
EM Pump Hydraulic and Stress Analysis 1989	GE	72	9
Input conditions and results of EM Pump thermal analysis	GE	11	21
Large EM Pump Test Matrix 2001	GE	199	<1
Prototype Electromagnetic Pump Design Status Report YL-270D-89175	GE	179	<1
Response to Prototype EM Pump Interim Design Review Comments.	GE	8	8
Review of EM Pump Design Changes 1989	GE	40	11
Testing Data and Analysis for EM Pump Collection	GE	627	12
Toshiba Data Evaluation for Large EM Pump Test 2001	Toshiba	32	1
Evaluation Of Inner Stator Radial Clamping	GE	321	75
Flux Testing of Lamination Blocks	GE	94	2
Lamination Block and Clamping Design	GE	142	<1
Large EM Pump Lamination File	GE	529	36
Large Scale EMP Development Program Plan: Stator Clamping Design and Thermal Analysis	GE	13	134
Magnetic Test Data of Lamination Stacks	ANL	25	<1
ARP Presentation of Test Results 2002	ARP	58	2
GE Prepared Documents for 160 m3/min EM Pump Project	GE	937	10
JAPC, Toshiba, and KHI Prepared Documents for Large EM Pump Project	JAPC	561	26
JFY 1997 Development Study of Sodium Immersed Large EM Pump – Design and Fabrication of Inner Stator and Support Structures	Japan	209	26
Large EM Pump Test Matrix 2001 (different document)	GE	125	140
Toshiba-GE Technical Meeting on 160m3/min EM Pump Project.	Toshiba	116	4
EM Pump MHD Instability	GE	148	3
EM Pump MHD Stability Update 1997	GE	16	<1
Large EM Pump Design Questions	Japan	66	<1
Magnetic Analysis of Axial Gaps at Stator Back Iron	GE	19	1
MHD Instability in Electromagnetic Pumps.	GE	31	1
EM Pump Miscellaneous Assumption Descriptions	GE	5	<1
GE 2D Electric and Magnetic Finite Element Analysis Package	GE	264	84

Document Title	Entity	Page Count	Size (MB)
LINEAR INDUCTION MOTOR EXPERIMENTS IN COMPARISON WITH MESHMATRIX ANALYSIS	JPL	10	1
Matrix Analysis of Linear Induction Machines Select Report	GE	417	10
MATRIX code runs and basic information on EAGLE code	GE	58	1
NTIS Matrix Analysis of Linear Induction Machines complete report	NTIS	739	14
Selected EM Pump Cross Section Flux Analysis Results	GE	51	1
Test Pump Electrical Parameters	ANL	30	1
Two-dimensional EM Pump code development 2001	GE	105	2
Upwind Galerkin Finite Element Analysis of Linear Induction Motors	Galerkin	5	<1
Compilation of Meeting Reports between GE and Toshiba for Large EM Pump project	Toshiba	1159	15
EM Pump Development Review Meeting July 1986	DOE	66	278
EM Pump Stator Segment Test Readiness Evaluation Report YL-270-88139-A1	ANL	57	1
Segment Stator Test Article Design Review July 1987	GE	109	2
Design and Fabrication Drawing Compilation	GE	333	<1
Design Drawings for 160 m3/min Large EM Pump Tested at ETEC	DOE	583	87
Design Guide	GE	79	2
Layout Drawings of Double Stator EM Pump	GE	4	139
PRISM core shielding model assembly	GE	7	5
Prototype EM Pump Design Requirements Specification 23A3907	GE	58	3
Selected Stator Segment Model Pump Drawings	GE	9	<1
SS3 EM Pump Design Drawings	GE	50	<1
160m3/min EM Pump Inner Stator Design and Assembly Sequence Presentation	GE	47	8
ANL-PRISM-39 OCR	ANL	46	1
Byron Jackson EM Pump Design Status Report.	Byron	78	2
Byron Jackson EM Pump Fabrication and Inspection Reference Plan.	Byron	39	<1
Design and Fabrication of Inner Stator JFY1999	Japan	99	5
Design and Fabrication of Inner Stator JFY2001	Japan	233	10
Design Report: Inner Stator 3-Coil Mockup for Large Scale EM Pump	GE	95	5
Development Study of Sodium Immersed Electromagnetic Pump (EMP) (Part 2) – Design and Fabrication of Inner Stator and Support Structures JFY1998	Japan	99	5
Development Study of Sodium Immersed Electromagnetic Pump (EMP) (Part 2) JFY 1999	Japan	215	20
Development Study of Sodium Immersed Electromagnetic Pump (EMP) (Part 2) JFY 1999	Japan	215	20

Document Title	Entity	Page Count	Size (MB)
Development Study of Sodium Immersed Electromagnetic Pump: Design and Fabrication of Inner Stator Support Structures	GE	198	47
EM Pump Fabrication Operations and Equipment Requirements	GE	214	3
EM Pump Fabrication Operations and Equipment Requirements 1989	GE	194	3
Inner Stator 3-Coil Mockup for Large-Scale EM Pump	ANL	109	31
Instrumentation Requirements for EM Pump	GE	151	9
Interface and Wiring Schematic for Large EM Pump	GE	59	2
Primary Sodium Electromagnetic Pump, Task A, Fabrication Technique Summary Report.	GE	32	9
PRISM EM Pump Assembly Sequence Diagrams and DLD.	GE	28	9
PRISM EM Pump Special Fabrication Methods.	GE	41	9
SS3 Fabrication and Key Feature Testing Photos	GE	95	24
Stator Segment 3 Test Article Design Report.	GE	278	5
Stator Segment Test Description and Experience 1989	GE	79	3
Adhesives Information and Development Collection	GE	95	41
Assessment of EM Pump materials under irradiation JFY90	GE	60	1
Bar Testing and Insulation Development Collection 1988	ANL	77	7
CVD/High Temperature Actuation	GE	26	1
Data, Graphical Representation, and Pictures from Insulation bar material testing 1986-1988	GE	261	18
EBR-II material test plan August 1992	ANL	10	<1
EM Pump coil insulation operating environment	GE	4	<1
EM Pump insulation test sample picture	ANL	4	<1
EM Pump material radiation assessment with cost info Jan 1991	ANL	15	<1
GE High Temperature Insulation System Design Philosophy and Experience	GE	4	<1
High Temperature Coil Insulation accelerated aging test - development study of sodium immersed	ANL	79	18
High temperature insulation materials for self-cooled EM Pump	GE	13	<1
Input data for EM Pump materials radiation assessment	GE	7	<1
Insulation Material and EM Pump Development at Argonne National Laboratory 1986-1996	ANL	231	13
Insulation Material Development Bruce Dunn Material	Dunn	116	5
Insulation Material Development Ken Mathes	Mathes	128	7
Insulation Material Review by Oak Ridge National Laboratory	ORNL	213	10
Insulation Material testing descriptions pre-1989	GE	21	1
Insulation sample irradiation test plan	ANL	8	<1
International Collaboration for LMR FY 87 Summary Status Report	DOE	55	3

Document Title	Entity	Page Count	Size (MB)
Investigation on Deterioration of Insulation (FMEA Analysis).	ANL	11	<1
Irradiation maximum dose level in APR	DOE	3	<1
Irradiation of Electromagnetic Pump Insulation Samples for ALMR	DOE	130	3
JFY 90 EM Pump assessment of insulation materials under irradiation	Japan	22	<1
Literature Search and Miscellaneous Insulation Material Development	GE	129	7
ORNL Report on Alternate Insulation Systems for EM Pump	ORNL	254	20
Secon Analysis and Insulation Material Testing w cover	GE	18	<1
Selected Correspondence Between General Electric and Argonne National Laboratory on Insulation Material Testing	GE/ANL	86	5
Selected Data from Insulation Material Testing 1988	GE	210	15
Thermal Performance Study of Liquid Metal Fast Breeder Reactor Insulations	DOE	259	12
Properties of magnetic materials for use in high-temperature space power systems	NASA	4	<1
Radiation-resistant magnet wire for use in air and vacuum at 850C	GE	6	<1
Standard Specification for Copper Sheet	GE	6	<1
Technical data from Carpenter	Carpenter	5	<1
Disassemble and Inspection Request 1996	GE	7	<1
Electromagnetic Pump Stator Segment Model Post Test Disassembly and Inspection, Final Report (DRAFT), 1GSV496-2	DOE	255	73
JFY Annual Report 1995	Japan	346	3
JFY Annual Report 1996	Japan	560	9
Outer Stator Disassembly and Inspection Requirements	GE	7	<1
GEFR-00869 EM Pump Stator Segment Test	ALMR	46	1
Prototype EM Pump Test Requirements Specification 23A3908	GE	63	<1
Power Supply Reports from Alstom and Olsun	Alstom	1045	3
Specification and Inspection Documentation for Large EM Pump	GE	356	91
Coil Fabrication Photos	GE	7	3
Duct Extension Photos	GE	6	4
Duct Segments	GE	49	46
Instrumentation	GE	9	5
Lamination Block Fabrication	GE	21	11
Pole Connections	GE	35	24
Poles	GE	21	8
Pump Lift at ETEC	Japan	3	<1
Shipping	GE	48	31
Upper Adapter	GE	36	24

Document Title	Entity	Page Count	Size (MB)
Large EM Pump Photos	GE	7	24
Pole 8 Pics	GE	27	13
GRC Tear down	GRC	1	<1
160 m3/min EM Pump Test Descriptions	GE	54	10
Application Data for Induction EM Pumps	GE	28	4
Brief EM Pump Overview Presentations	ALMR	25	<1
Cavitation background	GE	21	2
Comparison of Current Reference Single Stator and Alternate Double Stator EM Pumps.	GE	12	<1
EM Pump Actual Costs Vs. Estimated Costs	GE	22	<1
EM Pumps for Space Applications	GE	260	7
Feasibility Study of a Magnetically Coupled Pump for Use in a Fast-Reactor Coolant Circuit	DOE	32	1
Large EM Pump Development Plan_1974	DOE	51	11
Large EM Pump Procurement Activities	GE	302	6
Operating Experience with Sodium Pumps at EBR-II	ANL	55	12
Presentation to JAPC during visit to GE May 2000	Japan	17	1
Primary Sodium Electromagnetic Pump WBS4.1.3.1 1989	--	9	2
Response to TEPCO Questions on EM Pump	Japan	32	1
Selected Conference and Journal Papers on EM Pumps	--	46	3
Space Power EM Pump Program Review 1964	NASA	78	3
Steel Sales Bulletin with Sourcing Request	--	23	1
Electrical Conductor and Electrical Insulation Materials Topical Report	GE	782	23
Mechanical Properties Design Data Program	GE	310	13
Hiperco Soft magnetic alloy for high flux levels	Hiperco	5	<1
Materials Data Collection for Reference	--	223	12
Thermal Analysis Development	GE	31	2
Analysis Results	--	21	<1
THERMAL_MOD	GE	1	<1
MATRIX_Input_File	GE	1	<1
MATRIX_06252015	GE	1	<1
Copper Conductor Package	GE	1	2
Copper Conductor Package	GE	1	<1
Lamination Block	GE	1	3
Lamination Block	GE	1	<1
EM Pump Overview -PRISM Intermediate and Primary Pumps	GE	15	<1

Document Title	Entity	Page Count	Size (MB)
EM Pump Overview	GE	79	15
Linear Induction Motor Experiments in Comparison with Mesh Matrix Analysis	GE	10	1
EMP PES Final Dec 2005 Fanning	GE	9	1
India 2 SFR IGCAR	India	31	5
PRISM NT	ALMR	15	1
1991 Advanced Self Cooled Pump Testing at ANL	ANL	9	<1
1996 Progress in Japan in high temperature electrical insulation	Japan	12	1
Design and Development of Large Scale coil for high temps	GE	10	1
Design and Development of Large Scale coil for high temps	GE	10	1
EM Pump Thrust Calculations	GEH	16	1
Matrix Code Update Presentation	GEH	16	1
Matrix Code Project 5 21 14 presentation	GEH	5	2
EM Pump Insulation update 10/30/2013	GRC	14	3
EM Pump Insulation update 12/4/2013	GRC	25	8
EM Pump Insulation update 2/5/2014	GRC	21	5
EM Pump Insulation update 3/7/2014	GRC	32	10
EM Pump Insulation update 4/23/2014	GRC	13	3
EM Pump Insulation update 5/7/2014	GRC	18	6
EM Pump Insulation update 5/21/2014	GRC	9	6
EM Pump Insulation update 6/3/2014	GRC	7	1
EM Pump Insulation update 6/18/2014	GRC	19	5
EM Pump Insulation update 7/16/2014	GRC	22	6
EM Pump Insulation update 7/29/2014	GRC	24	7
EM Pump Insulation update 8/13/2014	GRC	12	5
EM Pump Insulation update 8/27/2014	GRC	7	2
EM Pump Insulation update 9/24/2014	GRC	21	4
EM Pump Insulation update 11/18/2014	GRC	6	<1
EM Pump Insulation update 12/17/2014	GRC	15	2
EM Pump Insulation update 7/1/2015	GRC	7	3
EM Pump Insulation update 7/15/2015	GRC	23	8
EM Pump Special Telecon 10/30/2014	GRC	6	3
ANL Project Status Update GE ALIP Forces on Coils	ANL	4	4
ANL Project Status Update Test Status 10/30/2014	ANL	19	4
ANL Project Status Update Testing Status 11/19/2014	ANL	42	5
ANL Project Status Update ANL Slides 2/3/2014	ANL	67	5
ANL Project Status Update Status 2014-12-17	ANL	14	<1

Document Title	Entity	Page Count	Size (MB)
ANL Project Status Update GE Insulation R4	ANL	23	70
ANL Project Status Update GE Insulation 3/12/15	ANL	13	1
ANL Project Status Update 3/12/2015 Pics	ANL	13	77
ANL Project Status Update 3/24/15	ANL	13	1
ANL Project Status Update 4/8/15	ANL	11	<1
ANL Project Status Update 4-22-15	ANL	14	2
ANL Project Status Update 5/20/15	ANL	12	3
ANL Project Status Update 5/13/15	ANL	17	4
ANL Project Status Update 6/3/15	ANL	15	1
ANL Project Status Update 6/16/15	ANL	31	5

This page intentionally left blank

Appendix B - Federal Assistance Reporting (FAR) Checklist

Federal Grant Identification Number: DE-NE0000613

Recipient Organization: GE-Hitachi Nuclear Energy Americas LLC
3901 Castle Hayne Road
Wilmington, NC 28401

Project Title: Qualification of EM Pumps: Next Generation Electromagnetic Pump: Analysis Tools and Insulation Materials Development

Report # DOEGEHA00613

Principal Investigator: Eric P. Loewen, Ph.D.
Chief Consulting Engineer, Advanced Plants
T 910-819-5190 F 910-363-5190
Email: eric.loewen@ge.com

Submitter: James Robinson
Project Manager
T 910-819-6215 F 910- 342-6215
Email: ne22472@ge.com

Other Team Members: Argonne National Laboratory
9700 South Cass Avenue
Argonne, IL 60439

3. Executive Summary

Research on the next generation electromagnetic (EM) pump analysis tool, i.e., the improved MATRIX code, revealed the importance of current carrying sodium velocity profile on the pressure head developed by the pump. It was found that application of a suitable correction factor or equation to the “flat” velocity profile results in a more accurate pump pressure head prediction, alleviating the need for multiplying the MATRIX results by an arbitrary factor of 0.7. The present research also added the thermal analysis directly to the improved MATRIX code thereby removing the need to run a separate code AGENA. The research on winding insulation materials development resulted in a better understanding of many

competing requirements for the insulating material and finally produced the Silicon-Bonded Mica Hard Board (SBMHB) slot-liner concept as the preferred approach. Multi-stress testing of this slot-liner insulation concept, however, was not complete under this research.

The analysis tool, MATRIX, was modernized to operate on a fully supported computer platform in the GE DTA format, improved its accuracy of pressure head prediction, and updated to incorporate both materials and thermal analysis into an all-purpose analysis tool. Post-processing tools were added to MATRIX, which simplified data processing, allowing the user to evaluate the data more efficiently and effectively. Systematic approach was used to identify the suitable insulation materials including tapes, binders and slot-liners. Laboratory equipment was designed and built to conduct prototypic, multi-stress testing at temperature; however, such testing was not complete under the present research project.

The research produced an improved EM pump analysis tool and an improved approach for winding insulation, which would make EM pumps with no rotating parts more attractive to be employed in liquid-metal cooled nuclear reactors. The public, in general, would benefit when such nuclear reactors are deployed to generate electricity from the spent or used nuclear fuel and for reducing the volume of nuclear waste to be placed in permanent repository.

4. Accomplishments of the Project

A comparison of the actual accomplishment with the original goals and objectives of the project is provided below in Table B-1, Project Task Summary. This table was derived from the original proposal, and the right column provides actual accomplishments.

Table B-1: Project Task Summary

Task #	Description	Owner	*Report(s) and Section(s)	Status
1.1	Update databank environments in a product lifecycle management system	GEH	Section 2.0 and Appendix A	Done
1.2	Collect and organize relevant existing design drawing, documents, and operation experience on EM pumps.	GEH	Section 2.0 and Appendix A	Done
1.3	Identify and document applicable nuclear and non-nuclear standards that apply to EM pumps	GEH	Section 2.0	Done – (DOC-0004-7828)
2.1	Review prior EM Pump insulation research	GRC	Insulation Report Sections 1.2, 3.1, and Appendix A	Done
	Summary report of EM Pump insulation history	GRC	Insulation Report Section 3.1	Done
	Dielectric characterization of prior insulation system	GRC	Insulation Report Section 3.2	Done
2.2	Develop new insulation materials & designs	GRC	Insulation Report Section 3.3	Done
	Binder candidates (selection and screening)	GRC	Insulation Report Section 3.3.1 and Appendix E	Done
	Fiber candidates (selection and screening)	GRC	Insulation Report Section 3.3.2 and Appendix E	Done
	New insulation designs	GRC	Insulation Report Sections 3.3.3 through 3.5	Done
2.3	Develop new Insulation test & specimens	Shared	--	--
	Model forces & motion	GEH/GRC/ANL	Insulation Report Sections 4.0 and 5.0	Done
	Develop multi-stress insulation test	ANL	Insulation Report Sections 6.1 and 6.2; Appendix G and H	Partial, tester had issues
	Benchmark prior insulation system	ANL	Insulation Report Sections 6.5 and 6.6	Partial, tester had issues
	Develop new insulation specimens for ANL to test	GRC	Insulation Report Sections 3.4.7 and 3.4.10	Partial
2.4	Perform multi-stress insulation tests	ANL	Insulation Report Section 6.0	Reported but incomplete
	Replicate tests on binder/fiber candidates	ANL	Not Reported	Incomplete
	Replicate tests on new insulation design	ANL	Not Reported	Incomplete
	Optimize fiber/binder candidates	ANL	Not Reported	Incomplete
	Optimize new design	ANL	Not Reported	Incomplete
3.1	Review current EM pump computational methods used at GEH and GRC	GEH	MATRIX Report Section 3.1	Done

Task #	Description	Owner	*Report(s) and Section(s)	Status
3.2	Capture knowledge of existing methods on best computational practices for capture in Task 1 activities	GEH	MATRIX Report Section 2.3 and 3.2	Done
3.3	Update MATRIX for current computing environment	GEH	MATRIX Report Sections 3.2 and 3.3	Done
3.4	Create a MATRIX user's manual with explanation of analysis method	GEH	MATRIX Software User's Manual (PLM DOC-0003-7657 Rev. 0)	Done
4.1	Investigation into development of new or adaptation of existing commercially available analysis tools for EM pump modeling. This investigation will be based on knowledge gained from Task 1 and 3	GEH	MATRIX Report Sections 2, 3 and 4	Done
4.2	Analysis tools will be modified to analyze an EM pump. These tools will be benchmarked against experimental data from Task 1 and the MATRIX model when possible	GEH	MATRIX Report Sections 3.3 and 5.0	Done
Deliverables	**Final Technical Reports**	**Shared**	--	--
***Insulation Report**	ELECTROMAGNETIC PUMP INSULATION MATERIALS DEVELOPMENT AND TESTING (PLM-DOC-0005-2465)	GRC	Sections 1.0, 3.0, 4.0, and 5.0; Appendix B - F	Done
	Insulation testing	ANL	Sections 4.0, 6.0; Appendix G - I	Reported but incomplete
***MATRIX Report**	NEXT-GENERATION ELECTROMAGNETIC PUMP ANALYSIS TOOLS (PLM DOC-0005-2188)	GEH	All Sections (Except 4.2 and 4.3)	Done
	Finite Element Analysis (FEA)	GRC	Section 4.2	Done
	Coil force comparisons	ANL	Section 4.3	Done

As shown in Table B-1, the actual accomplishments are indicated with the original goals. The research team struggled with the completion of subtask 2.4 due to difficulty of performing the multi-stress test. The Project underestimated the difficulty in the confluence of establishing a low oxygen gas environment, at elevated temperatures, with applied high voltage, with relative movement at a fixed force. The repeatability of this environment (gas, temperature, voltage and motion under force) on previous binder/fiber system and developed binder/fiber candidates could not be attained. Thus the ability to perform replicate tests on new insulation designs was not completed; therefore, no optimization fiber/binder candidates of the new design were completed.

5. Project Activities

(a) Project Activities Summary:

In 2013, the Department of Energy (DOE) announced a $3.5 million investment opportunity for the further improvement of Advanced Nuclear Power Reactors to expand clean energy leadership and to empower a low-carbon economy. For the past two years, GE Hitachi Nuclear Energy Americas LLC (GEH) with GE Global Research Center (GRC) teamed with Argonne National Laboratory (ANL) to perform Research and Development (R&D) for the next-generation analysis tools and insulation materials for Electro-Magnetic (EM) Pumps. These tools and insulation materials are necessary for the development and qualification of EM Pumps used in advanced liquid-metal reactor (ALMR) designs.

GEH led the research efforts to ensure the relevant pockets of individual expertise within industry and one of the DOE laboratories were incorporated into industry products for the benefits of the U.S. In GEH's 2009 Technology Development Roadmap: Facilities for Closing the Fuel Cycle (#DE FC01-07NE24504), the self-cooled EM Pump is defined as a "critical technology element" for the development.

The project was kicked off with the GEH team (PI, PM, and one individual contributor) traveling to both GRC and ANL for individual project alignment meetings. In these meetings, the project schedule, project reporting, project technical deliverables, and approaches were discussed.

Once the approach was defined, the project started on Task 1 and 2. GEH started the update of the EM Pump databank environments in a product lifecycle management system. This process resulted in the collection and organization of the relevant existing design drawing, documents, and operation experience on EM pumps. ANL came to GEH to review progress and provide prioritization of which document to place into the databank.

GRC led the efforts of Task 2. Task 2 leveraged the initial progress of GEH Task 1 activities to review the prior EM Pump insulation research that was being loaded in the databank. This allowed GRC to produce a summary report of EM Pump insulation history so that the proper direction of the research could be started. GRC started the dielectric characterization of the prior insulation system to obtain a baseline. With this baseline established, GRC then set out to develop a new insulation system that include both selection of materials and the designs of those materials to make a better insulation system.

About three months into the project, GEH started Task 3. Leveraging Task 1 results, a review of current EM pump computational methods used at GEH, GRC, and ANL was investigated. This was captured knowledge of existing methods on best computational practices. Then the MATRIX code was updated for current commercial computing environment used at GEH. While the code was being updated, a MATRIX user's manual with explanation of analysis method was drafted.

Task 2 advanced to the next subtasks. GRC worked with several commercial companies to determine which candidate binder materials would work. This involved many screening tests of the selected materials. Next, the fiber candidates went through a similar selection and screening process. In the course of this effort, a completely new insulation design was developed and submitted to the United States Patent and Trademark Office (USPTO) for a future patent.

At this point at GEH, the investigation into development of new or adaptation of existing commercially available analysis tools for EM pump modeling was evaluated. At this point, the MATRIX code was fully functional with a new operating approach. After modernization, it was benchmarked against experimental data from Task 1 and the MATRIX model to validate its operation. This was completed in December of 2014.

ANL subtasks were started about one quarter late from the original proposed scheduled. The entire team worked on what are the key parameters to establish a multi-stress test environment. The more the team looked into the technical details, the more complex the simulated environment (the inside of a submerged EM Pump) became. Recreating an environment became more difficult than originally thought. The model predictive forces and the actual motion in the multi-stress tester continued forward.

In January of 2015, GEH started on Task 4 activities, which continued until project close on August 5, 2015. The investigation into the adaptation of existing commercially available analysis tools, within or coupled to MATRIX, did not prove to be as viable as initially expected. What the investigation showed is the development of new analysis tools with MATRIX was easier in the new computing environment. This investigation was based on knowledge gained from Task 1 and success of the Task 3 updates to the code. The MATRIX model was then updated for flow correction in the duct, ability to input material properties, and a thermal analysis module.

The efforts to start multi-stress testing at ANL started in earnest in the fourth quarter of 2014. Initial development of the multi-stress tester began in first quarter 2015 with controlling the oxygen environment and the development of a movement device that was all coupled to a high-voltage source. GRC provided ANL testing samples, as needed. Weekly meetings regarding the progress of the ANL testing sought to provide ANL different solutions/success paths in order to obtain a stable multi-stress platform. The details of the difficulties are provided in the final technical report (Electromagnetic Pump Insulation Materials Development and Testing (PLM-DOC-0005-2465). In summary, the following was not completed: replicate tests on binder/fiber candidates developed by GRC; replicate tests on new insulation designs to determine reliability; conduct tests to optimize fiber/binder candidates; and optimized new design that was developed by GRC.

The project was stopped and the project deliverables documented in two final technical reports: Final Technical Report: Electromagnetic Pump Insulation Materials Development and Testing (GEH #PLM DOC-0005-2465); Final Technical Report: Next-Generation Electromagnetic Pump Analysis Tools (GEH #PLM DOC-0005-2188)

(b) Original Hypotheses:

This project had two original hypotheses:

- The past insulation system is not workable.

- The MATRIX code was non-functional as current day analysis tool.

Some background on the two hypotheses:

Insulation system not workable

The company that originally manufactured and sold part of the insulation material for the 160m^3/min EM pump no longer existed, and access to the ore body for the mineral from which this material is made was no longer available. The original insulation had been 'pedigreed' by previous ANL long-term, thermal cycle testing, and material behavior had been observed under neutron flux. The approach to overcome the hypotheses was to validate the constituents of the previous insulation material in order to seek a modern alternative insulation material that closely matched or exceeded the properties (i.e., electrical and mechanical properties) of the insulation in the 160m^3/min EM pump.

MATRIX Code was non-functional

GEH's proprietary EM pump analysis model, MATRIX, was created by Dr. David G. Elliott at the Jet Propulsion Laboratory in Pasadena, California, in 1975 for use on mainframe computers. In 1990, this model was modified by GE for more flexibility in its analysis method on DEC Alpha Platform. In 1999, it was modified again to run on a PC platform but has been dormant since 2001. The approach to overcome the hypotheses was to modernize this analysis model to run on current computing platforms (clusters), update the documentation for the new computing environment, and update the analysis methods therein. With the MATIX code operational on the new platform, it was updated for flow correction, materials, and heat transfer to become the next-generation ALIP design and analysis tools with improved electromagnetic (EM), magnetohydrodynamic (MHD), and thermal in steady-state.

(c) Approaches Used:

Our approach to overcome these two negative hypotheses was to break the problem into four Tasks. Simply: What do we know from the past that we can apply to the two problem hypotheses (Task 1);

Understand the original insulation and come up with an equivalent or better insulation system and then perform multi-stress tests (Task 2); Bring the MATRIX Code out of electronic storage and update for operation on current day computing platforms (Task 3); Develop the next generation EM Pump analysis tools (Task 4). Below are the approaches used for each of these Tasks:

Task 1: Update EM Pump Databank (GE)

GEH created a legacy ALIP pump databank for searchability from Super-PRISM (S-PRISM), ALMR, Integral Fast Reactor (IFR), and the Large EM Pump programs. This databank includes previous GEH design and analysis tools and results, as well as drawings of EM pump prototype and proof-of-principle components. The experimental test data from the 160 m^3/min pump test program was digitized, as well as publicly-available literature from other EM pump experiments. Finally, the relevant PRISM reactor pump design specifications where collected. The information was stored on a product lifecycle management system. Task 1 was divided into three subtasks:

Subtask 1.1 Update databank environments in a product lifecycle management system.

Subtask 1.2 Collect and organize relevant existing design drawing, documents, and operation experience on EM pumps.

Subtask 1.3 Identify and document applicable nuclear and non-nuclear standards that apply to EM pumps.

Task 2: Insulation Materials Development and Evaluation (GE, ANL)

The company that originally manufactured and sold part of the insulation material for the 160m^3/min EM pump no longer exists, and access to the ore body for the mineral from which this material is made is no longer available. The original insulation had been 'pedigreed' by previous ANL long-term thermal cycle testing, and material behavior had been observed under neutron flux. This tasking follows Task 1 quantification to validate the constituents of the previous insulation material in order to seek a modern alternative insulation material that closely matches or exceeds the properties (i.e., electrical and mechanical properties) of the insulation in the 160m³/min EM pump. GRC identified and produce alternative insulation materials. GEH provided the testing requirements for ANL and GRC to work collaboratively to test insulation samples. ANL built a multi-stress tester to subject the sample to thermal cycle and stress tests. Task 2 was divided into four subtasks:

Subtask 2.1 Identify properties of old insulation material. Compare with previous documentation (design specs, testing, etc.) contained in databank from Task 1 and perform limited direct testing (as needed) to provide a link with previous data.

Subtask 2.2 Development of a chemical composition of new insulation material along with material structural properties evaluation.

Subtask 2.3 Develop and produce samples of insulation materials for further evaluation.

Subtask 2.4 Evaluate alternative materials through thermal, electrical, and mechanical testing to qualify longevity of insulation performance.

Task 3: Modernize Existing EM pump Analysis Model (GE)

GEH's proprietary EM pump analysis model, MATRIX, was created by Dr. David G. Elliott at the Jet Propulsion Laboratory in Pasadena, California in 1975 for use on main frame computers. In 1990 this model was modified by GE for more flexibility in its analysis method on DEC Alpha Platform. In 1999, it was modified again to run on a PC platform and has been dormant since 2001. GEH modernized this analysis model to run on current computing platforms (clusters), updated the documentation for the new computing environment, and updated the analysis methods therein. GEH also created a manual of MATRIX that discusses not only how to use the model, but an explanation of its analysis method. This exercise was documented and serves as a theoretical knowledge transfer of the EM Pump technology for potential licensing and design work. Task 3 was divided into four subtasks:

Subtask 3.1 Review current EM pump computational methods used at GEH and GRC.

Subtask 3.2 Capture knowledge of existing methods on best computational practices for capture in Task 1 activities.

Subtask 3.3 Update MATRIX for current computing environment.

Subtask 3.4 Create a MATRIX user's manual with explanation of analysis method.

Task 4: Develop Next-Generation EM Pump Design and Analysis Tools (GE)

The research team developed the next-generation ALIP design and analysis tools informed by Task 1 through 3 activities. The next-generation ALIP design and analysis tool was developed, increasing MATRIX's MHD, thermal, and mechanical aspects in steady-state. Task 4 was divided into two subtasks:

Subtask 4.1 Investigation into development of new or adaptation of existing commercially available analysis tools for EM pump modeling. This investigation will be based on knowledge gained from Tasks 1 and 3.

Subtask 4.2 Analysis tools will be modified to analyze an EM pump. These tools will be benchmarked against experimental data from Task 1 and the MATRIX model when possible.

(d) Problems Encountered:

The project faced the biggest problems in Subtask 2.4. Specifically, the test team was unable to control the oxygen content in the furnace at elevated temperate below the previous requirements. The tests were unable to apply the high voltage to the insulating system without arcing within the furnace or external control circuitry. The movement of the sample with the combination of low oxygen and high temperature with high voltage applied had problems this project could not overcome. Figures B-1 and B-2 show some examples of difficulties with the multi-stress testing.

Figure B-1: Hot Testing Before and After Samples, Test #4

Figure B-2: HV Wire Clip Failure

The project faced problems in Tasks 4.2 in the integration of CFD and mechanical analysis within the MATRIX code for transient analysis. The linage of MATRIX
(a FORTAN based language) with present day CFD Codes was not made due to incompatibility issues. The same issue was faced when seeking to couple or embed a mechanical (Finite Element code) with MATRIX presented a large incompatible problem this project could not overcome.

(e) Departure from Planned Methodology:

No departure from the planned methodology was made.

(f) Assessment of their impact:

The positive impact of this project was:

1. A searchable databank of EM Pump design, development, operation and post-operation was created. Figures B-3 through B-5 show some examples.

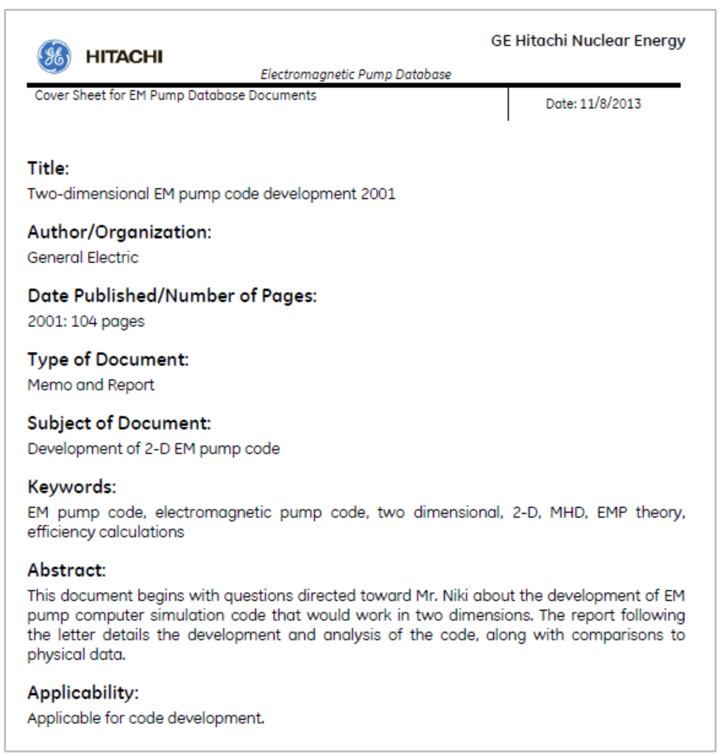

HITACHI
GE Hitachi Nuclear Energy
Electromagnetic Pump Database
Cover Sheet for EM Pump Database Documents
Date: 11/8/2013

Title:
Two-dimensional EM pump code development 2001

Author/Organization:
General Electric

Date Published/Number of Pages:
2001: 104 pages

Type of Document:
Memo and Report

Subject of Document:
Development of 2-D EM pump code

Keywords:
EM pump code, electromagnetic pump code, two dimensional, 2-D, MHD, EMP theory, efficiency calculations

Abstract:
This document begins with questions directed toward Mr. Niki about the development of EM pump computer simulation code that would work in two dimensions. The report following the letter details the development and analysis of the code, along with comparisons to physical data.

Applicability:
Applicable for code development.

Figure B-3: Example Searchable Cover Sheet

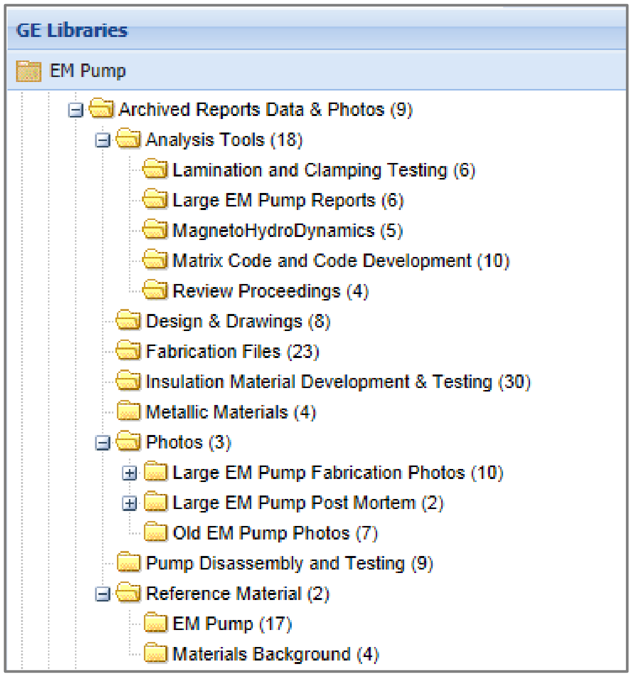

Figure B-4: EM Pump Databank Structure

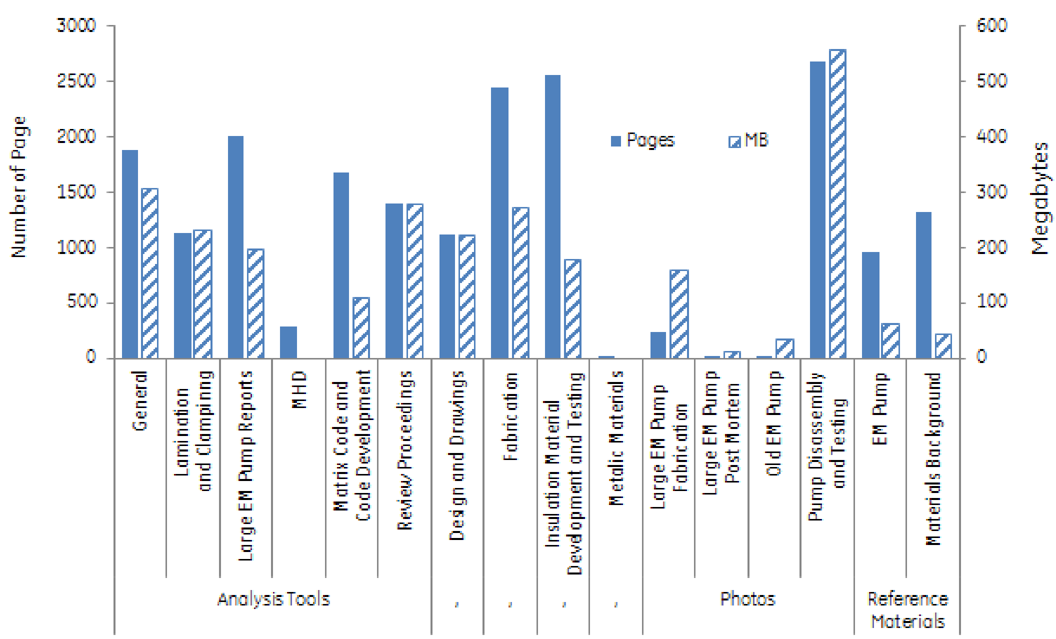

Figure B-5: EM Pump File Size and Number

2. Advanced insulation materials for winding insulation of the pump coil with resilient, engineered material was selected and screened for faster EM pump construction. Figures B-6 and B-7 show some examples.

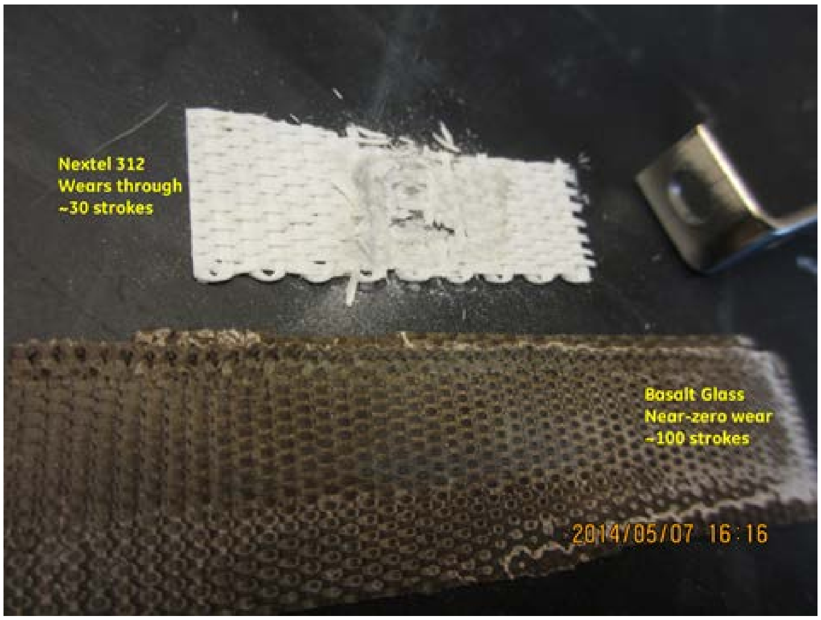

Figure B-6: Polysilazane Binder Abrasion Resistance of Nextel 312 (top) vs CFB Tape

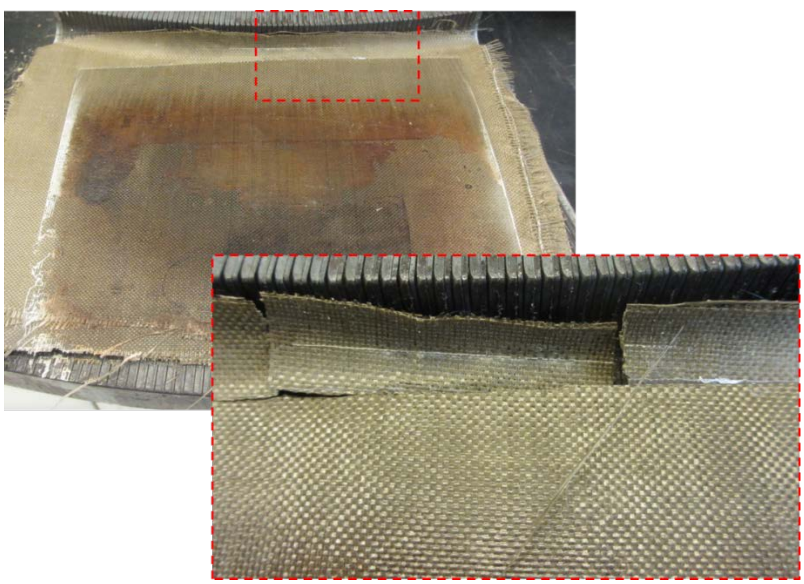

Figure B-7: Molded CFB Laminate Fracturing of Polysilazane (VL20) Binder

This advanced insulation system would lower the pump internal operating temperature, as shown in Figure B-8 from improved MATRIX analysis.

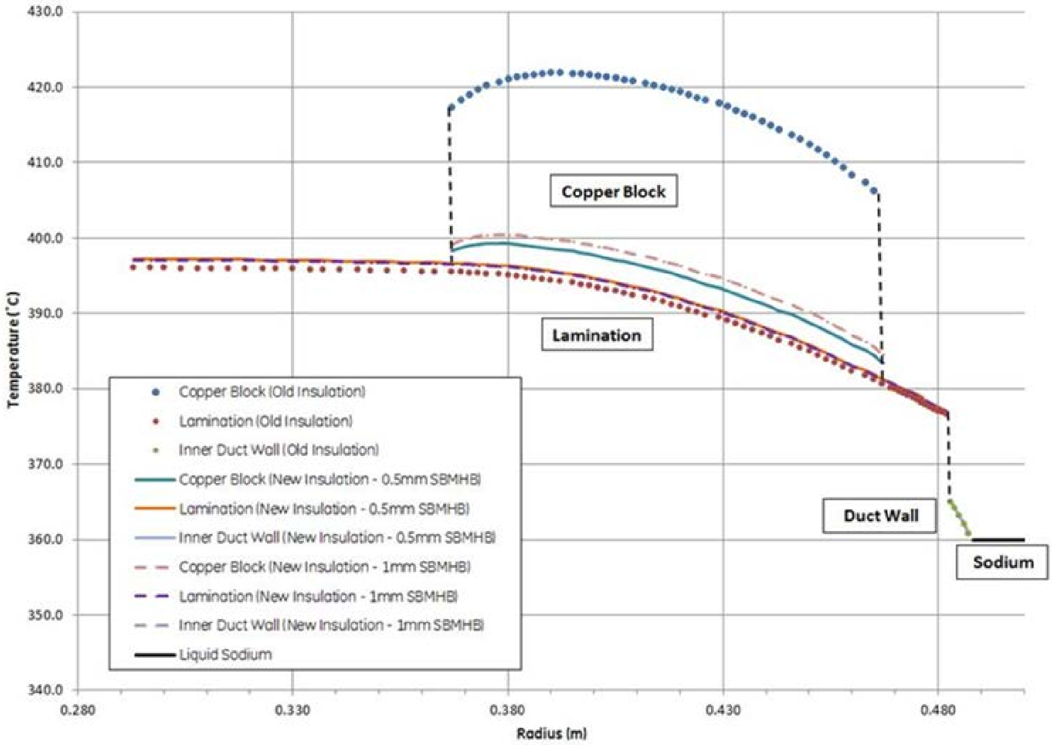

Figure B-8: MATRIX Thermal Profile of the Benchmark and SBMHB Insulation System

3. The MATRIX legacy performance code was modernized using early career engineers (see Figure B-9).

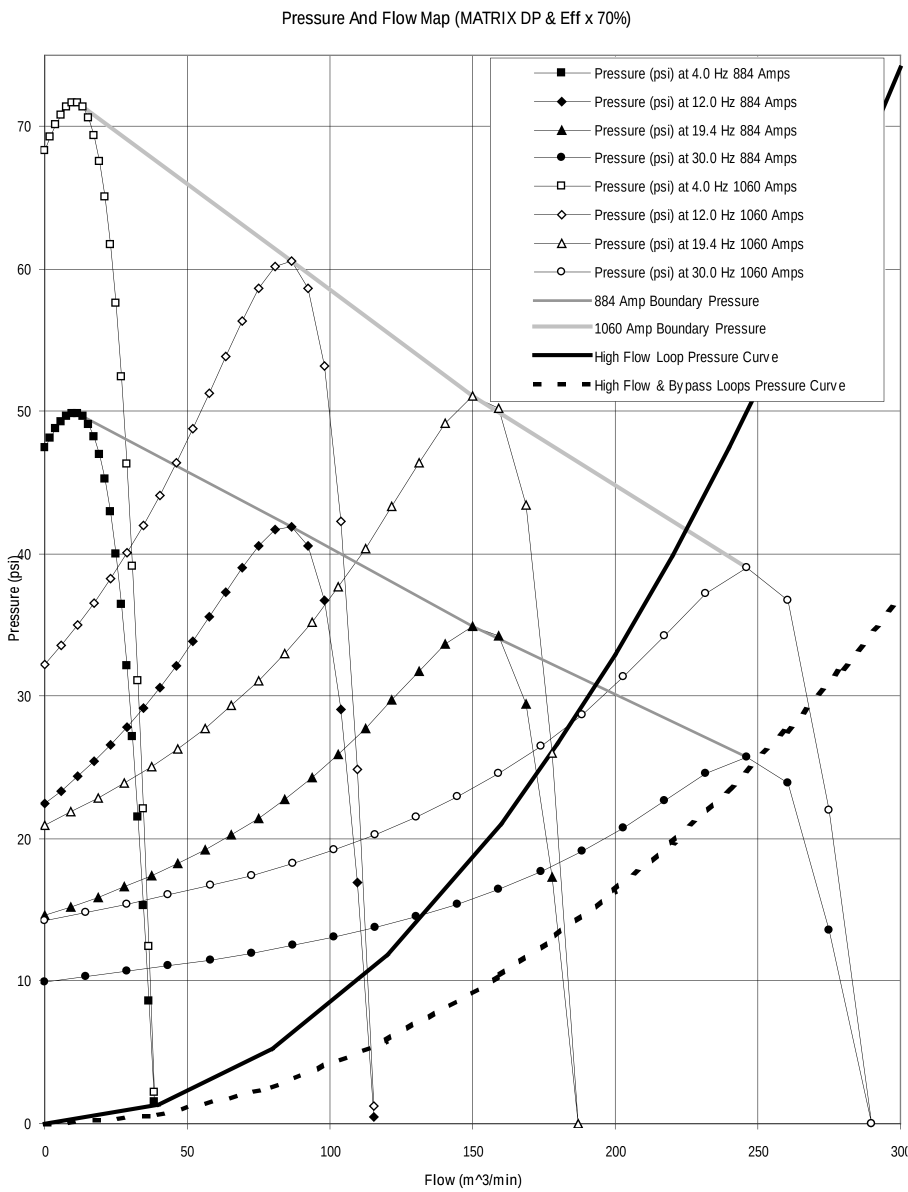

Figure B-9: 2015 MATRIX Pressure Map (with 0.7 Multiplier)

4. With these early career engineers, MATRIX was developed further to better understand the magnetic field and flux profiles as they relate to thermal cycling and pumping efficacy of molten metal. MATRIX results with flow correction are shown in Figure B-10.

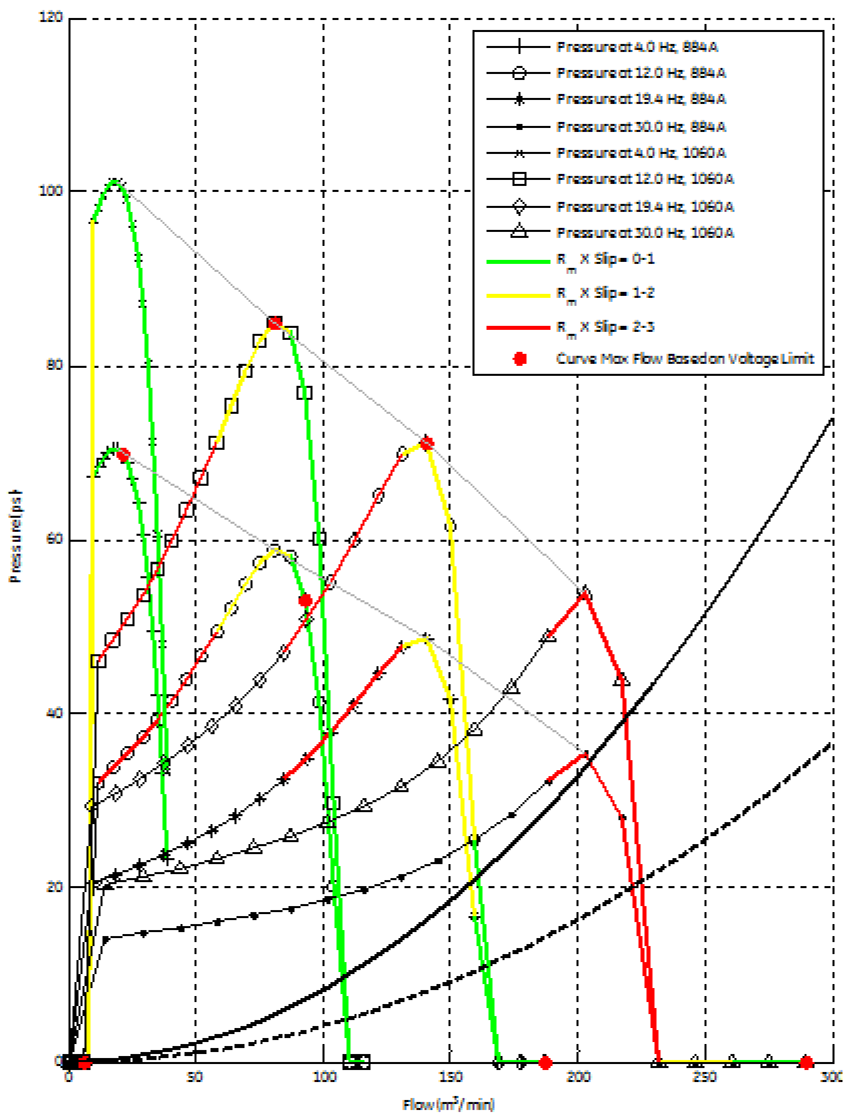

Figure B-10: 3rd Order Flow Corrected MATRIX Developed Head versus Flow Rate .

5. This project provided GEH the ability to conduct collaborative research with ANL. Figure B-11 shows the multi-stress test facility built under this collaboration.

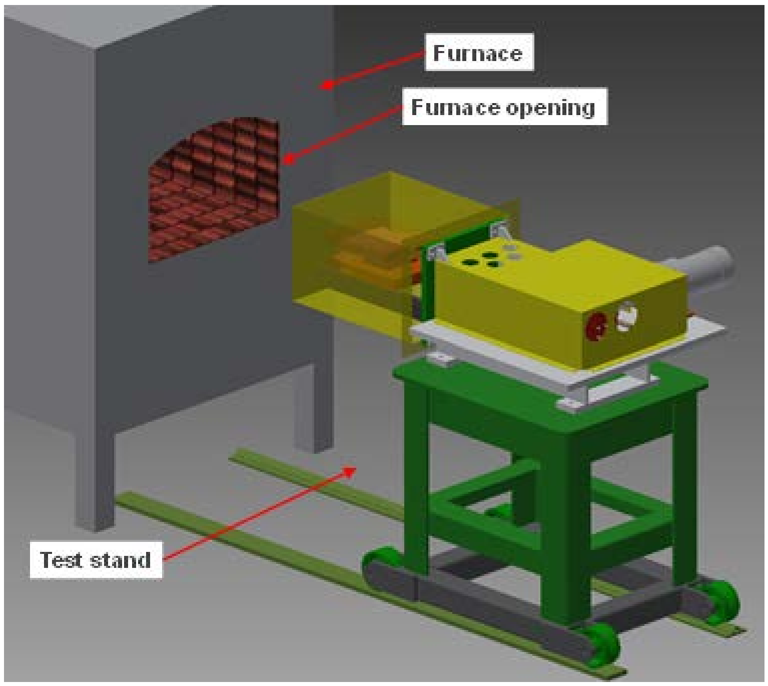

Figure B-11: Sketch of the Multi-Stress Test Facility

6. Products Developed

(a) Publications:

Modernization and Capability Investigation of the MATRIX Electromagnetic Pump Analysis Code. Seth Strege, Serkan Yilmaz, Pradip Saha, and Eric P. Loewen. (Submitted to Nuclear Technology: 2015)

Capability Enhancement of MATRIX EM Pump Analysis Code by Including Thermal Analysis. Ana Da Silva, Pradip Saha, and Eric P. Loewen. (Drafted for Internal Review, submittal to *Nuclear Technology* planned in fourth quarter 2015).

(b) Web Site or other Internet Sites:

Not applicable.

(c) Networks or Collaborations Fostered:

This project allowed GEH to better collaborate with ANL in the development of EM Pumps. ANL provided access to all levels of their technical team to solve problems encountered.

The Project fostered technical discussion with GEH not normally attended at the following two venues:

2013 American Nuclear Society National Winter Meeting, SMR Session, Department of Energy Investments in Advance Nuclear Power, Session Chair: Craig D. Welling

Colloquium titled "PRISM Fast Reactor and Clean Nuclear Fuel Cycle" at University of Nevada, Los Vegas on April 14, 2015 by Dr. E.P. Loewen. A portion of the presentation discussed the project deliverable to students and faculty

(d) Technologies/Techniques

The MATRIX code was modernized in order to streamline the batch running process that had previously been in place, by reconstructing the code into the GE Data Transfer Array (DTA) format. The DTA structure, which is based on common data memory blocks, vastly improved the data transfer and running efficiency of the code without using a fixed sized data structure. In addition, the reorganization eases the maintenance and the ability for future modification of MATRIX. The original code which was split up into three main FORTRAN files, PREMAT.FOR, MATRIX.FOR, and POSTMAT.FOR; Then they were simplified into one main routine controlled by MAIN.FOR. The elimination of the separated FORTRAN source files, which originally all had to be compiled separately for each MATRIX run, streamlined code performance. The process now only uses one generic compiled FORTRAN file.

Technologies: "Slot-Liner

Approach"

The slot-liner approach replaces the traditional ground wall insulation wrap around the coils by using either an insulating coating on the lamination blocks or providing an insulation liner in which the coils can expand and contract. The thermal resistance of the slot-liner system is only about 20% of the thermal resistance that the original pump system demonstrated. Since the slot-liner approach employs a material with a much improved dielectric strength, the total ground wall insulation thickness can be reduced. Due to the CTE mismatch of copper (~17ppm/°C) to that of most high temperature dielectric materials (typically 3 to 6 ppm/°C) and the lack of tensile strength in those materials (and/or embrittlement when combined with binders), following the traditional ground-wall insulation strategy of wrapping the copper coils with insulation will always result in fractured insulation systems. Those fractures within the ground-wall degrade the dielectric strength of the insulation and, as a result, the insulation builds are relatively thick, operating at relatively low dielectric stress. The benefit of a dielectric is not leveraged, and the insulation becomes simply a spacer, relying more on the dielectric strength of the air gap. If a design could be found that did not fracture, then the full entitlement of dielectric strength of the ground-wall materials could be achieved. Furthermore, this results in thinner insulation systems, which translates into higher heat flow and lower copper and insulation temperatures. This, in turn, results in opportunities for higher pump efficiencies, cooler pump temperatures, higher pump energy/power densities, and/or longer insulation life.

The "slot-liner approaches" is summarized in Figure B-12.

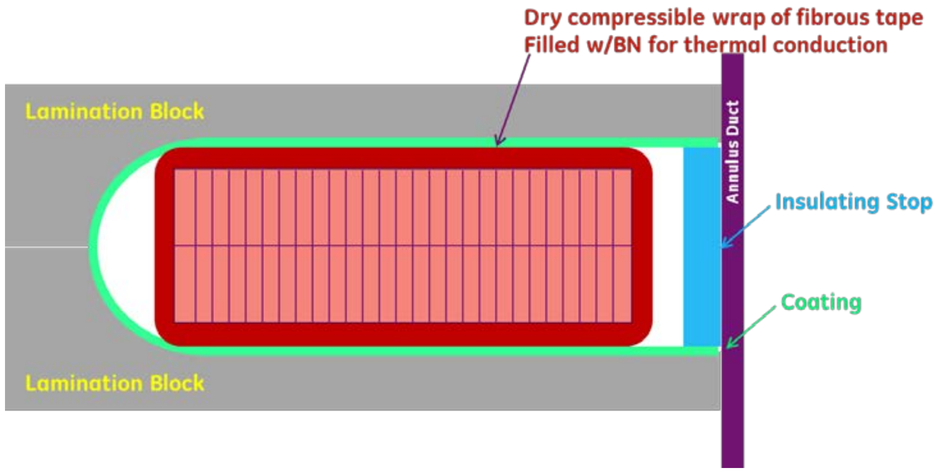

Figure B-12: Cross-Sectional View for the General Concept of Either Slot-Liner Approach

Techniques: To streamline the batch running process from the 1999 MATRIX code, the 2015 MATRIX code was restructured into the GE Data Transfer Array (DTA) format. The DTA structure, which is based on common data memory blocks, vastly improved the data transfer and running efficiency of the code, without using a fixed sized data structure. In addition, the reorganization eases the maintenance and the ability for future modification of MATRIX. The original code, which was split into three main FORTRAN files, PREMAT.FOR, MATRIX.FOR, and POSTMAT.FOR, was consolidated into one, main routine controlled by MAIN.FOR. The modernized MATRIX block flow is illustrated in Figure B-13.

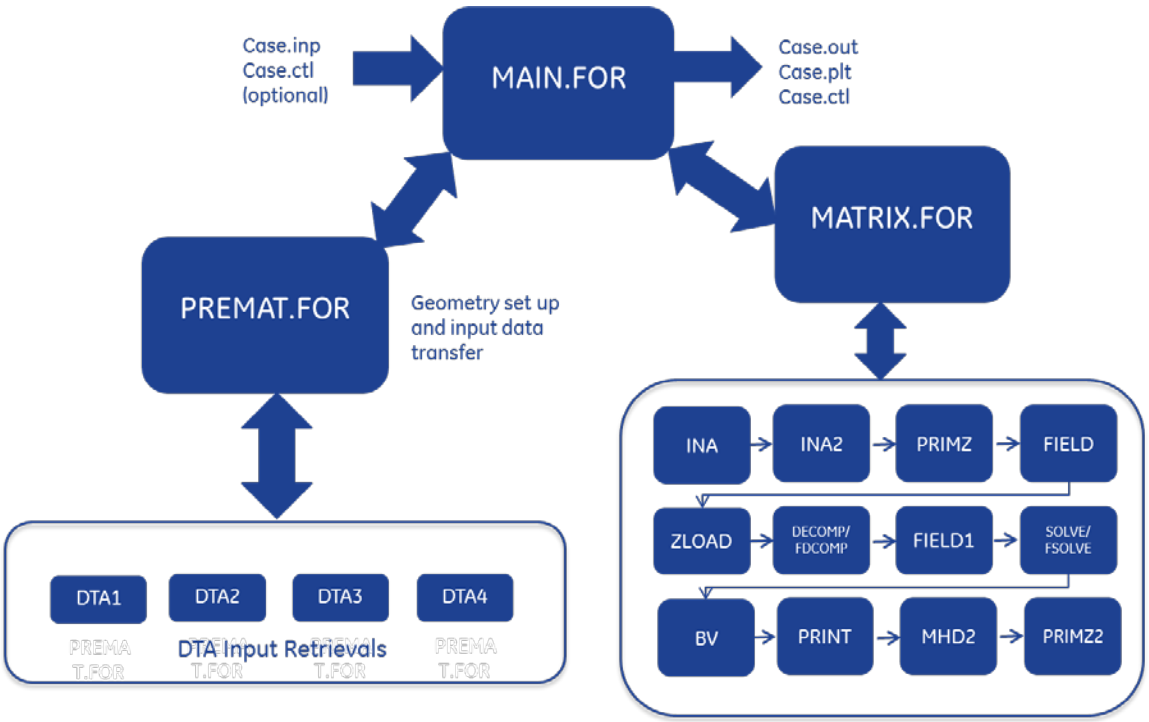

Figure B-13: 2015 MATRIX Code Computation and Data Flow (circa 2015)

The elimination of the three, separate FORTRAN source files which had to be compiled separately for each file and each MATRIX run streamlined code performance. Figure B-14 illustrates the modernized process flow for running a single test case through MATRIX. The process now only uses one, generic compiled FORTRAN file.

A pre-preprocessing executable was created to work in conjunction with a multiple case post-processing tool, which takes output text files from multiple MATRIX test cases and automatically creates output and plot files corresponding to the data.

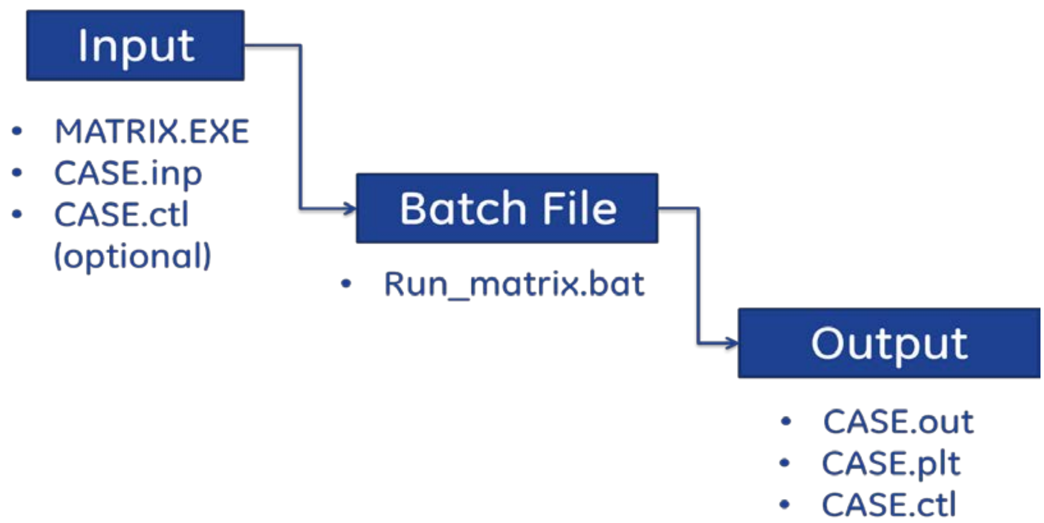

Figure B-14: Modernized DTA MATRIX Basic Process Flow

(e) Inventions/Patent Applications, Licensing Agreements:

Invention disclosure letter for GE patent docket 279303 was submitted to DOE on April 9, 2015 covering the insulation design employing silicon-bonded mica hard board in a slot-liner approach to provide ground wall insulation.

Patent Application, Confirmatory License, and associated documents for GE patent docket 279303 were submitted to DOE on September 17, 2015.

(f) Other Products:

Understanding the need for better electrical insulation, thermal hydraulics, and operation of the plant in general proved a difficult technical problem for the project that required many engineering disciplines for project success. Table 1-1 provided a listing of the key personnel and their technical disciplines. The six different technical disciplines listed (nuclear, electrical, mechanical, materials science, thermal-hydraulics, and electromagnetic) provided an interesting confluence of EM Pump technical areas:

- High voltage that needs separation by insulation

- Frequency and current that produces heat and forces
- An electrical insulation that must transfer heat
- Duct sodium flow altered by the magnetic field
- Variety of materials from metals (steels and iron) to non-metals (glass and ceramics)

During the bi-weekly project meetings, team members from these engineering disciplines shared information and learned from each other.

Engineers are learning about electricity, magnetism, and MHD. They are re-discovering a suitable high-temperature electrical insulation material that will enable sodium-cooled, fast reactor plants performance and reliability improvements, in addition to the continued development of performance analysis tools to better predict EM Pump operation.

The world needs engineers coming together and working on these types of co-discipline problems. In the advanced reactor engineering community, there is an acceptance for the need/use of EM Pumps. However, the current nuclear generation community has a 'pathological fear' of EM Pumps. This fear leads not only to opposition of advanced reactor concepts in the nuclear generation community, but also results in 'political' engineering decisions that do more harm than good.

This project is important as it taught more engineers about the possibilities of EM Pumps. It was the unique nature of this project, with a broad spectrum of engineers; that makes EM Pumps positioned for commercial adaptation in the future.

During the opening stages of this project while creating the databank, current engineers came to appreciate the excellent engineering previously accomplished with EM Pumps.

At several venues, this project's technical accomplishments were shared with other engineers.

The value of engineered testing should never be underestimated. Testing and test set-up is always threatened by the unknowns in the ability to collect worthwhile data.

While progress was made towards an improved, replacement insulation system for EM Pumps, unfortunately, not all of the multi-stress testing objectives were completed. To support advanced cooled reactor engineering and research, the engineering completed and the lessons learned during this project need to be widely distributed.

From a Human Resources perspective, the project re-established the relevant technical expertise in the current generation of scientists and engineers at GEH, GRC, and ANL.

Past insulation systems are not available in the market today; therefore, development of 21st century versions of the laboratory equipment needed to perform high temperature insulation material testing is crucial for future U.S. development of EM Pumps.

The MATRIX Code was updated by two current generation, GE electrical engineers for both code enhancements, post processing tools, and mechanical and thermal properties, as supervised by senior Ph.D. engineers. The MATRIX outputs were compared with other calculations from other organizations (GRC, ANL) with the next generation of scientists providing a broad increase in relevant technical expertise.

As the project lead organization, GEH sought to capture knowledge and support this project with early career engineers in GE's best company leadership program, Edison Engineer Development Program (EEDP). During the conduct of this project, four EEDP engineers (mechanical, chemical and two electrical) worked on the project. This grew the Human Resource capital within GEH for the future commercialization of advanced reactors. Members of the EEDP program today are the engineer leaders of tomorrow.

7. Computer Modeling Projects

(a) Model Description

The MATRIX analysis code is a tool used to analyze the overall electrical, magnetic, and fluid performance of EM pumps. The code uses the well-established "matrix method" for the analysis of linear induction machines, including linear induction motors, both single- and double-sided, and linear induction liquid-metal pumps and generators, both flat and annular. MATRIX incorporates features which allow a finite-length stator to be modeled on a slot-by-slot basis, with magnetic end effects explicitly considered. The code is based on a narrow gap magnetic circuit approximation with correction factors for the various fringing fluxes, stator ends, and skin effects.

The MATRIX code was originally created in 1975 and has been modified/modernized several times. Table B-2, MATRIX Code Development, shows a summary of the MATRIX code development. The current version of the code is MATRIX 2015.

Table B-2: MATRIX Code Development

MATRIX Version	Change	Description
MATRIX 1975	Base code from Jet Propulsion Lab (JPL)	
MATRIX 1999	Addition of magnetohydrodynamic capabilities for detailed EM pump characteristic design	Base Fortran code for GE EM pump analysis and design
MATRIX 1999 (PC Update)	Modernized to run on PC	No change in old code
MATRIX 2014	Modernized to run on new Intel PC compilers (change to DTA file structure). Sodium Flow correction added	New inputs for flow adjustments
MATRIX 2014A	EM pump material code added	New inputs for materials
MATRIX 2015	EM pump thermal code added	New inputs for thermal capabilities

The MATRIX code can be used to model the operational characteristics of a defined (flat or annular linear induction) electromagnetic (EM) pump. The results from MATRIX can be used as EM pump analysis data and supplement pump design.

(b) Performance Criteria

The MATRIX analysis code shall provide the basic electrical and MHD operating characteristics of a specified annular or flat linear induction EM pump. These operating characteristics include electrical power curves as well as developed pressure head versus flow.

(c) Test Results

The current MATRIX2015 analysis code was verified using both legacy MATRIX output files, as well as EM pump test data from the EM pump program funded by the Japan Atomic Power Company (JAPC) from the early 1990's through the early 2000's.

See the "Results" section of the "Modernization and Capability Investigation of the Matrix Electromagnetic Pump Analysis Code" paper for a detailed review of the code verification. Alternately, please see Sections 3 and 5 of the MATRIX report (GEH# PLM DOC-0005-2188).

(d) Theory:

The MATRIX analysis code uses the "matrix method," which solves Maxwell's equations in a series of mesh calculations, for the analysis of linear induction machines. Linear induction machines utilize the rotating magnetic fields created by the AC current passing through their stator coils to generate a force or torque. In an induction motor this force turns a rotor, and in the case of a pump, this force pushes a conductive fluid. In an EM pump, the rotating magnetic field of the stator induces a current in the fluid, so no mechanical rotor is necessary, and the resultant axial force on the fluid induces a directional flow.

(e) Mathematics:

See the "Methodology" section of the "Modernization and Capability Investigation of the Matrix Electromagnetic Pump Analysis Code" paper for a detailed review of the code mathematics. Alternately, please see Sections 3 and 5 of the MATRIX report (GEH# PLM DOC-0005-2188).

Utilizing the "matrix method," The main principle in linear induction machine analysis is, given the primary currents, to find the secondary currents within the system. After MATRIX solves for these currents, the performance of the machine can be found using basic electromagnetic principles. The ALIP inner and outer stator coils are first energized with a power supply to create a circulating current around the pump. The coils are energized using three-phase alternating current (AC) ranging from 600 to 1,000A at a voltage ranging from 500 to 1,700 V (line-to-line). This circulating AC current induces a magnetic field, ranging from 0.5 T to 0.65 T, within the inner and outer stator iron cores. The changing magnetic field, with a magnitude of around 0.1 T, inside the flow annulus further induces a current in the pump fluid. The resultant axial force on the fluid induces a directional flow. This axial force is derived from a phenomenon known as the Lorentz force, which is defined as:

$$dP_z = J_x \times B_y \qquad \text{(B. 1)}$$

In Equation B.1, Jx is the current density of the sodium, By is the magnetic field in the pump flow annulus, and dPz is the incremental pressure rise in the axial direction of the pump. During the modernization of MATRIX several functional structures were combined to help the code run more efficiently; however, the main electromagnetic MATRIX computing structure was not altered.

During the modernization of the code, additional velocity profile capabilities were added for increased accuracy. The original MATRIX code calculated pressure rise and efficiency results 30% greater than measured pump values. The code used a flat velocity profile; however a series of experiments conducted by S. Eckert and G. Gerbeth (2002) revealed that when sodium flows under a strong transverse magnetic field, an M-shaped velocity profile occurs within the flow duct. The application of an electromagnetic field causes a different flow structure phenomenon to occur within a duct than expected in non-conducting fluid. As the magnetic field is increased, the sodium velocity in the core of the flow is slowed while the velocities on the edges of the flow are enhanced. A relation to estimate the ratio between the velocity rises seen in the edges of the flow compared to the core of the flow δu and the mean velocity u is as follows:

$$\frac{\delta u}{u} \approx 10 * \beta \, \frac{\mathrm{Ha}}{\mathrm{Re}} \qquad \text{(B. 2)}$$

The Re and the Ha variables in Equation B.2 are the Reynolds Number and the Hartmann number, respectively. The aspect ratio of the flow duct for the subject experiment was unity. The Hartmann number (Ha) is a non-dimensional parameter (ratio of the electromagnetic force to the viscous force) defined by:

$$Ha = B * a \sqrt{\frac{\sigma}{\rho * v}} \qquad \text{(B. 3)}$$

The variables B, a, ρ, σ, and v stand for the magnetic flux density, half-width of the duct, fluid density, electrical conductivity, and kinematic viscosity, respectively. As the Hartmann number increases, corresponding to an increasing transverse magnetic field, the M-shape profile becomes apparent (see Figure B-15).

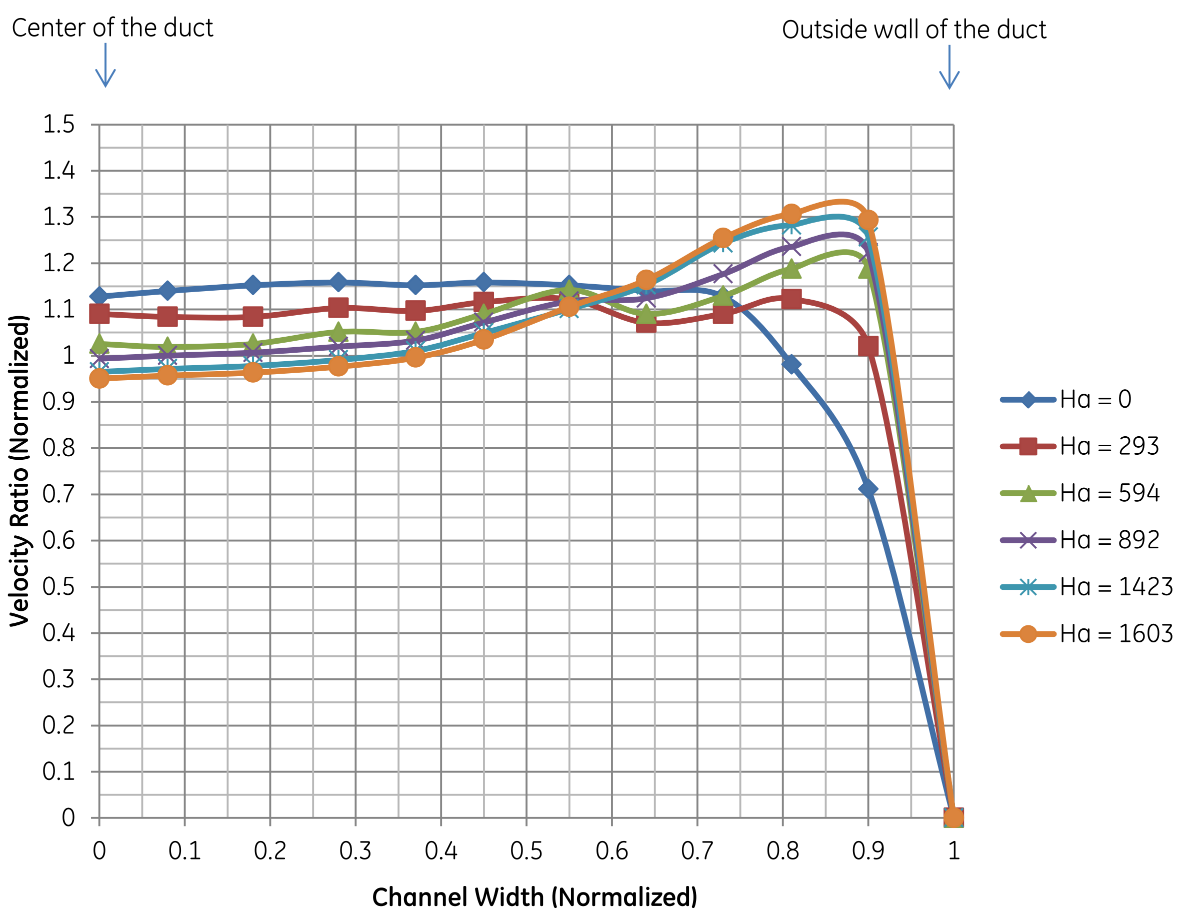

Figure B-15: Transverse Magnetic Field Effects on the Mean Velocity Profile at a Reynolds Number of 57,000

For an EM pump operating in the intermediate loop of the PRISM reactor system (sodium temperatures near 335°C) the Hartmann number is near 500. In the operating case of Figure B-15, a Reynolds number of about 60000 is seen. For a much higher Reynolds number, typical for EM pump operation, but at a Hartmann number of about 500, the sodium velocity profile would most probably resemble a "turbulent" flow. Instead of a flat sodium velocity flow profile, originally assumed in MATRIX, this turbulent velocity profile would alter the magnetic flux. Thus a flow correction (see Figure B-16) to MATRIX input velocity adjusts for the actual velocity profile, and much improved MATRIX results are obtained (see Figure B-17).

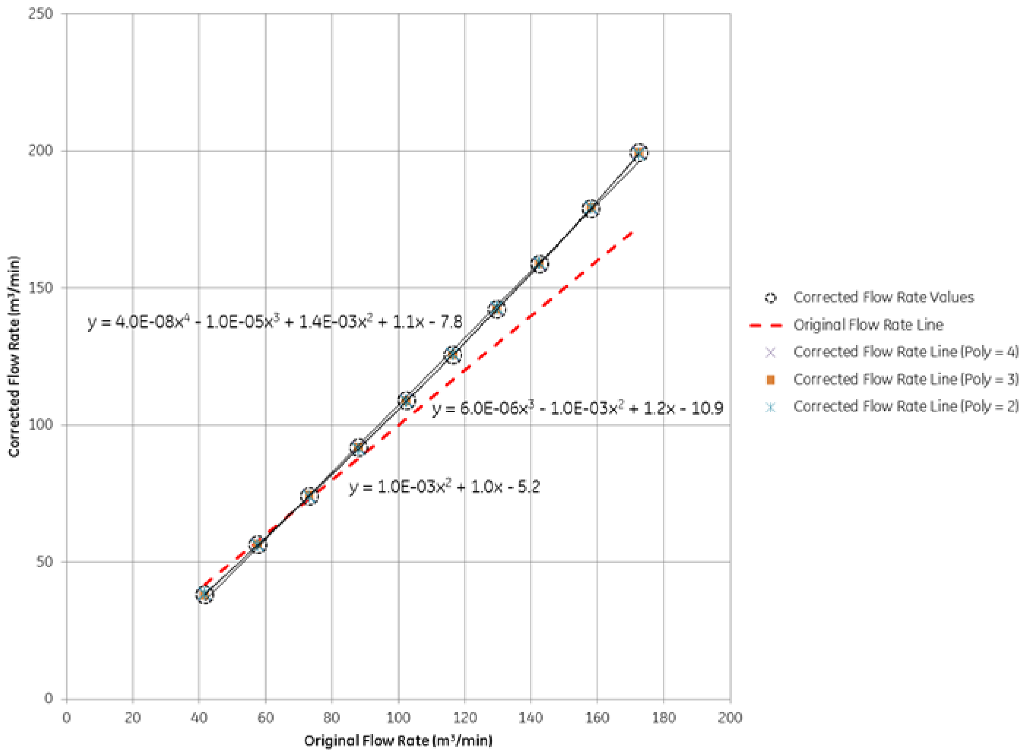

Figure B-16: MATRIX Flow Rate Correction Equations

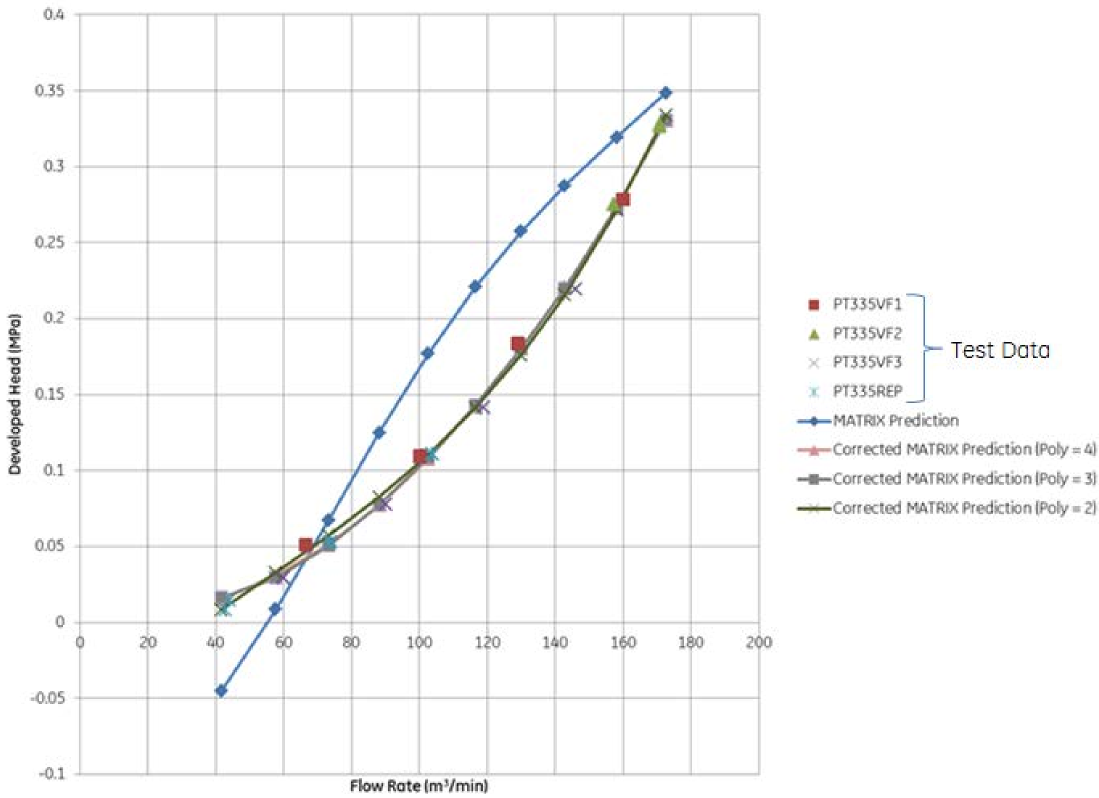

Figure B-17: Corrected MATRIX Developed Head versus Original Flow Rate

(f) Peer Review Summary:

As this is not a confirmed GEH Level 2 code, the mathematical algorithms were not peer-reviewed based on our commercial safety code process.

Through the modernization and verification process of the MATRIX2015 code, it was seen that the updated code output results matched the results seen from the legacy MATRIX code within + 5%. Through the addition of flow rate correction equations within the code (2nd, 3rd, or 4th order polynomial), the effective sodium velocity can be adjusted, thus improving the overall predictability of the MATRIX code for developed pressure head. Using a 4th order polynomial correction equation on the flow rate allows the predicted, developed pressure to be within + 10% of the measured data taken from a 160 m3/min EM pump used in the JAPC program.

Even though the improvement to the MATRIX code has improved the overall predictability of tool, the code is still limited to a 1-D analysis of annular and flat geometry linear induction pumps. Any other type of geometry would require further improvement/modification for pump analysis. In addition, further verification of the added flow velocity correction should be performed using measured data from various EM pumps, if and when available. The current code is only verified for the 160 m^3/min EM pump test pump.

(g) Hardware Requirements:

Not Applicable.

(h) Documentation

Modernization and Capability Investigation of the Matrix Electromagnetic Pump Analysis Code – Documentation on the Modernization and Verification of the MATRIX 2015 Code (Strege, Yilmaz, Saha, and Loewen)

MATRIX Software User's Manual (PLM DOC-0003-7657) – User's manual for the MATRIX2015 code (Strege)

MATRIX Analysis of Linear Induction Machines (FRA-OR&D-75/77) – Original MATRIX code manual created by the Jet Propulsion Lab (JPL) in 1975 (Elliott)